

A System for the Detection of Concealed Nuclear Weapons and Fissile Material aboard Cargo Containerships

by

Shawn P. Gallagher

SUBMITTED TO THE DEPARTMENT OF NUCLEAR SCIENCE AND ENGINEERING IN PARTIAL FULFILLMENT OF THE REQUIREMENTS FOR THE DEGREE OF

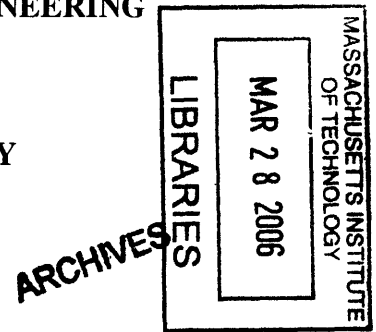
MASTER OF SCIENCE IN NUCLEAR SCIENCE AND ENGINEERING

at the

MASSACHUSETTS INSTITUTE OF TECHNOLOGY

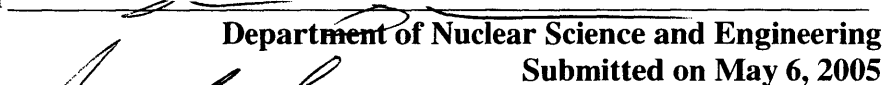
June 2005

© 2005 Shawn Gallagher
All rights reserved

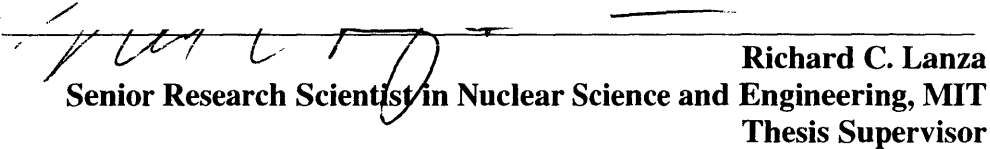


The author hereby grants to MIT permission to reproduce and to distribute publicly paper and electronic copies of this thesis document in whole or in part.

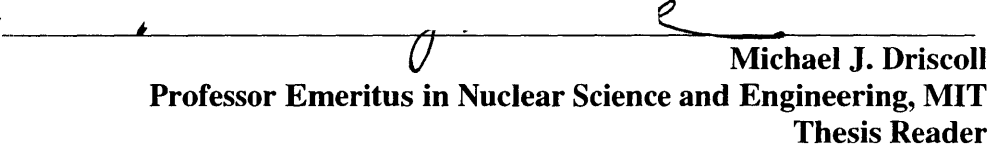
Signature of Author


Department of Nuclear Science and Engineering
Submitted on May 6, 2005

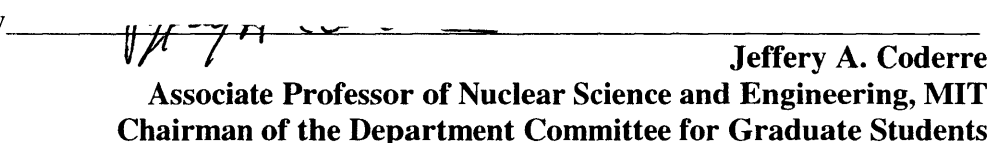
Certified by


Richard C. Lanza
Senior Research Scientist in Nuclear Science and Engineering, MIT
Thesis Supervisor

Certified by


Michael J. Driscoll
Professor Emeritus in Nuclear Science and Engineering, MIT
Thesis Reader

Accepted by


Jeffery A. Coderre
Associate Professor of Nuclear Science and Engineering, MIT
Chairman of the Department Committee for Graduate Students

A System for the Detection of Concealed Nuclear Weapons and Fissile Material aboard Cargo Containerships

Submitted to the Department of Nuclear Science and Engineering On May 6, 2004 in Partial Fulfillment of the Requirements for the Degree of Master of Science in Nuclear Science and Engineering

Abstract

A new approach to the detection of concealed nuclear weapons and fissile material aboard cargo containerships is proposed. The ship-based approach removes the constraints of current thinking by addressing the threat of containerized nuclear terror in a novel way. Critical tactical misjudgments exist in currently deployed detection systems, which expose U.S. cities to an act of nuclear terrorism. Current port-based systems position defenses within the perimeter of each coastal city and the assumption that terrorists would not remotely detonate the weapon while taxiing past urban areas en route to the port is irrational. The new approach protects this hole in national security by moving defenses outside the perimeter and onto the containership. A networked system of radiation detectors, aboard all inbound containerships, does not allow a concealed nuclear weapon to ever approach the U.S. homeland.

This thesis describes the ship-based system in detail, outlines its capabilities and suggests possible deployment scenarios. The basic concept of the ship-based system is to hide detectors in empty standard 40-foot shipping containers and send them back and forth across the ocean alongside normal cargo. Containerized arrays of gamma and neutron detectors are linked to small data processing and transmitting devices. Data is transmitted to a central U.S. location for collection, assessment, and possible dissemination to responders in the event of threat identification. Upon positive detection, an alarm condition is signaled and interception of the containership occurs while still at sea.

Monte Carlo based simulations suggest that due to long count times during typical two week voyages, radiation transport is significant enough such that containerized units will detect weapons grade uranium and plutonium in implosion-type configurations with three-sigma confidence from distances averaging 22.0 and 23.5 meters of cargo respectively. The vast majority of containerships require between 3 and 15 units deployed on each ship depending on its capacity and degree of control over container placement. Given the low number of units required for each ship, deployment of a containerized detector network is practical and an initial limited deployment increases the level of deterrence by denial against containerized nuclear terror.

Thesis Supervisor: Richard C. Lanza

Title: Senior Research Scientist in Nuclear Science and Engineering

Acknowledgements

I would like to thank Dr. Richard Lanza who has not only been a thesis and research advisor for this project, but has served to exemplify a concert of scientific idealism and integrity. Going far beyond the duties of an MIT professor, he has set aside countless hours of personal time to both elevate this idea to top levels of the government and to ensure that a scientifically sound message was heard.

I would also like to recognize the contributions of Brett Broderick, who was instrumental in the development and concise definition of the ship-based approach. The conclusions of this thesis would not be possible without the invaluable work that Brett performed in writing his thesis. It was Brett's enthusiasm that helped me fully realize the potential of the system. I am truly impressed with his unselfish dedication to improving national security and it is the hope that our two theses combine to provide a blueprint to accomplish such a lofty goal.

MIT Professor Emeritus Michael Driscoll has been an extremely valuable reader of this thesis. Through his tireless editing and insightful suggestions, Dr. Driscoll has ensured the high quality expected of an MIT thesis.

I would like to thank Whitney Raas for helping in the editing process and pointing out important concerns that needed to be addressed.

Without the financial assistance of the Department of Nuclear Science and Engineering and the work of Clare Egan and Carmen Velez, I would have been forced to leave MIT and this thesis would not have been possible.

I would like to mention Tyler Ellis, who donated his personal time and computer resources to expedite the simulation process.

Most importantly, I would like to recognize my wife Marisa and daughter Makayla for their continued patience while I embarked on this endeavor. Without their support, this thesis would have been a much more formidable task and would have taken significantly longer to complete.

Table of Contents

Abstract.....	2
Acknowledgments.....	3
Table of Figures.....	7
List of Tables.....	9
Forward.....	10
1. The Threat of Nuclear Terrorism.....	11
1.1 Introduction.....	11
1.2 Problem Definition.....	14
1.2.1 Threat Characterization.....	15
1.2.2 Detection Constraints.....	17
2. Current Approaches to Fissile Material Detection	19
2.1 Port-Based Systems.....	19
2.1.1 Passive Detectors.....	19
2.1.2 Active Detectors.....	22
2.1.3 Irrational Port-Based Assumptions.....	23
2.2 Smart Containers.....	24
3. Ship-Based System Description.....	27
3.1 Advantages over Current Technology.....	28
3.1.1 Standoff.....	29
3.1.2 Sensitivity.....	31
3.1.3 Stealth.....	32
3.2 Physical Description.....	33
3.2.1 Commercial Off-the-shelf Technology.....	34
3.2.2 Gamma Detectors.....	34
3.2.3 Neutron Detectors.....	36
3.2.4 Array Configuration.....	37
3.2.5 Coded Aperture.....	38
3.2.6 Electronics and Data Processor.....	39
3.2.7 Transmitter.....	40
3.2.8 Power.....	41
3.2.9 Dissemination and Response.....	41
4. Unique Radiation Signatures from Fissile Material.....	43
4.1 Weapon Geometry Model.....	43
4.2 Fissile Material Model.....	44
4.3 Detecting Uranium.....	46
4.3.1 Gamma Detection.....	46
4.3.2 Weapons Grade Uranium Spectrum.....	47
4.3.3 ²³² U Concentration.....	48
4.3.4 Neutrons from Uranium.....	50
4.3.5 Virgin Uranium.....	51
4.4 Detecting Plutonium.....	52
4.4.1 Neutron Detection.....	53
4.4.2 Neutron Sources.....	53

4.4.3	Interactions within the Weapon.....	53
4.4.4	Interactions within the Cargo.....	54
4.5	Detecting Fissile Material.....	56
5.	Background Radiation.....	57
5.1	General Background.....	58
5.2	Neutron Background.....	60
5.2.1	Neutron Sources.....	60
5.2.2	Neutron Background Quantification.....	61
5.3	Gamma Background.....	63
5.3.1	Gammas from the Ocean.....	64
5.3.2	Gammas from the Ship.....	65
5.3.3	Gammas from the Cargo.....	66
5.3.4	Reducing False Alarms.....	69
5.3.4.1	Shipping Manifesto Cross-Reference.....	69
5.3.4.2	Spectroscopic Source Identification.....	69
5.3.4.2.1	The Use of ²³⁸ U Gammas.....	69
5.3.4.2.2	The Use of ²²⁸ Ac Gammas.....	70
5.3.5	Gamma Background Quantification.....	71
5.4	Detectability.....	72
6.	Cargo Characterization.....	75
6.1	Importance of Cargo Constituents and Density.....	75
6.2	Modeling of Cargo for MCNP.....	78
6.2.1	Redistribution of Density.....	79
6.2.2	Cargo Materials.....	81
6.2.3	Air Percent by Volume.....	82
6.3	Pixel Approach.....	86
6.4	Discussion of Pixel Approach.....	89
6.5	Cargo Model Summary.....	92
7.	Results and Discussion.....	93
7.1	Control and Variable Description.....	93
7.2	Number of Particles.....	95
7.3	Model Dimensions.....	96
7.4	Additional MCNP Modeling Comments.....	96
7.5	Distance to Threshold.....	96
7.6	Energy Resolution.....	97
7.7	Results.....	98
7.7.1	Spectral Simulation.....	98
7.7.2	Signal Attenuation in Air.....	105
7.7.3	Signal Attenuation in a Uniform Density Model.....	109
7.7.4	Results with Pixelized Cargo.....	113
7.7.4.1	2615 keV Gamma Transport.....	114
7.7.4.1.1	12 Kilograms of Uranium.....	114
7.7.4.1.2	50 Kilograms of Uranium.....	119
7.7.4.2	1001 keV Gamma Transport.....	122
7.7.4.3	Neutron Transport.....	125
7.7.4.3.1	4 Kilograms of Plutonium.....	126

7.7.4.3.2	12 Kilograms of Plutonium.....	129
7.7.4.4	Shielded Gamma Transport.....	133
7.7.4.4.1	12 Kilograms of Uranium, Shielded.....	134
7.7.4.4.2	50 Kilograms of Uranium, Shielded.....	139
7.7.4.5	Shielded Neutron Transport.....	141
7.7.4.5.1	4 Kilograms of Plutonium, Shielded.....	141
7.7.4.5.2	12 Kilograms of Plutonium, Shielded.....	144
7.7.4.5.3	Concrete Filled Container.....	148
7.8	Summary of Results.....	149
8.	Deployment of the Ship-Based Detector Network	151
8.1	Detectors Needed on a Typical Containership.....	153
8.2	Load Factor Adjustment.....	155
8.3	Deployment Scenarios.....	157
8.3.1	Containerized Units Required for Complete Coverage.....	158
8.3.2	Deployment Outline.....	158
8.3.3	Initial Deployment.....	159
8.3.4	Extended Deployment.....	161
8.3.5	Final Deployment.....	162
8.3.6	Deployment Enhancements.....	162
8.4	Cost.....	164
9.	Reassessment and Conclusions	166
9.1	Reassessment of Assumptions.....	166
9.2	Conclusion.....	167
Appendix A:	2615 keV Gamma Origin Determination Procedure.....	170
Appendix B:	Radioactive Cargo.....	175
Appendix C:	Thorium Series Relative Gamma Intensities.....	178
Appendix D:	²³⁶ Pu/ ²³² U Series Relative Gamma Intensities.....	180
Appendix E:	Self-Shielding Effect in 50 kilograms of Uranium.....	183
Appendix F:	Randomized Pixel Arrays of Materials.....	184
Appendix G:	Cargo Imported to the Port of New York/New Jersey.....	193
References.....		196

Table of Figures

Figure 2-1: Port-based scanners for semi-trucks.....	20
Figure 2-2: Detectors mounted on quay cranes.....	21
Figure 2-3: Smart detector location.....	25
Figure 3-1: Containership taxiing passageways at Port of New York/New Jersey.....	30
Figure 3-2: Containerized unit component diagram.....	33
Figure 3-3: Example of a half-pyramid array configuration.....	38
Figure 3-4: Coded aperture schematic diagram.....	39
Figure 4-1: Weapon model.....	44
Figure 4-2: Critical mass of uranium versus enrichment of ^{235}U	46
Figure 4-3: Weapons Grade Uranium spectrum.....	48
Figure 4-4: ^{232}U parts per trillion in U.S. or alloy.....	50
Figure 4-5: Spectrum from a Soviet warhead.....	52
Figure 6-1: Cargo density redistribution.....	79
Figure 6-2: Container packing examples.....	82
Figure 6-3: Pixel array example, top-down view (left) and side view (right).....	87
Figure 6-4: Linearity of space.....	90
Figure 6-5: Extra low angle scattering events into the detector.....	90
Figure 6-6: Loss of low angle scattering events due to pixelized geometry.....	90
Figure 7-1: ^{232}U spectrum through core.....	99
Figure 7-2: ^{232}U spectrum through reflector.....	100
Figure 7-3: ^{232}U spectrum through tamper.....	101
Figure 7-4: ^{232}U spectrum through high explosives.....	102
Figure 7-5: ^{232}U spectrum at 1.28 meters.....	103
Figure 7-6: ^{232}U spectrum at 2.78 meters.....	104
Figure 7-7: ^{232}U spectrum at 4.28 meters.....	104
Figure 7-8: 2615 keV flux 12 kg U in air.....	106
Figure 7-9: 2615 keV flux 50 kg U in air.....	107
Figure 7-10: Neutron flux 4 kg Pu in air.....	108
Figure 7-11: Neutron flux 12 kg Pu in air.....	109
Figure 7-12: 2615 keV flux 12 kg U, uniform density model.....	110
Figure 7-13: 2615 keV flux 50 kg U, uniform density model.....	110
Figure 7-14: 1001 keV flux 12 kg U, uniform density model	111
Figure 7-15: Neutron flux 4 kg Pu, uniform density model	112
Figure 7-16: Neutron flux 12 kg Pu, uniform density model.....	113
Figure 7-17: 2615 keV flux 12 kg U, pixel array #1.....	115
Figure 7-18: 2615 keV flux per source particle, 12 kg U, pixel array #1.....	116
Figure 7-19: 2615 keV flux 12 kg U, pixel array #2.....	117
Figure 7-20: 2615 keV flux 12 kg U, pixel array #3.....	118
Figure 7-21: 2615 keV flux 50 kg U, pixel array #1.....	120
Figure 7-22: Ratio of 50 kg/12 kg fluxes, pixel array #1.....	121
Figure 7-23: 2615 keV flux 50 kg U, pixel array #2.....	122
Figure 7-24: 2615 keV flux 12 kg U, pixel array #1.....	123

Figure 7-25: 1001 keV flux 12 kg U, pixel array #1.....	123
Figure 7-26: 1001 keV flux 12 kg U, pixel array #2.....	124
Figure 7-27: 1001 keV flux 12 kg U, pixel array #3.....	125
Figure 7-28: Neutron flux 4 kg Pu, pixel array #1.....	126
Figure 7-29: Neutron flux 4 kg Pu, pixel array #2.....	127
Figure 7-30: Neutron flux 4 kg Pu, pixel array #3.....	128
Figure 7-31: Neutron flux 12 kg Pu, pixel array #1.....	129
Figure 7-32: Ratio of 12 kg/4 kg Pu fluxes, pixel array #1.....	130
Figure 7-33: Neutron flux 12 kg Pu, pixel array #2.....	131
Figure 7-34: Neutron flux 12 kg Pu, pixel array #3.....	132
Figure 7-35: 2615 keV flux 12 kg U, shielded with 2 cm of lead, pixel array #1.....	134
Figure 7-36: Ratio of unshielded/shielded flux 12 kg U, pixel array #1.....	135
Figure 7-37: 2615 keV flux 12 kg U, shielded with 2 cm of lead, pixel array #2.....	136
Figure 7-38: Ratio of unshielded/shielded flux 12 kg U, pixel array #2.....	137
Figure 7-39: 2615 keV flux 12 kg U, shielded with 2 cm of lead, pixel array #3.....	138
Figure 7-40: Ratio of unshielded/shielded flux 12 kg U, pixel array #3.....	138
Figure 7-41: 2615 keV flux 50 kg U, shielded with 2 cm of lead, pixel array #1.....	139
Figure 7-42: 2615 keV flux 50 kg U, shielded with 2 cm of lead, pixel array #2.....	140
Figure 7-43: 2615 keV flux 50 kg U, shielded with 2 cm of lead, pixel array #3.....	140
Figure 7-44: Neutron flux 4 kg Pu, shielded with 5 cm of water, pixel array #1.....	141
Figure 7-45: Ratio of unshielded/shielded flux 4 kg Pu, shielded with 5 cm of water, pixel array #1.....	142
Figure 7-46: Neutron flux 4 kg Pu, shielded with 5 cm of water, pixel array #2.....	143
Figure 7-47: Neutron flux 4 kg Pu, shielded with 5 cm of water, pixel array #3.....	144
Figure 7-48: Neutron flux 12 kg Pu, shielded with 20 cm of polyethylene, pixel array #1.....	145
Figure 7-49: Ratio of unshielded/shielded flux 12 kg Pu, shielded with 20 cm polyethylene, pixel array #1.....	146
Figure 7-50: Neutron flux 12 kg Pu, shielded with 20 cm of polyethylene, pixel array #2.....	147
Figure 7-51: Neutron flux 12 kg Pu, shielded with 20 cm of polyethylene, pixel array #3.....	148
Figure 7-52: Neutron flux 4 kg Pu, container backfilled with concrete, pixel array #2..	149
Figure 8-1: Coverage volume in two dimensions.....	152
Figure 8-2: Coverage volume inefficiencies due to loading factor.....	155
Figure A-1: NaI Scintillator efficiency.....	174

List of Tables

Table 3-1: Hourly temperature change example.....	35
Table 4-1: Weapon geometry and materials used in simulation.....	45
Table 4-2: Isotopic composition of fissile material.....	45
Table 5-1: Decay series comparison.....	59
Table 5-2: Common medical and industrial radionuclides.....	60
Table 5-3: Expected neutron background.....	61
Table 5-4: Thorium concentrations in the ocean.....	64
Table 5-5: 2615 keV gamma background from the ship.....	65
Table 5-6: Intensity factor for granite.....	68
Table 5-7: Expected 2615 keV gamma background.....	72
Table 5-8: Three-sigma detectability limits.....	74
Table 6-1: Material for MCNP model.....	80
Table 6-2: Average density of cargo.....	83
Table 6-3: Material volume probability calculation.....	87
Table 6-4. Example of a random array of materials, side view.....	89
Table 7-1: Average distance to threshold.....	150
Table 8-1: Containerized detectors needed per containership.....	154
Table 8-2: Containerized detectors needed on containerships with 65% loading factor.....	156
Table 8-3: Containerized detectors needed to cover all incoming containerships.....	157
Table 8-4: Containerized detectors needed for an initial deployment.....	160
Table 8-5: Containerized detectors needed for secondary deployment.....	161
Table A-1: Important values of η , the weapon to background intensity ratio.....	171
Table B-1: Gamma energies from common background isotopes.....	176
Table C-1: Thorium series relative gamma intensities.....	178
Table D-1: Thorium series and ^{236}Pu and ^{232}U relative isotopic gamma intensities.....	180
Table F-1: Pixel array arrangement.....	184
Table G-1: Port of NY/NJ import material tonnages.....	193

Foreword

I would like to instill a degree of patriotism and innovation to you, the reader. As with any system, process or idea, the ship-based approach can always be improved and it is through collaborative inventiveness and ingenuity that the system described below will realize maximum effectiveness. In the interest of national security, I challenge you to absorb the ideas presented here with the intent of improving upon them. It is our collective effort that will win the day.

The ultimate value of the ship-based system lies in the degree of deterrence achieved by the simple knowledge that it might be deployed. Once the adversary realizes that this system might be overtly or covertly operating, he cannot overlook its implications and a level of deterrence by denial is achieved. I therefore humbly request your cooperation in the sharing of information presented here.

Finally, I offer a note to any terrorist group or rogue nation with the intent of committing nuclear terror against the United States and who might obtain a copy of this thesis: as I write these words, the ship-based approach is in its infancy; as you read them, whether visible or not, it has matured. Do not misjudge the ability of the scientific community to provide secure solutions to all threats that might arise. *And do not underestimate the resolve of the American nation, as we stand united against you.*

Chapter 1: The Threat of Nuclear Terrorism

1.1 Introduction

The dawn of the nuclear age fundamentally changed the United States' defense posture; but after half a century, current strategies are outdated and incomplete. The threat from the Soviet Union prompted the U.S. to develop a second-strike counter-value capability to deter nuclear attack, but that capability no longer applies to the current spectrum of possible nuclear events. A new dynamic in the form of organized global terrorism has emerged that requires a reassessment of the nuclear deterrent achieved during the Cold War era as non-state actors may now threaten new modes of nuclear attack. Gaps in fissile material security following the collapse of the Soviet Union [Allison, 1996] have now combined with the one-stop-shopping provided by the A.Q. Khan nuclear proliferation network to ease the burden of obtaining sufficient fissile material to construct a crude nuclear device [Bush, 2004; Slavin, 2004]. A well-funded terrorist group could have taken advantage of extremely poor security and working conditions at Russian nuclear facilities to obtain fissile materials and simply paid a Khan representative to provide requisite nuclear knowledge. Without borders to defend or citizens to protect, a terrorist group is left undeterred from using a nuclear weapon against the United States, effectively rendering the U.S. nuclear stockpile incapable of non-state intimidation or coercion.

The rise of organized international terrorism has thus changed the traditional nuclear deterrence landscape. The principle that nuclear weapons would never be used against the U.S. because of assured retaliatory destruction is no longer valid. Non-state actors and terrorist groups may now threaten the U.S. homeland with unconventional modes of attack by concealing a nuclear device with the intent to deliver a clandestine blow. With no practical retaliatory option against a terrorist group using nuclear force, the mutually assured destruction (MAD) safety net falls apart. Thus, the threat of nuclear terrorism may now even compete with the threat of a conventional nuclear attack. This claim is

substantiated by a comprehensive report from the Defense Science Board Task Force (DSBTF) for the Department of Defense, which suggests that the possibility of clandestine nuclear terror should be treated with attention “as serious as that devoted missile defense” [DSBTF, 2004].

The new dynamic of religiously motivated, suicidal terrorist groups operating on an international level and targeting U.S. interests has expanded the number of possible modes of nuclear attack. Traditional methods—such as ICBMs, submarine-launched cruise missiles and manned bombers—are no longer the only means of delivery. A terrorist group or rogue nation wishing to detonate a nuclear weapon on American soil have much more insidious options available. Possible delivery methods of clandestine nuclear attack include border-crossings with large trucks or trains as well as port landings with small boats and airplanes. As evidenced by recent comments from top-level government representatives, one thought that has caused particular concern in Washington is the possibility that a terrorist group would conceal a nuclear weapon among common cargo aboard a containership [Schumer, 2003; CNN:Ashcroft, 2005]. Identified as the most unprotected and insecure method of nuclear delivery, nearly 19,000 cargo containers enter U.S. seaports every day, any of which could be concealing an assembled nuclear device. In the new nuclear landscape, the list of delivery options has expanded to include the weaponization of cargo.

Since the possibility of nuclear smuggling aboard containerships appears to be the most threatening and least secured, a new method of both nuclear defense and deterrence is required. It is therefore of the utmost importance to national security that a new deterrent is developed to address the rational enemy and a new line of defense is deployed to respond to the irrational adversary. This thesis aims to address the threat of nuclear terrorism as it has evolved and will describe a new approach to the detection of a nuclear weapon concealed aboard cargo containerships and a system which has the ability to mitigate the threat before it ever comes close enough to destroy an American city.

The basic concept of the ship-based system is to hide radiation detectors in otherwise empty standard 40-foot shipping containers and send them back and forth across the ocean alongside normal cargo. The system is capable of detecting weapons grade uranium and plutonium in an assembled and operational geometry. It also detects unassembled fissile material and, while not at all a focus but certainly an added benefit, the system can also detect material used in Radiological Dispersal Devices (RDDs), commonly known as “dirty bombs”. Containerized arrays of gamma and neutron detectors are linked to small data processing and transmitting devices. Continuous or discrete data is transmitted to a central U.S. location for collection, assessment, and possible dissemination to responders, in the event of threat identification. Upon positive detection, an alarm condition is initiated and interception of the containership occurs while still at sea.

Current port-based solutions offer no deterrence against the use of an assembled nuclear device concealed in a containership; and worse, set the final line of defense within the perimeter of U.S. cities. Given the implicit assumption that a terrorist group has the capability to weaponize fissile material or procure a functional nuclear weapon, it is unreasonable to conclude that they will not have the ability to remotely detonate the weapon. It is then a straightforward risk assessment on the part of the terrorist to opt to detonate the device while taxiing past urban areas, not ever having reached port-based detection systems. This could be done either by remote activation or via stowaway suicide bomber. The ship-based system sets a line of defense offshore, outside the perimeter, thus not ever allowing the weapon to threaten the U.S. homeland.

The new approach described in these pages makes no claim to solve the entirety of the nuclear terrorism problem; rather, it solves the containerized nuclear terrorism problem, the one identified as the most likely mode of attack and most difficult to defend. Subsequent work from different parties will have to address other smuggling routes and, once closed off, the hope is that the threat of nuclear terrorism will have been significantly deflected from the United States.

The system described in this thesis achieves a dual counter-terrorism effect. It offers an increased degree of deterrence by denial and establishes a crucial line of defense. Deterrence by denial requires a defense such that the enemy realizes his chances of success are minimal and that his goals are unachievable [Mearsheimer, 1983; Bowen, 2002]. Denial is enhanced if the cost of failure is immense, and in the case of obtaining a nuclear weapon, the cost to terrorists is assumed high and failure unacceptable [Powers, 2001]. By reducing the chances of a successful act of containerized nuclear terror to extremely low levels, the ship-based approach achieves deterrence by denial for the rational enemy. But, for the undeterrable, non-calculating adversary, the deployment of a ship-based network of detectors inserts an extra layer of at-sea defense. It may also be possible to enhance the efficacy of other layers with the ship-based system. If believable enough and if combined with other systems that protect secondary attack modes, the deployment of a system based on deterrence by denial might deter the attempted acquisition of nuclear weapons or even prevent it as a form of warfare [DSBTF, 2004; Powers, 2001].

A suicidal, nuclear-armed terrorist with a motivation to inflict catastrophic damage on the United States may now be a possibility. This thesis will describe a system, based on currently available technology, simply rearranged in a new way, that will enhance national security by offering an increased degree of deterrence by denial, which is backed by a believable and capable line of defense.

1.2 Problem Definition

This brief section defines the difficulty of finding a solution that effectively addresses the problem of containerized nuclear terror. Rather than viewing the problem as a whole, the approach taken in the conception of the ship-based system was to analyze the problem from a 'top-down' viewpoint. Potential constraints in current thinking were then identified and solutions that lie outside of these constraints were considered. A synthesis of viable sub-solutions was then formed and the result is the system described in this thesis. A conscious effort was made to proceed with this 'top-down' method of scientific

advancement, rather than working on one facet of the containerized terrorism problem and contributing only a small piece of the puzzle. Before taking such a broad perspective; however, a clear characterization of the threat must be made.

1.2.1 Threat characterization

One of the underlying assumptions in this thesis is that terrorists either have or could have the capability to deliver a nuclear weapon via cargo containership to a U.S. seaport and detonate it. There certainly are intense debates in Washington as to whether or not this scenario is even possible, let alone likely. However, the fact that the government has spent large sums of money on radiation detectors for port security at least indicates that some of those with budgetary power are convinced that the threat is real [AP, 2005]. The degree to which the government believes that a terrorist group could carry out such an attack is not openly discussed and therefore carries an element of ambiguity. However, given the events of September 11th, there can be little question that terrorist groups have the organizational and operational capability to carry out a complex attack. The question that remains is whether or not a terrorist group has the technical proficiency to construct or procure a nuclear device.

The question as posed is essentially unanswerable. There is no way to gauge the nuclear competence of an organization such as al-Qaeda that has apparently eluded international efforts to uncover all its intentions. However, the motivation of terrorist groups to commit nuclear terrorism is evident. Osama bin Laden has stated that the acquisition of nuclear weapons is a “religious duty” and in an al-Qaeda *fatwa*, the group authorizes all Muslims to use a nuclear device against Americans [Garamone, 2002; Uphoff, 2004]. Traditional terror methods have focused on committing attacks that seek to maximize their psychological effect or kill key personnel, rather than maximize their destructive effect and kill at random [Stern, 1999]. Conversely, the new format of terror displayed by al-Qaeda on September 11th clearly seeks to maximize destruction and number of casualties. It would seem that weapons of mass destruction, especially nuclear, fit this new format.

A nuclear attack on an American city requires no description of its destructive and indiscriminate consequences. However, considering not only the tremendous loss of life and the political and social disruption which would be the results of such an act, it is clear that the U.S. cannot afford the purely economic consequences that a nuclear attack would initiate. For example, the present discounted value of Lower Manhattan is around two trillion dollars and given the public fear and uncertainty of radiation, it is unlikely that a post-nuclear Manhattan would be return to its current state in short order [Allison, 1996].¹ Worldwide, the consequences of an attack involving the U. S. maritime shipping infrastructure would likely halt international commerce (\$1.4 billion in goods exchanged per day) for an extended period of time [Koch, 2004]. The above scenarios are mentioned not to overstate the consequences, because it should already be clear that nuclear terrorism must be disallowed, but rather to highlight the need for a system that can at least prevent containerized nuclear terrorism.

To mitigate this threat, several layers of defense are necessary including source (fissile material) security, detection and homeland defense. Securing the source and defending the homeland are clearly necessary and much of the available national resource pool has been poured into these areas. In the detection layer, the unique radiation signal given off from the fissile material inside the core of the nuclear weapon must be identified before it is close enough to unleash any destructive power on the U.S. homeland. It is impractical for customs officers to perform daily hand searches of 19,000 containers [Koch, 2004]; therefore, along with some hand-held detection devices, wide-area radiation scanners have been developed and deployed. Billions of dollars have also been spent on securing loose fissile material in Russia and considerable national resources have been devoted to tracking would-be terrorists, both with the idea of removing the source of fissile material from the equation [NTI, 2005]. Cutting off the threat at the source and placing detectors at the destination are two important layers, but these alone cannot to provide a competent defense; an extra layer is required between the source and destination to address any

¹ This value was figured from an estimated \$260 billion gross product, a discount rate of 5 percent and a ten year life span. The estimate was taken from Allison, et al., page 129.

source breaches that may already have occurred and to defend against the enemy who will remote detonate a device just before reaching the destination.

1.2.2 Detection Constraints

Before proceeding in an attempt to solve such a difficult problem, it is important to completely characterize the constraints and freedoms that exist. As formed, the dilemma is simple to understand, but complex to solve. It is generally accepted that a viable solution must include the following:

- Positive detection claims should not disrupt commerce in more than a minimal way because the economic inefficiencies of a bottlenecked detection system might prove vastly cost-prohibitive.
- Any solution should provide confident detection such that when false positives occur, as they inevitably will, there is not a significant effect on the flow of containers.
- The probability of false negatives should be vanishingly small.
- The system should be deployable without building an impractical infrastructure that requires the rerouting of all containers.
- Detectors should be situated such that they are tamper-proof, and ideally autonomous.
- A degree of deterrence by denial would be achieved through the demonstrated use of any radiation detection system.

The unneeded constraints this places on a solution, as generally perceived prior to this thesis, are the following.

- The system must be able to quickly scan only suspicious containers as they are loaded or unloaded so as not to disrupt commerce.
- Detectors must be attached to existing infrastructure at ports such as on cranes or near roads and railways within the port grounds.

- The detection units must be based mostly in U.S. ports to minimize adversary tampering.
- Layers of defense covering the source and destination are enough to address the threat.
- Deterrence by denial is achieved with port-based radiation detectors because the terrorist will not risk the loss of his weapon without a chance to use it.

The ship-based approach described in this thesis relieves all of these prior unnecessarily imposed constraints and offers a new perspective with clear advantages over existing and proposed technology by stepping beyond current thinking. The solution begins with the observations that allow additional freedoms not previously conceived or realized.

- Every container, not just those deemed suspicious, must be checked to ensure that there is no chance of a weapon slipping past defenses.
- The constraint that detectors should be placed at port is unnecessary and due to their location, leave a large gap in national security.
- Deterrence by denial is achieved through believable defenses. Only a line of defense outside the U.S. homeland is sufficient.
- Most importantly, no foreign nuclear weapon should ever, *under any circumstances*, be allowed within the borders of a U.S. city.

The solution provided in this thesis achieves all the above objectives in a practical and fully implementable manner in such an effective way that the adversary will likely be deterred from committing containerized nuclear terror.

Chapter 2: Current Approaches to Fissile Material Detection

The currently prevailing strategy for the detection of fissile material concealed in cargo containers is what will be termed a port-based approach. In much the same way airplane luggage is scanned by an x-ray machine for conventional weapons or other contraband, U.S. seaports have installed radiation detectors to find fissile material. The port-based approach usually involves a simple array of radiation detectors placed such that each suspect container is scanned either while it is unloaded from the ship or when it is loaded onto a truck or train. The method places a potential bottleneck on the flow of containers off the boat, but great effort by many engineers and scientists has minimized the pinch on container flow such that commerce moves relatively unconstrained. The system is far from perfect and often the method applied to relieve a potential bottleneck is to simply not scan every container [Koch, 2004]. Some containers are labeled as higher risk and interrogated while many pass through unchecked. False alarms also cause some procedural disruption for a small percentage of containers scanned. Despite some drawbacks, the port-based approach has been well implemented and given the improvement over previous ineffective methods, should be considered a successful first step towards prevention of containerized nuclear terror.

2.1 Port-Based Systems

2.1.1 Passive Detectors

There are many ways to apply the port-based approach including both passive detectors, which scan for the normal radiation signal from fissile material, and active systems, which beam neutrons or photons towards the cargo causing a unique return signal from subsequent fission events. Most systems have focused on the placement of detector arrays in a wall, mounted on or near the docks. Some of the ground-mounted arrays are situated such that semi-trucks or trains pass through detector portals along their normal routes. Almost all of these systems require the vehicle to stop for a few minutes so that a

statistically significant number of counts can be collected. The type and geometry of detectors varies depending on the manufacturer and determines the time needed to scan each container. An example of a port-based scanner is shown in Figure 2-1 [Kok, 2004].

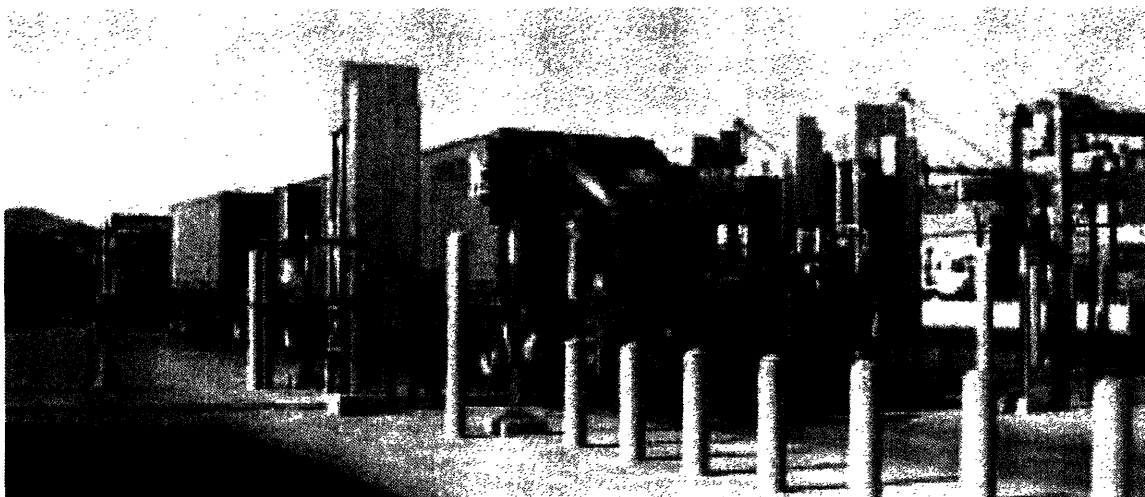


Figure 2-1: Port-based scanners for semi-trucks

Other port-based approaches propose mounting an array of detectors at some place in the unloading process. For instance, it has been suggested that mounting detectors on large quay cranes would give enough time for confident detection (see Figure 2-2). Also, the gantry assemblies that drop the containers onto the truck or train could house a series of detectors and have been considered as possible mounting locations [Kok, 2004].

Additionally, a cadre of hand held detectors has been distributed to customs personnel for mobile monitoring. These detectors are by necessity small and often require a few minutes of count time to distinguish the radiation from natural background. Some personnel carry dosimeters with them at all times so that an increase in radiation dose will signal an alarm condition [Hasson, 2005].

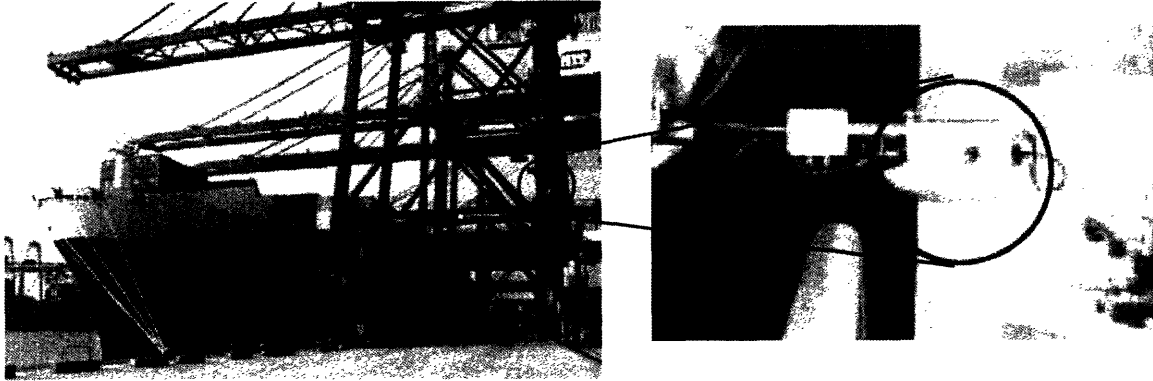


Figure 2-2: Detectors mounted on quay cranes

Still more creative approaches have been proposed, but not yet implemented. For example, researchers at Lawrence Livermore National Laboratory (LLNL) have designed a cell phone based system that would hide a small detector inside a series of cell phones. Each phone would then act as a node for an entire detection network. LLNL has also proposed (and built to prototype) a buoy based detection system that would theoretically detect radiation from a ship passing by [Wampler, 2004]. It has also been suggested that a large array of detectors could be deployed on barrier islands or peninsulas surrounding some ports or on bridges such as the Golden Gate Bridge in San Francisco or the Sunshine Skyway Bridge over Tampa Bay. It is not clear how these systems intend to receive enough counts from passing containerships at such long distances and short proximity times.

Mobile detectors mounted on vehicles are also currently being considered. LLNL has built a prototype radiation detector mounted in the back of a moving truck for finding fissile material in buildings and other places, but it could theoretically be used to search containers at port [Ziock, 2004]. Similarly, small coast guard boats outfitted with radiation detectors could drive by the hull of each incoming containership or other vessel. It has also been proposed that a helicopter, carrying a large array of detectors on its underside, could fly across the bow of each ship and hover for a few minutes.

2.1.2 Active Detectors

Active interrogation methods are receiving much more attention than passive systems for port-based applications because of their superior ability to distinguish threatening signals from benign background. Focused beams of photons and neutrons intended to excite the fissile material offer unique signals by returning either high-energy (>3000 keV) de-excitation gammas or high neutron fluxes. The use of an active system on a containership is not practical because the two-week long dose that crew members would receive rises above unacceptable levels. Still, a survey of current approaches to fissile material detection would not be complete without a brief mention of active systems.

Lawrence Livermore National Laboratory (LLNL) has devoted considerable resources to developing an active approach using neutrons. The idea is to focus enough neutrons towards the concealed fissile material to cause a significant number of fissions. High-energy gammas emitted from the fission process and from fission fragment decays provide a unique signature of fissile material. It turns out that firing a stream of neutrons at cargo will only return significant numbers of greater than 3,000 keV gammas if the cargo contains fissile material [Slaughter, 2003].

One other developing technology that has been proposed as a possible way to detect fissile material is by active interrogation using high-energy photons [Bertozzi, 2003]. This approach would take advantage of photo-excitation of the fissile nuclei through nuclear resonance fluorescence (NRF). For the safety reasons already identified above, the approach is not useful aboard containerships. The dose given to the crew would likely be far above acceptable limits and it would be both illegal and unacceptable to the international shipping community for the crew to absorb doses out of the normal range. Nevertheless, NRF could be used at port to scan suspect cargo given that a proper amount of shielding is present. An important application of these active interrogation technologies may be of use as another layer of the overall defense.

2.1.3 Irrational Port-Based Assumptions

The port-based approach has a fatal flaw, which if exploited, could expose a hole in the entire nuclear defense of the United States. Before a nuclear device is in range of the systems described above, the weapon could be remotely detonated. The minute that the containership enters a bay, inlet or other docking area, it could be remotely activated or set off by suicide bombers stowed in the container such that it would destroy surrounding urban areas and infrastructure.

While not explicitly stated or considered, the fundamental assumption of the port-based approach is that the weapon will not be remotely detonated or equipped with countermeasures such as booby-traps. It is already implicitly assumed that a terrorist group has the ability to procure or manufacture a complex nuclear device. Therefore, it is illogical to assume that the group will be unable to accomplish simple engineering feats such as remote detonation and countermeasures. As seen in the recent Madrid train bombings, a cell phone is sufficient for an initial firing signal [CBS/AP, 2004]. Furthermore, it can be argued that the terrorist might also booby-trap the weapon such that any opening of the container or other inspection would detonate the device. It might even be the case that the terrorist arranges his own embedded radiation detector such that the high fluxes from an active probe would set off the firing sequence.

It can be argued that the terrorist would smuggle the fissile material into the country in small pieces for later assembly. From the nefarious view of the terrorist group, it would seem to diminish the potential for success if the weapon were assembled in the country, where it would be subject to the watchful eye of various government entities and other policing agencies. Furthermore, many attractive target cities are by the ocean and have dense urban areas near major seaports so adding the extra step of in-country assembly would only increase the chances of being caught – there appears to be no motivation to attack an interior city like St. Louis or Denver, when larger and more economically important cities such as New York are accessible with less risk. From the terrorist's perspective, it is irrational to risk detection at port when one could simply detonate before

even reaching current U.S. homeland defenses, especially if already within range to inflict damage on an American city.

Given the assumption of rational enemy, there seems little reason to expect the nuclear device will ever reach port-based detectors. The current maritime security utilizing only a port-based approach is therefore not offering an optimal last line of defense. Moreover, it is not offering the terrorists any deterrent from the containership method of attack.

Rather, they will likely detonate the weapon at some optimal point while the containership is taxiing towards the port. It is under these pretexts that a new approach is not only required, but also essential for national security.

2.2 Smart Containers

The only other approach currently suggested that attempts to make detection aboard the ship might seem, at first, to be very similar to the containerized detector system but the utility of the “smart container” is extremely limited. The smart container approach, which has been proposed by Klann and McGregor at Argonne National Laboratory, consists of tiny wafers of solid-state neutron detectors inserted inside every imported container [ANL, 2003]. These small, thin wafers are attached or are in some way connected to the electronic seals soon to be prominent on all incoming containers. The would-be location of the detector is shown in Figure 2-3 [Kok, 2004].

There are several differences with this sort of approach, all of which point to the advantages of the containerized detector described in this thesis. Perhaps an obvious difference is that the small wafers are shipped alongside cargo while the approach described here entails detectors shipped in empty, dedicated containers (see section 3.1.3 for more detail). Smart containers are therefore not a clandestine approach, which leads to severe security problems. Most importantly, a terrorist group would, upon obtaining their container, simply remove, disable or otherwise deceive the detection unit [Koch, 2004]. While each smart container will be part of a network and an alarm signaled when

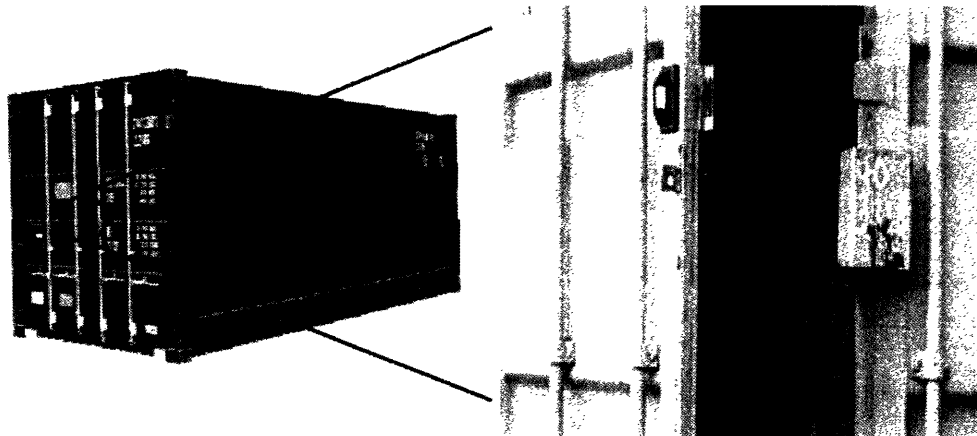


Figure 2-3: Smart detector location

one has been disabled, it is safe to assert that, considering the nearly 11 million containers, the number of broken smart container detectors at any given time will be too high to account for every disturbance without disrupting commerce. The tampering would likely go unnoticed.

Furthermore, the small, thin detectors offer such a low solid angle (even relative to a weapon concealed in its smart container) and not enough thickness to slow down neutrons, that the detector will likely not resolve a confident signal. Also, the cost of fabricating 11 million detection units, even if made cheaply for around \$1000, would balloon to 11 billion without including significant operation and maintenance costs. And, the implementation of the smart containers would be useless until they were attached to all 11 million containers because it only takes one container to smuggle a weapon.

Finally, an ultimately overwhelming disadvantage of smart containers is that they are set up to only look for neutrons. The neutron signal from uranium is almost non-existent and smart containers are therefore limited to detecting plutonium (see section 5.3). It is not practical to also include large gamma detectors with enough efficiency in 11 million containers. Less significantly, the smart detector approach would be unlikely to detect

dirty bomb material because most radioisotopes emit gamma radiation and not neutrons. Clearly, the limitations of the smart containers preclude any realistic chance of their practical implementation.

Chapter 3: Ship-Based System Description

The basic concept of the ship-based system is to hide detectors in empty standard 40-foot shipping containers and send them back and forth across the ocean alongside normal cargo. Upon positive detection, an alarm condition is transmitted to the United States and an interception of the containership occurs while still at sea. This novel approach employs the inherent advantages of standoff, sensitivity and stealth to more effectively achieve its objective of detecting a concealed nuclear weapon before it can be detonated. The most important advantage, standoff, offers the benefit of detection at sea before the weapon is in range of a U.S. city and while an effective response is still possible.

The ship-based system is essentially a detector in a box. Containerized arrays of cesium iodide (CsI) gamma detectors and boron tri-fluoride (BF₃) neutron detectors are linked to small data processing and transmitting devices. Continuous data is transmitted to a central U.S. location for collection, assessment, and possible dissemination to responders in the event of threat identification. If a positive detection is made, data transmission, processing and reporting should take on the order of minutes and will allow for the formulation of an appropriate preventative response.

The system is capable of detecting both weapons-grade uranium and plutonium. Using the ²³²U impurity daughter nuclide, ²⁰⁸Tl, which emits an energetic 2615 keV gamma, in combination with the ²³⁸U daughter ^{234m}Pa 1001 keV gamma, the system will detect uranium. For plutonium, the system will detect mostly neutrons from spontaneous fission, but will also be equipped for identifying high-energy gammas (>3000 keV) from fission products and secondary radiation via (n, γ) reactions in the surrounding cargo. While signal attenuation in dense material is high, long count times from voyages (often on the order of two weeks) and random pathways of air allow the transmission of even weak radiation signals through several cargo containers.

Each containerized gamma detector is held in a three-dimensional spectroscopic imaging array to maximize surface area and with corresponding coded apertures to reduce background. A three-dimensional gamma imaging system has previously been applied to high-resolution nuclear medicine and to passive imaging of radioactive sources at distances of 100 meters [Chen, 1989]. The method is both scalable in size and predictable in performance and is substantially more sensitive than conventional techniques. Using an iterative reconstruction approach, a single detector can obtain three-dimensional information without motion. The detectors are placed in such an array so that the system can distinguish between a distributed natural background and a concentrated point source. The use of a coded-aperture will reduce background, minimize false positives and improve detectability.

Each detector array is hidden by itself in an empty 40 foot, dedicated container. The non-descript nature of the containerized ship-based detection systems allows these units to operate covertly. The stealth of the containerized units will discourage attempts by adversaries to tamper with the system. Furthermore, the knowledge that a system is operational combines with the inability of the enemy to locate the detectors to achieve a degree of deterrence by denial.

One further benefit of the ship-based system is that it consists of commercial off the shelf (COTS) technology. No major technological advancements are required to reduce the system to practice. Components are made of commercially available gamma and neutron detectors; electronics developed for similar purposes; a small computer for data acquisition and processing; and transmission devices that have been available for decades. Effectively, the new approach entails only a rearrangement of available technology in a new way to address a burgeoning threat.

3.1 Advantages over Current Technology

As compared to currently envisioned and deployed technology—categorized port-based systems—the ship-based approach boasts the advantages of standoff, sensitivity and

stealth. Standoff allows for detection at sea, before the weapon ever becomes a threat to a U.S. city. The ship-based system attains enormous gains in sensitivity due to both the long count times during a two-week oceanic voyage and the nearly million-fold reduction of natural background signal interference while at sea. Stealth is achieved by shipping each detection unit inside a standard, non-descript container such that the adversary is not aware of its exact location, thereby offering the advantage of covert deployment and self-defense. The unique advantages of the ship-based system over current technology are outlined in this section.

3.1.1 Standoff

Operating under the assumption that a terrorist group or rogue nation can either weaponize fissile material or procure a functional nuclear weapon and reverse engineer any inherent safety features, it is unreasonable to assume that they would not be able to achieve remote detonation capability. Terrorists have already demonstrated such a capability, albeit on a smaller scale, in the pre-election Madrid train bombings [CBS/AP, 2004]. It is therefore likely that the terrorist, not taking a chance on detection at port, will opt to remotely detonate the weapon while taxiing through urban areas and before port-based detectors have a chance to operate. Furthermore, a terrorist group might send a contingent of suicide bombers along with the weapon in hope of ensuring its delivery. Put simply, once the weapon is in range of urban areas or other targets, the game is already over. It is therefore necessary to make a positive detection away from U.S. shores, while an effective response is still possible.

In order to further illustrate the inherent and crucial difference between a port-based detection regime and a ship-based detection regime, the concept of perimeter defense is employed. Depending on the yield of the smuggled nuclear device, a perimeter can be defined such that detonation outside its boundaries would not produce any damage to a U.S. city. The idea is, of course, that the perimeter must be defended. Placing detectors far within the perimeter (e.g. port-based scanners) still allows the possibility of catastrophic damage because the weapon could be brought just inside the perimeter and

detonated without ever reaching port-based detectors. *The city is left defenseless.* With a ship-based detector network, the weapon would never be allowed inside the perimeter and the threat is therefore mitigated.

Another perhaps more instructive way to view the perimeter defense concept is through the eyes of the terrorist. Given remote detonation capability, when assessing a target city outfitted with port-based detectors, the terrorist sees no defense against perimeter breach. Under the current port-based detector regime, the enemy is confident in success and is therefore undeterred. When evaluating targets, a delivery method that offers no chance for perimeter breach, such as one defended by the ship-based network of detectors, is clearly not attractive and the adversary will likely move on to the next target. A ship-based network of detectors covering all American cities likely removes the U.S. homeland from the target list.

A visualization of perimeter breach is perhaps useful through example. Figure 3-1 depicts the most common routes containerships take into the Port of New York/Port of New Jersey, shown in blue [CPIP, 2003].

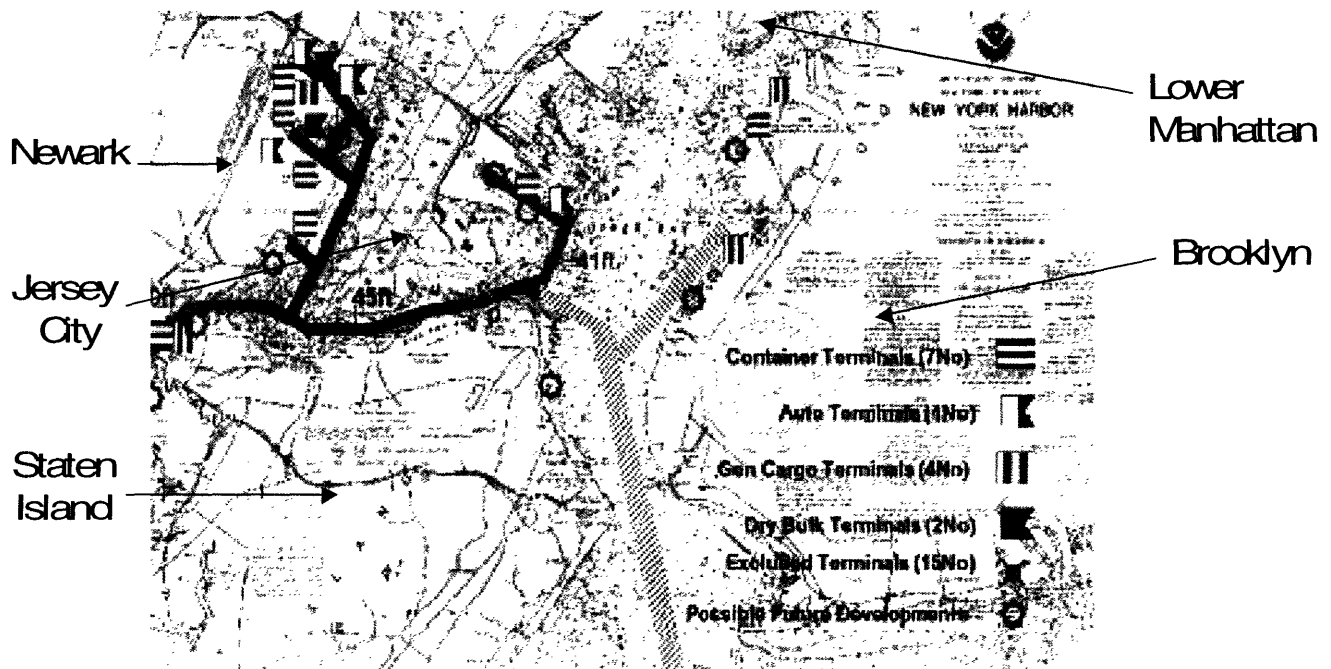


Figure 3-1: Containership taxiing passageways at Port of New York/New Jersey

Containerships without detectors aboard can easily breach the perimeter as densely populated centers such as Brooklyn, Lower Manhattan, Staten Island, Newark and Jersey City are all in range of a potential nuclear blast. A rational adversary would not take the chance of detection at port when the target is already in range and would detonate while taxiing along the blue paths shown Figure 3-1. The advantage in standoff of a ship-based system should be crystal clear at this point.

3.1.2 Sensitivity

One further improvement that the ship-based approach has over existing technology is its sensitivity. Background from natural radioactive sources, such as thorium, can interfere with the signal from the weapon. On land, the concentration of thorium is significant enough that a noticeable background is seen; but due to the extremely low concentrations of thorium in the ocean, background contributions from natural sources are virtually non-existent [Ivanovich, 1982]. Background characterization is a major part of this thesis and much more detail is given in Chapter 5. Lower background radiation from the environment increases sensitivity because the signal can more easily be distinguished. Thus, at sea, detection confidence is increased and the number of false positives is decreased.

More importantly from a sensitivity perspective, Broderick has found that the average voyage time for a U.S. bound containerships is around two weeks [Broderick, 2004]. A long voyage time affords the ship-based detection system on the order of two weeks to make a measurement instead of the approximately two minutes that common port-based solutions allow. Given a longer time for measurement, a resolvable signal can be seen through much more cargo. The extra time more than offsets the potential proximity to the weapon of port-based scanners (this will be clear once results of the simulations are presented in Chapter 7).

3.1.3 Stealth

Each detector unit and all data processing and transmission equipment will be placed in a non-descript container so that the adversary will not know the location of the detectors. There are several advantages to this necessary part of the detector network; the most important of which is a degree of both indirect and direct self-defense. Because the enemy will not know the location of the detectors, he will have no way of opening the container and tampering with the system. It is not difficult to imagine an indirect tampering scenario where a well-financed terrorist organization would manipulate a foreign port's human infrastructure such that detection units could be disabled either by tampering or by purposely dropping the container. Even worse, the crane operator could be paid to place the weapon on the ship in a location far away from detectors. This would be especially easy to accomplish if a crane operator were also paid to place all containerized detectors on one end of the ship and place the weapon at the other end. As long as no one knows which containers hold detector systems, the terrorist will have no chance to manipulate port workers.

A second advantage of covert operation is an increase in deterrence by denial because the adversary does not know which ships are covered with detector units. A terrorist will most likely look for the easiest mode of attack and if one avenue appears blocked, he will look for other options. Again assuming the viewpoint of the adversary, considering the resources likely tied up in the procurement of a nuclear weapon, it does not make sense to risk a mode of attack where the chances of success are diminished because of a deployed network of ship-based detectors. At this point it is useful to reiterate earlier statements about the problem the ship-based system solves. The ship-based solution seeks to solve the containerized nuclear terrorism problem, not the entire nuclear terrorism problem.

A third advantage of operating covertly is an inherent self-defense against direct tampering. Following traditional military strategy, if the adversary has no knowledge of a unit's location, he has no way to attack it. Similarly, if the terrorist has no knowledge of the containerized detector's location on the ship (or in the loading area) then there is little

hope of disabling it. Even though the containerized units will not be physically defended, covert operation ensures a high level of confidence that they will not be disabled; however, as a countermeasure just in case their location is discovered, the container might also be secured with an alarm system that will signal a central U.S. location that the container has been opened. This alarm condition might also be initiated if the unit suddenly stops sending data.

3.2 Physical Description

Already conceptually outlined, some more detail on the physical components of the system is provided in this section. For reference and to aid in visualization of component arrangement, a data flow chart is provided in Figure 3-2.

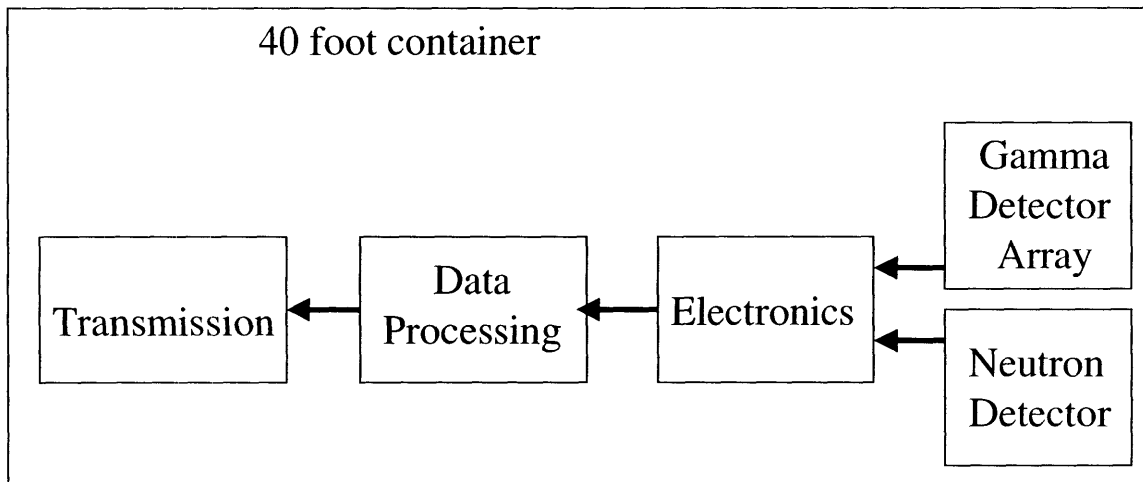


Figure 3-2: Containerized unit component diagram

3.2.1 Commercial Off-the-Shelf Technology

As currently envisioned, a ship-based detection unit consists completely of commercial-off-the-shelf technology (COTS). A reliance on COTS affords the advantage of rapid development and implementation. Because there is no requirement for development of new technology, it is likely that a prototype ship-based detection unit could be engineered

and fabricated on the order of months. Furthermore, all elements of the containerized detectors have been in extensive use in the past and are therefore robust. Some detail of each component is given below.

3.2.2 Gamma Detectors

The currently envisioned type of gamma detector is a cesium iodide crystal activated with thallium. CsI is preferred not only because of its relatively high efficiency, but most importantly, its resistance to thermal and mechanical shock [Knoll(1), 2000]. Relatively high cost is the downside to CsI, which is more expensive than commonly used sodium iodide. These cost/benefit analyses are beyond the scope of this thesis, but should be carried out by the ultimate vendor per government budgetary constraints. It is important to delineate the reason for an initial preference of CsI crystals, especially over the much more common and cheaper sodium iodide crystals.

Sodium iodide is the standard crystal for gamma detection where cooling is not possible, but NaI is not the most attractive option because of its susceptibility to both mechanical and thermal shock [Knoll(1), 2000]. It is common knowledge that while loading a ship, crane operators tend to drop containers from time to time. The mechanical shock of such an event could cause the NaI crystal to crack. Additionally, the possibility of large temperature swings might cause some degree of thermal shock. NaI manufacturers indicate that a common crystal will not withstand a change of more than 15 degrees Fahrenheit per hour [Bicron, 1992]. As an illustration to provide intuition of common temperature swings, a survey of hourly temperature data in the United States shows that temperature gradients of this magnitude actually occur around 2.5 times per year [NWS, 2003].

Table 3-1: Hourly temperature change example

Hourly Temperature Change for stations in Indiana for 1996-1998			
Station Call	Year	Change >10F	Change >15F
IND	1996	7	0
EYE	1996	7	3
IND	1997	6	0
EYE	1997	10	2
IND	1998	12	4
EYE	1998	14	6
Average		9.33	2.5

The above data is not meant to be conclusive, but rather suggestive. It shows that temperature changes of 15 degrees per hour are at least possible. As part of the cost/benefit analysis, the government might elect to insulate the cheaper sodium iodide detectors with a material of low density such as Styrofoam. Additionally, placing the crystal array on springs might alleviate some degree of mechanical shock.

It should be noted that due to the high cost of CsI detectors, it is possible that the final product will consist of some other crystal, liquid or plastic scintillator. Given the large volume of a standard 40-ft. container, there is plenty of room for large tanks of liquid scintillator or large enough blocks of plastic scintillator to ensure a high efficiency of 2615 keV gamma capture. Gas filled detectors, such as high-pressure xenon tanks, are not considered because of degraded energy resolution due to acoustic effects and because of their extremely high cost [Lasche].

It is also fairly straightforward to eliminate germanium from consideration. Despite a large increase in energy resolution over CsI, the detector requires cooling, which is not feasible in the remote containerized setting. There are also several scintillators that can be eliminated because of high cost and low availability. Lutetium orthosilicate (LSO) and yttrium aluminum phosphate (YAP) fall into the high cost/low availability category, while also having lower resolution than NaI [Knoll(1), 1997]. Finally, if cadmium

zirconium telluride (CZT) could be engineered to eliminate high energy peak “tailing”, the semiconductor may prove an interesting option that should be considered in the cost/benefit analysis, but the extremely low availability of the material with large enough surface area will likely prove prohibitive.

3.2.3 Neutron Detectors

As with gamma detector selection, the choice of neutron detector will depend on a cost/benefit analysis carried out at the engineering and commercialization stage. The recommended choice of neutron detector is either a standard ^3He or BF_3 tube commercially available through many vendors. ^3He would be chosen because of its high detection efficiency [Knoll(2), 2000], however, the rare gas is more expensive; whereas BF_3 might be chosen as a slight downgrade in efficiency but at a much cheaper price. A ^3He detector at 4 atm with a diameter of 2.5 cm has a thermal neutron detection efficiency of around 79%, while a BF_3 detector with around twice the diameter at just under half the pressure has an efficiency of 46% [Crane]. It is not necessary to choose a neutron detector with an attached moderator because neutrons will be well thermalized by the time they traverse the weapon (especially the high-explosives) and intermittent cargo. The low energy neutron spectrum reaching the detector also eliminates the possibility of using proton recoil detectors, which are more suitable for a high energy spectrum [Knoll(2) 2000]. The commonly stated disadvantage of ^3He neutron detectors is their poor energy resolution and subsequent inability to produce a spectrum. For this application, there is no need to obtain a neutron spectrum for energy discrimination so the disadvantage does not present a problem.

Stand-alone plastic and liquid scintillators are not considered for neutron detection because of their general efficiency bias towards high-energy neutrons. However, the possibility of using plastic scintillators as substitutions for CsI in an array to detect both neutrons and gammas has not been overlooked. Pulse-shaping techniques developed in the last decade have increased the possibility of employing this type of dual-use detector; however, plastic scintillators are still less efficient for thermal neutrons than ^3He tubes

and it is not necessary to image neutrons. Furthermore, the increased gamma background in a plastic scintillator from neutron interactions would decrease detection confidence in the 2615 keV gamma signal. It has therefore been determined that a separation of neutron and gamma detectors is advantageous.

3.2.4 Array Configuration

The array of scintillator crystals should maximize surface area in all three dimensions. It is not sufficient to build the common planar imaging scanners seen at ports or border crossings. The weapon could be in any direction relative to the detector and a planar array only “looks” in one dimension efficiently. Three arrangements of detectors are given in this section, but the ultimate configuration will again depend on the cost/benefit analysis made by the government and vendor. The first, and perhaps most efficient configuration would be a sphere of outward pointing detectors. However, another constraint is the desirability of a coded aperture mask, which has been developed only for flat surface reconstruction and it is not clear that the same technology would be applicable to a spherical surface. In the interest of maintaining a complete system of COTS components, the spherical arrangement is not given further consideration. Another possible arrangement is to configure the detectors in a cube, with a coded-aperture in front of each face. While probably the most practical, the cube of detectors might not prove to be the most efficient design. A more efficient design might be to arrange the detectors in a half-pyramid such as seen in the sculpture at the National Mall in Washington D.C., shown in Figure 3-3.

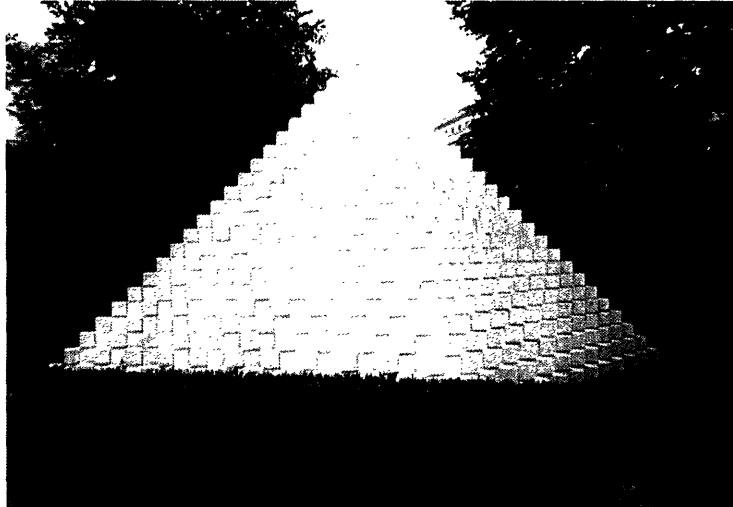


Figure 3-3: Example of a half-pyramid array configuration (photo taken July, 2004 at the National Mall, Washington D.C.)

The staggered nature of the pyramid would provide a maximum exposure of detector surface area, thus minimizing the number of detectors needed for the entire three-dimensional array. Only two of a typical pyramid's four triangular faces would be necessary as radiation could enter from the backside of each detector essentially unimpeded. The drawback of the half-pyramid is that some images would be triangular, but this will not affect detection confidence. Coded apertures would still surround the pyramid, but fewer detectors would be required. The distance between the flat face of the aperture and indented portions of the half-pyramid should not adversely affect the reconstruction process; however, a more detailed analysis of this effect will be necessary if the half-pyramid is chosen.

3.2.5 Coded-Aperture

Each face of the 3-D detector array will be outfitted with a coded aperture. The use of these coded apertures significantly reduces background through an image reconstruction process. On a basic level, the coded-aperture is essentially a partially opened mask that allows some photons through, while blocking others. The pattern of photons that are allowed to pass can be used through detailed reconstruction algorithms to reduce

background, thus enhancing point-like or relatively point-like images. Coded-aperture technology has been available for years and has been successfully applied to a wide variety of applications including medical imaging; but most importantly it has been applied specifically to searches for fissile material [Ziock, 2004].

More detail on the advantage of the coded aperture is necessary, but the value of imaging to reduce background is not completely appreciated until a background is fully characterized in Chapter 5. To better illustrate the coded-aperture process, a concept diagram has been reproduced in Figure 3-3 below from other work at MIT [Accorsi, 2001].

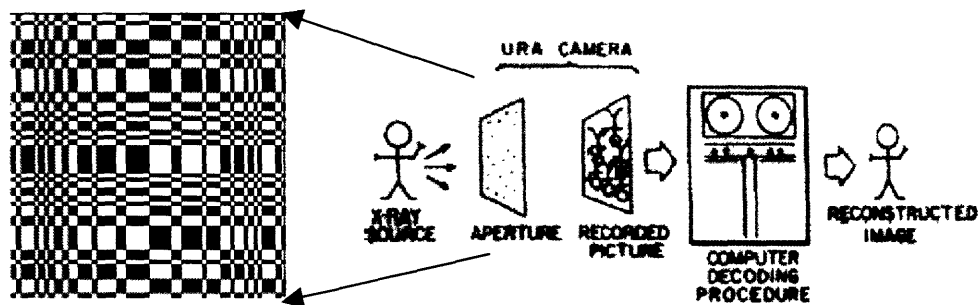


Figure 3-4: Coded aperture schematic diagram

Essentially, the source projects only one shadow on the detector array, while the distributed background projects many shadows on the array. The reconstruction process takes into account different projections and significantly reduces background, leaving mostly the source in the image. In this way, background from the ocean, ship and cargo can be reduced to increase confidence in detectability and limit false positives.

3.2.6 Electronics and Data Processing

Electronics for similar applications have been developed and are readily available [Ziock, 2004]. Problems with signal processing from multiple detectors are not underestimated, but have been solved in the past for imagers intended to search for fissile material. One problem that can be particularly difficult when dealing with a large array of many detectors is spectral and electronic drift. For this reason, periodically, the detector units will require some maintenance and calibration, which can be performed upon each arrival in the United States (see section 8.3 for more on deployment). It is not clear how often this maintenance will occur without having shipped these detectors across the ocean several times.

The computational power necessary for data processing in a ship-based system is not prohibitive. Each containerized unit will likely need less processing power than a normal personal computer. The computer will essentially take data from a multi-channel analyzer and process the information. Data processing will include not only normal background reduction algorithms, but also reconstruction of the coded aperture image. It will be directly linked to the transmission device.

3.2.7 Transmitter

A transmitter will be included with each detector unit to send data back to a centralized U.S. location for analysis and possible dissemination to responders. Transmission could occur through direct broadcast to the United States or more likely would arrive via satellite link. One option identified that would minimize the number of signals bounced off satellites is to design containerized detectors with the ability talk to each other and have at least one master unit on each ship that would broadcast the signal to the satellite. This would, however, complicate the deployment of the system because the master units would have to be distinguished and assurance made that each ship has at least one master unit. A master unit would also introduce a single-point failure mode that could severely weaken the entire system and is therefore not recommended.

Secure and clandestine transmission of data is desired so as not to give away the detector's location. The study of these techniques is outside the scope of this work, but will have to be implemented by knowledgeable officials. It suffices to state that this type of technology has been around for decades and should not be difficult to use for this application.

Concern has been raised that the containership's external communication systems would interfere with the electronics of the detector array. However, radiation detection measurements made by Kernan for this explicit purpose aboard the USNS Regulus with the radar and other communications systems in operation indicated no interference [Kernan, 2003].

3.2.8 Power

Power requirements for each detector unit will not be challenging. It has been estimated that the total power required for the detectors and electronics is on the order of 100-200 Watts. Data processing should not significantly exceed the power requirement for the electronics. There exists a great degree of variance in power requirements necessary for signal transmission depending on the type of transmitter employed. There are several options for power generation but the preferred method would be to use fuel cells, which are commercially available and relatively inexpensive. Fuel cells offer advantages over conventional generators in that they are exhaust free and relatively quiet. A containerized unit operating with a mechanical generator would emit exhaust that could be detected by the adversary. Similarly, the noise associated with conventional generators would signal the location of detector units.

3.2.9 Dissemination and Response

The final component of the ship-based network is the human element, which concerns procedure if an alarm condition is signaled. Little attention has been given to this portion

of the system because it has been deemed too early to delineate procedures for responders and it is not within the scope of this thesis to analyze response scenarios. The likely course of action in case of a positive detection would be to blockade the suspected ship and board for further inspection. One important point to note is that once the data has been processed and sent to a central location, some contingent of permanent staff should be on hand to make rational decisions about positive detections and make appropriate recommendations about the nature of the threat. For instance, if close enough to a detector, the image may show, geometrically, whether there is an assembled weapon or a fissile material smuggling attempt. Also, spectral analysis could show if the signal received indicates a large activity of some material for a dirty bomb. Some human element should be involved in the decision making process once the image has been received so that a more effective response can be implemented.

Chapter 4: Unique Radiation Signatures from Fissile Material

Nature has shaped nuclear structure such that its most powerful and destructive isotopes are not easy to detect. Finding fissile material is a difficult task not only because most gamma radiation from weapon materials is emitted at low energies and is therefore easily shielded and but also because neutron emission from highly fissile isotopes, ^{235}U and ^{239}Pu , is almost non-existent. Nature's apparent opaqueness is not without weakness; ironically, it is the methodology necessary to create materials of mass destruction that introduces a detectable signature. The enrichment process preferentially increases the concentration of the impurity ^{232}U in reprocessed weapons grade uranium and the creation of plutonium in a reactor produces significant quantities of ^{240}Pu , both of which are not found in nature, but are highly detectable.

The measured radiation signature of a nuclear weapon greatly depends on its design and the quality of material used. A gun-type weapon is in a fundamentally different geometry than an implosion-type weapon and will have different self-shielding signal attenuation [Fetter(1) 1992]. Also, depending on the size and specific design, self-shielding due to the tamper and high explosives may vary. The scope of this work has been strictly constrained from suggesting any detail of design geometry; however, some weapon model had to be adopted to ensure the accuracy of radiation transport simulations. More germane to this work is the type and quality of the fissile material used in the weapon and the radiation produced. Primary radiation and secondary interactions with both the material surrounding the fissile isotopes and the cargo are also considered in detail. Before proceeding with spectroscopic analysis, it is important to outline the setting for self-attenuation by defining the weapon geometry.

4.1 Weapon Geometry Model

It is not the intention of this work to research possible configurations of fissile material and the constituent parts of a nuclear weapon. However, it is necessary to find a balance

between detail and reality when assuming a model. Early nuclear weapon designs have been declassified by the U.S. government and are easily obtained with a brief literature search [DOE, 2001]. These declassified designs will serve as an upper-bound constraint to the level of detail assumed in this study. As such, the weapon model adopted for the analysis of radiation signatures and as input for computer simulations is exactly the same as assumed by Fetter, et al. in “Detection of Nuclear Weapons”, a pioneering work in this field [Fetter(1), 1992]. A diagram of Fetter’s model, which is intentionally described here to exact specifications to minimize ambiguity, is deliberately copied into the simulation without modification and shown in Figure 4-1. The model might prove to have some degree of accuracy as it might also be asserted, though in no way assumed, that a terrorist weapon might follow open literature design to an extent.

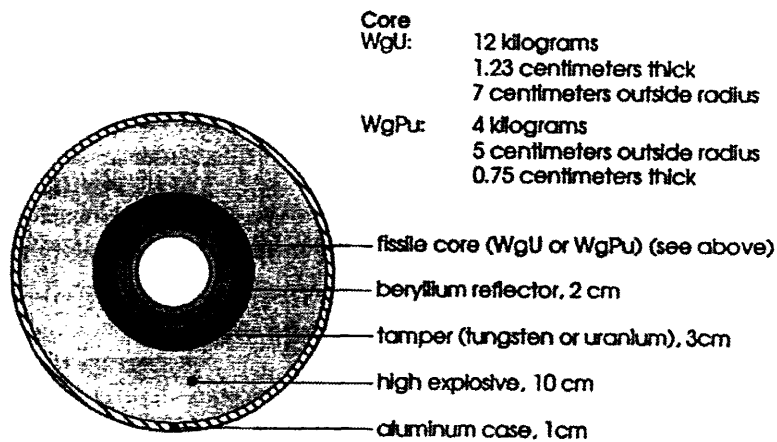


Figure 4-1: Weapon Model

4.2 Fissile Material Model

The exact amount of fissile material necessary to ensure a run-away chain reaction before subcritical separation is not openly accessible and depends in detail on the design of the

high explosives and tamper as well as the yield desired. In keeping with the Fetter model described above, the amounts of uranium and plutonium assumed for the analysis and simulation are shown in Table 4-1.

Table 4-1: Weapon geometry and materials used in simulation

12 kg Uranium Model				4 kg Plutonium Model			
Material	Radius (cm)	Density (gm/cm ³)	Mass (kg)	Material	Radius (cm)	Density (gm/cm ³)	Mass (kg)
Air	5.75	0.001	0.0	Air	5.75	0.001	0.0
Uranium	7	19.05	12.2	Plutonium	6.27	16.9	4.0
Aluminum	7.1	2.7	0.2	Aluminum	6.37	2.7	0.1
Beryllium	9	1.848	2.9	Beryllium	9	1.848	3.6
Depleted uranium	12	19.05	79.7	Depleted uranium	12	19.05	79.7
High explosives	22	1.9	71.0	High explosives	22	1.9	71.0
Aluminum	23	2.7	17.2	Aluminum	23	2.7	17.2
50 kg Uranium Model				12 kg Plutonium Model			
Material	Radius (cm)	Density (gm/cm ³)	Mass (kg)	Material	Radius (cm)	Density (gm/cm ³)	Mass (kg)
Air	5.75	0.001	0.0	Air	5.75	0.001	0.0
Uranium	9.34	19.05	49.8	Plutonium	7.11	16.9	12.0
Aluminum	9.44	2.7	0.3	Aluminum	7.21	2.7	0.2
Beryllium	11.44	1.848	5.1	Beryllium	9	1.848	2.7
Depleted uranium	14.44	19.05	120.8	Depleted uranium	12	19.05	79.7
High explosives	24.44	1.9	92.2	High explosives	22	1.9	71.0
Aluminum	25.44	2.7	21.1	Aluminum	23	2.7	17.2

The isotopic composition of the fissile material is shown in Table 4-2. Depleted uranium is assumed to originate from enrichment tails, but to have no concentration of ²³²U since there is no guarantee that a uranium tamper will be used. All other materials are modeled consistent with their natural isotopic concentrations.

Table 4-2: Isotopic composition of fissile material

Isotopic Composition of Fissile Material		
Uranium	Isotope	Weight Percent
	²³⁵ U	90.5
	²³⁸ U	8.5
	²³⁴ U	1.0
	²³² U	100 ppt
Plutonium	Isotope	Weight Percent
	²³⁹ Pu	93.5
	²⁴⁰ Pu	6.0
	²⁴¹ Pu	0.4

4.3 Detecting Uranium

4.3.1 Gamma Detection

One of the key variables that will ultimately describe the range at which a positive detection can be made is the isotopic composition of uranium in the weapon. It is generally accepted that weapons grade uranium (WgU) consists of 90% ^{235}U , just under 10% ^{238}U , and around 1% ^{234}U [Fetter(1), 1992]. There is no way to accurately predict the enrichment of uranium that a terrorist might use so a chart of enrichment vs. critical mass is provided in Figure 4-2 for reference, but it should be recognized that this curve is somewhat of an upper bound for the amount of material needed as implosion will increase the uranium density and decrease the critical mass [Bunn, 2004].

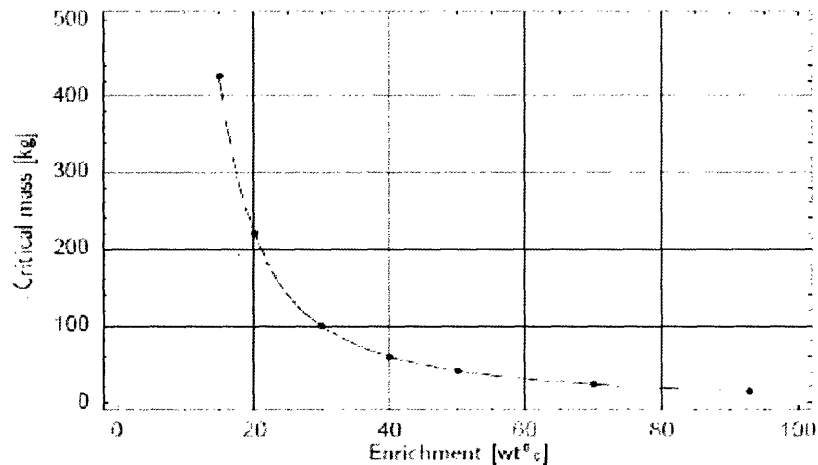


Figure 4-2: Critical mass of uranium versus enrichment of ^{235}U

It is not the enrichment of ^{235}U that provides the most important radiation for detection. Rather, it is the impurity ^{232}U —on the order of hundreds of parts per trillion in WgU—that provides the most active and energetic decay chain. Therefore, the concentration of ^{232}U is actually more important than the mass of uranium from an activity standpoint. However, WgU mass will prove important from a self-shielding perspective.

^{232}U decays through a long series of isotopes to ^{208}Tl , which emits a 2615 keV gamma. This high-energy gamma is extremely penetrating and can be detected through several containers of cargo. It is because of the energy and relative high intensity of this ^{208}Tl gamma that the thrust of the analysis going forward will focus on the concentration of ^{232}U . Experimental results indicate that the ^{232}U line is seen in spectral measurements of assembled warheads. In 1990, Fetter, et al. were allowed to make measurements of Soviet Cruise Missiles and found a high activity of ^{232}U [Fetter(2) 1990]. It remains to quantify the expected concentration of ^{232}U , but first a survey of other possible gamma signatures is provided.

4.2.2 Weapons Grade Uranium Spectrum

To provide more detail of the expected radiation signature, a measured high-resolution spectrum of 2.2 kg of WgU with 100 ppt ^{232}U is shown in Figure 4-3, from Gosnell at LLNL [Gosnell(1), 2000; Gosnell(2), 2000]. The 2615 keV line from ^{232}U is evident and is clearly the most attractive signature due to its high-energy and intensity. Other energetic gammas are also visible, including several ^{212}Bi lines between 1500 and 2000 keV, all of which will transport significantly through several containers of cargo, but are still not as intense as the ^{208}Tl line. Gamma intensities of each isotope in the ^{232}U decay chain are provided in Appendix D. While many identifiable gammas exist in the spectrum, the tendency to concentrate only on the ^{208}Tl line should not be curbed; it is difficult to imagine creating a more identifiable spectrum from a long-distance measurement standpoint.

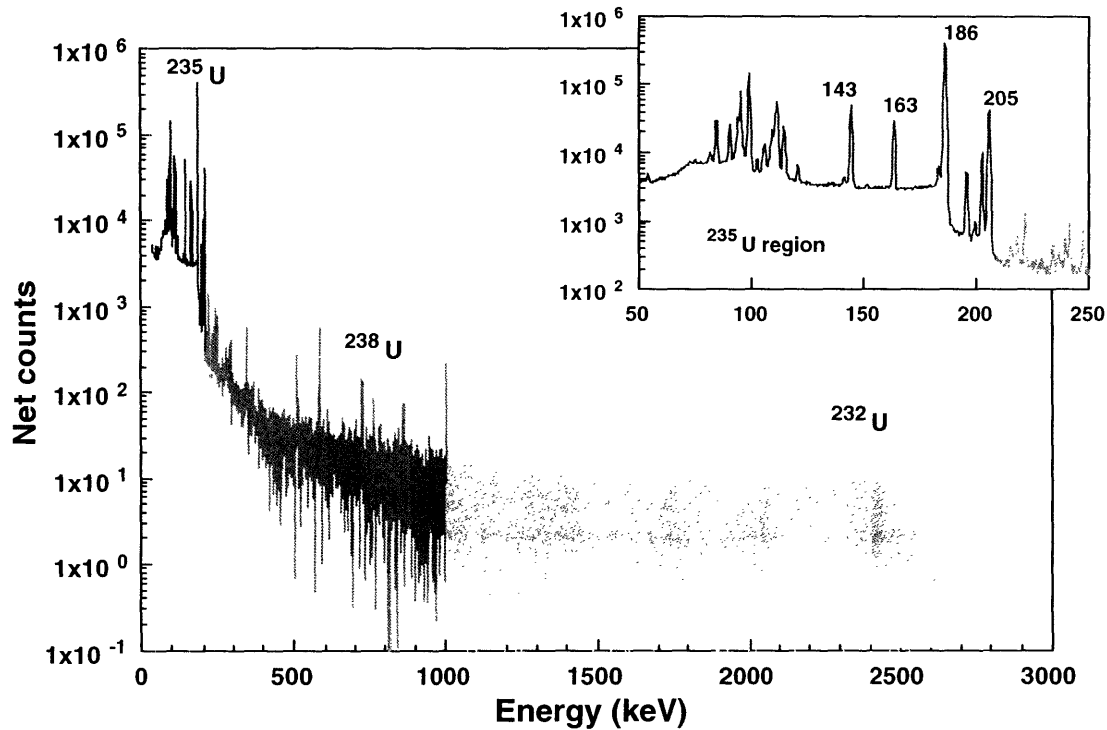


Figure 4-3: Highly enriched uranium spectrum

Away from the ^{232}U decay chain, the most interesting line comes from the 1001 keV gamma from the daughter product $^{234\text{m}}\text{Pa}$. Highly penetrating and a significant indicator of ^{238}U , close attention to this gamma is necessary because there is no guarantee that ^{232}U will be present (see section 4.3.5). Finally a brief look at the gamma spectrum of ^{235}U shows that there is nothing of high enough energy to garner interest and a more detailed study supports this conclusion.

4.3.3 ^{232}U Concentration in Weapons Grade Uranium

Clearly, the concentration of ^{232}U in fissile material is of great importance to the overall result of this study. ^{232}U does not occur in nature and is created only during irradiation in a reactor. Most of the ^{232}U concentration in WgU will have come from the enrichment of reprocessed uranium and will have been created through the following reactions [Perrung, 1998]:

$$(1) \quad {}^{235}\text{U} \xrightarrow{704\text{ My}} \alpha > {}^{231}\text{Th} \xrightarrow{25.5\text{ h}} \beta^- > {}^{231}\text{Pa} \xrightarrow{(n,\gamma)} > {}^{232}\text{Pa} \xrightarrow{31.4\text{ h}} \beta^- > {}^{232}\text{U}$$

$$(2) \quad {}^{234}\text{U} \xrightarrow{246\text{ ky}} \alpha > {}^{230}\text{Th} \xrightarrow{(n,\gamma)} > {}^{231}\text{Th} \xrightarrow{25.5\text{ h}} \beta^- > {}^{231}\text{Pa} \xrightarrow{(n,\gamma)} > {}^{232}\text{Pa} \xrightarrow{31.4\text{ h}} \beta^- > {}^{232}\text{U}$$

$$(3) \quad {}^{235}\text{U} \xrightarrow{(n,\gamma)} > {}^{236}\text{U} \xrightarrow{(n,\gamma)} > {}^{237}\text{U} \xrightarrow{6.8\text{ d}} \beta^- > {}^{237}\text{Np} \xrightarrow{(n,2n)} > \\ {}^{236m}\text{Np} \xrightarrow{22.5\text{ h}} \beta^- > {}^{236}\text{Pu} \xrightarrow{2.9\text{ y}} \alpha > {}^{232}\text{U}$$

$$(4) \quad {}^{238}\text{U} \xrightarrow{(n,2n)} > {}^{237}\text{U} \xrightarrow{6.8\text{ d}} \beta^- > {}^{237}\text{Np} \xrightarrow{(n,2n)} > {}^{236m}\text{Np} \xrightarrow{22.5\text{ h}} \beta^- > {}^{236}\text{Pu} \xrightarrow{2.9\text{ y}} \alpha > {}^{232}\text{U}$$

The United States used reprocessed uranium in its gaseous diffusion program in the 1960s and therefore much of U.S. oralloy is contaminated with ${}^{232}\text{U}$ [Gosnell(2), 2000; Rhodes, 1986]. While there is no evidence to substantiate the claim, it might be suggested that other countries would have undertaken similar methods to enrich their own fissile material. This might be especially true considering the economic advantage in separative work units (SWU) of using reprocessed uranium as opposed to natural uranium. It is important to stress that ${}^{232}\text{U}$ will not be present in significant quantities, if at all, for fissile material enriched from natural uranium feed (see section 4.3.5).

One final comment that deserves attention is the fact that a simple isotopic measurement of spent fuel is not a good approximation for the concentration of ${}^{232}\text{U}$ in weapons material. The enrichment process, almost by definition, takes advantage of the mass difference between ${}^{235}\text{U}$ and ${}^{238}\text{U}$. The same physical process that allows for streams of lighter ${}^{235}\text{U}$ to be enriched relative to ${}^{238}\text{U}$ should also preferentially enrich ${}^{232}\text{U}$ relative to ${}^{235}\text{U}$ (and ${}^{238}\text{U}$). The exact enrichment calculation is, of course, beyond the scope of this thesis. Instead, a ${}^{232}\text{U}$ concentration distribution for US oralloy is shown in Figure 4-4 [Gosnell(1), 2000].

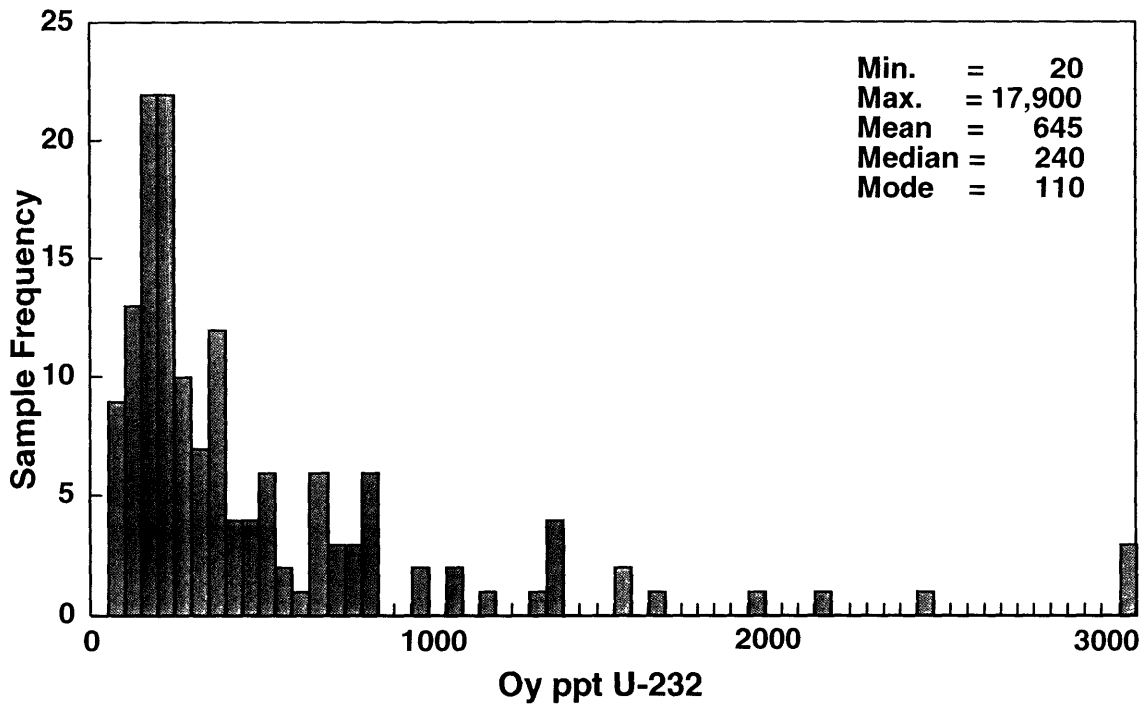


Figure 4-4: ^{232}U parts per trillion in U.S. oralloy

The fissile material model chosen for this study consisted of a baseline concentration of 100 parts per trillion ^{232}U . As can be seen from the above chart, this is a rather conservative estimate, at least for U.S. WgU. Simulation results presented in Chapter 7 will therefore be quoted at 100 parts per trillion; but can be scaled to good approximation if a non-linear term is included to account for self-attenuation.

4.3.4 Neutrons from Uranium

Neutron signatures from uranium are of little use. The spontaneous fission half-life of ^{235}U is 1.8×10^{18} years, or 1.2×10^{-26} per second, which is less than one neutron per second for the given model. The spontaneous fission half-life of ^{238}U is 1.01×10^{16} years, or 2.17×10^{-24} per second, which produces only a few neutrons per second. Also, accounting for (α, n) reactions in the material does not significantly increase the total

number of neutrons emitted from WgU [Fetter(1) 1992]. It is safe to assume, even given the long count times at sea, that passive detection of WgU with neutrons is not effective.

4.3.5 Virgin Uranium

One concern commonly expressed in the weapons detection field is that virgin uranium would be used as feed to enrich fissile material for use in the nuclear device. The problem is that ^{232}U does not occur in nature and if natural uranium were used as feed material for enrichment, there would be no ^{232}U present in the weapon. For all conceivable scenarios, it is safe to assume that ^{232}U is only present in uranium that has been irradiated in a reactor. The question as to what type of uranium would be used as feed material is left open but it can at least be stated that there are significant gains in efficiency by using previously enriched uranium, such as that from a reactor, for the feed material.

Furthermore, despite a likely superior budget, the United States clearly used reprocessed uranium as feed material for its enrichment process as evidenced by Figure 4-4. Perhaps more importantly, at least some Russian weapons material was enriched using reprocessed uranium. Measurements made by Fetter of a Soviet warhead, shown in Figure 4-5, reveal a large peak at 2615 keV and indicate the presence of ^{232}U in Russian assembled weapons [Fetter(1), 1990; Belyaev, 1990]. Given the poor security of fissile material in Russia after the fall of the Soviet Union, there is at least a chance that uranium obtained by a terrorist group would have the ^{232}U impurity.

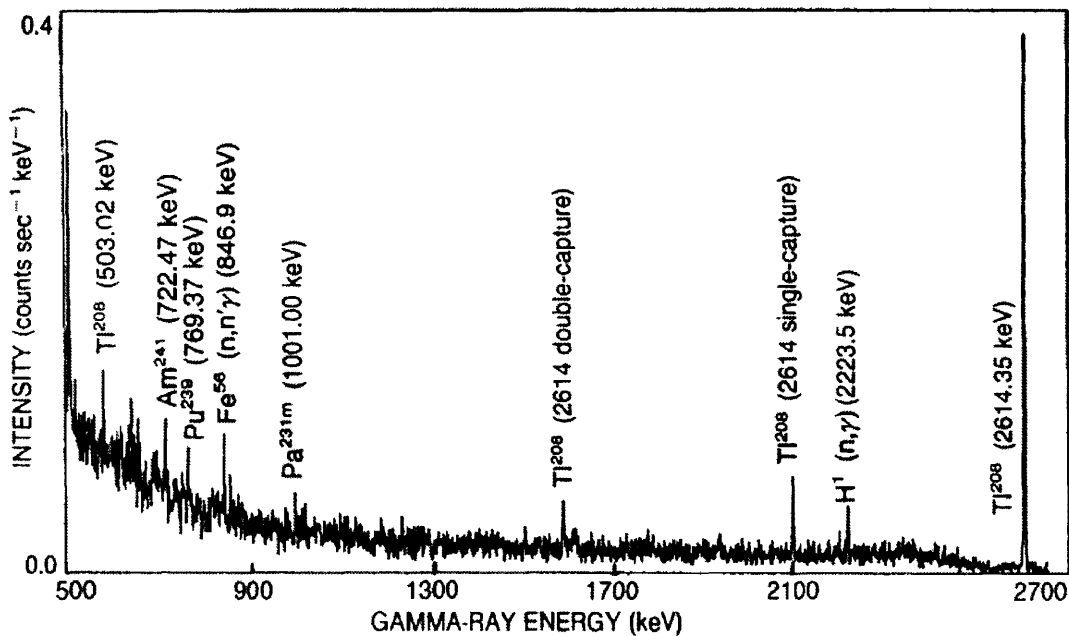


Figure 4-5: Spectrum from a Soviet warhead

4.4 Detecting Plutonium

4.4.1 Neutron Detection

Converse to the method of looking for uranium, the gamma radiation signature of plutonium is not strong. Plutonium does not, by itself or any of its daughters, give off any high-energy, high intensity gammas. The ^{239}Pu chain is almost exactly that of ^{235}U , which as seen above, is not of use. Of note, however, is the ^{241}Am daughter of ^{241}Pu , which emits a 662 keV gamma with relatively high intensity. This line will be indistinguishable from the ^{137}Cs line possibly found in benign medical isotopes within normal cargo so that by itself, the 662 keV line is not enough to assume a positive detection of weapons grade plutonium (WgPu).

Fortunately, plutonium can be detected by directly looking for neutrons or by inferring their presence from unique secondary reactions. Neutron interactions including radiative

capture and inelastic scatter will produce high-energy gammas that can be detected [Morgado, 2003]. There are virtually no sources of neutrons in common cargo and the background is therefore expected to be fairly constant and uniform. A very brief description (constrained not to include neutron interaction physics, which is easily found elsewhere [Lamarsh, 1966]) of neutron origins and subsequent interactions is given in the sections below.

4.4.1 Neutron Sources

WgPu is most likely to be detected using neutrons. The signal from spontaneous fission neutrons in WgPu is orders of magnitude stronger than that of uranium. The strength of the signal is highly dependent on the amount of ^{238}Pu and ^{240}Pu in the fissile material. The spontaneous fission half-life of ^{238}Pu is 5.0×10^{10} years and of ^{240}Pu is 1.2×10^{11} years, giving 4.39×10^{-19} and 1.83×10^{-19} per second per atom, respectively. ^{239}Pu spontaneous fission neutron intensity is of the same order as ^{238}U and therefore insignificant. When combined in the assumed weight percentages for the weapon model and accounting for (α, n) reactions, 56,000 neutrons per kilogram per second are produced [Fetter(1), 1992]. As will be discussed in section 7.7.4.3.2, significant multiplication, where spontaneous fission and (α, n) neutrons cause normal fission, can occur for larger quantities of plutonium. For 4 kilograms, the number of neutrons leaving the core surface per kilogram per second turns out to be around 110,000, which offers a huge advantage over the natural background.

4.4.2 Neutron Interactions within the Weapon

Direct measurement of neutrons is not the only way to detect the presence of plutonium. Secondary (n, γ) interactions with materials surrounding the weapon such as the tamper and explosive lenses as well as interactions with alloy stabilizing elements in the core cause a small, but high-energy flux of gammas [Morgado, 2003; Luke]. Moreover, a large percentage of the neutrons that do escape the weapon assembly will eventually interact with surrounding cargo.

An initial flux of around 110,000 neutrons per kilogram of WgPu per second can be expected from spontaneous fission and (α , n) reactions as well as multiplication within the weapon [Fetter(1) 1992]. These neutrons can interact with other materials both surrounding and inside the core causing radiative capture. Materials within the heavy metal tamper such as depleted uranium or tungsten do not give off high energy gammas; however, capture in hydrogen and nitrogen in the high explosive lenses will produce highly penetrating gammas. Alloyed materials, such as gallium, which were used to improve the properties of plutonium at Los Alamos in the 1940's, also offer high energy capture gammas [Hammel, 1998]. Gallium can be present on the order of 3% of the total core mass and ^{71}Ga emits a 2201 keV gamma when it captures a neutron [Hammel, 1998].

It is also possible to detect the presence of plutonium by looking for high-energy gammas emitted from spontaneous fission fragment decay. Slaughter, et al. at LLNL have performed a comprehensive study of this effect in terms of an active interrogation and have found that a significant number of gammas greater than 3 MeV are emitted from these fission fragments [Slaughter, 2003].

Neutrons may also undergo inelastic ($n, n' \gamma$) collisions while still slowing down in the weapon (and possibly in the cargo), which can produce high-energy gammas. While a considerably lower flux is expected without active interrogation, the number of gammas greater than 3 MeV from fission fragment decay will not be negligible, especially when contrasted with the essentially zero background at these energies.

4.4.3 Neutron Interactions within the Cargo

Neutrons that escape the weapon will interact with the surrounding cargo. Cargo could have almost any isotopic composition, but much of it is organic. This will allow for further interaction with hydrogen, oxygen and nitrogen, producing more high-energy gammas. If the weapon happens to be situated in the center of the containership, the

cargo will likely capture a significant portion of the neutron flux. Even if situated near the edge, high percentages of the total neutron flux will be captured before leaving the ship. The neutron flux will be well thermalized by the time it leaves the weapon, but there still exists the possibility of (n, n' γ) interactions in the cargo. A flux of gammas from 2-11 MeV significantly higher than background, would signal the presence of a large neutron flux and therefore fissile material.

Thus, it is important to quantify the flux of high-energy gammas from plutonium in a natural setting. Fortunately, this work has been carried out within the specific context of fissile material detection. Morgado, et al. made measurements with a 4.5 kg Pu “BRP ball” surrounded by 2 inches of moderator/absorber [Morgado, 2003]. The results of their measurement showed the existence of high-energy gammas from secondary neutron reactions with count rates at 1 meter of 100 per second from 1-2 MeV, 50 per second between 2-3 MeV, 30 per second from 3-6 MeV and 10 per second at 6+ MeV. Any measurement significantly above the background of gammas greater than 3 MeV would be cause for alarm.

Some mention of the possibility of trace amounts of ^{232}U in plutonium is necessary. Small amounts of ^{236}Pu , which decays with a 2.9-year half-life to ^{232}U , could be present in plutonium [Gosnell(2), 2000]. Also, the possibility exists that some small fraction of ^{232}U from spent fuel could still end up in WgPu after reprocessing. This possibility is identified only for completeness and will not be considered in any subsequent analysis.

It is also possible that a large flux of neutrons from a cosmic event such as a solar flare would cause a benign increase in high-energy gammas, but this would be an impulse event and could easily be distinguished from the constant flux of high energy gammas from spontaneous fission neutron capture. Moreover, a solar event would be simultaneously detected by other deployed units and various scientific endeavors throughout the world.

4.5 Detecting Fissile Material

In summary, the detection of fissile material depends on high-energy gammas and neutrons. ^{232}U impurities in reprocessed uranium provide an intense source of radiation that could indicate the presence of reprocessed WgU and the 1001 keV line from ^{238}U could indicate the presence of virgin WgU. Any significant neutron flux above background is cause for alarm and could indicate that plutonium is on board. High-energy gammas, greater than 3 MeV, also indicate the presence of plutonium. The next important step is to quantify the expected high-energy gamma and neutron background aboard a containership at sea.

Chapter 5: Background Radiation

The expected background radiation in a detector's field of view is one of the major constraints governing confident detection of any radioactive material. Given the nature of a potential interdiction of a containership at sea, extremely high confidence in positive detection is required. That is, a minimization of false positives is crucial to the practical operation of the ship-based network of detectors. It is not within the scope of this thesis to suggest possible interdiction methodologies; however, it can be assumed that if a positive detection were made, the U.S. Navy or Coast Guard would immediately stop the containership at sea and board for further inspection. False alarms causing significant disruption of commerce due to such interdictions are not acceptable; therefore, a minimization of false positives is necessary. It follows that a strong effort should be made to characterize the expected background radiation from the natural environment, from the containership and from the cargo.

The following sections will discuss a first attempt at the characterization of neutron and gamma backgrounds expected on a containership at sea. As yet, there appear to be no measurements of background radiation aboard a fully loaded containership; therefore the following assessment is constrained to theoretical calculation, in which inferences about likely background are made from known isotope activities in similar circumstances. Without actual measurement, the efficacy of the background estimate depends squarely on the transferability of radiation patterns in materials of known loading frequencies and measurements made on other ships. The limitations of theoretical background assessments should be specifically noted and the material presented here should therefore be taken only as an estimate. For this reason, reliance on measurement, where available and applicable, has been preferred over calculation.

It is worth noting that once the ship-based system is deployed, a database of typical backgrounds aboard containerships will be built by default [Lanza, 2005]. Most measurements will be benign, thereby at minimum producing a good characterization of

the background. These background spectra could be fed back into a central database for constant cross-reference and used in background subtraction algorithms. The longer the system is deployed, the more valuable the database will become.

5.1 General Background

Natural background from both cosmic and terrestrial sources is well documented and thoroughly measured. This thesis will not discuss the details of natural background unless directly applicable to detection aboard a containership; however, some mention of what the entire background spectrum might look like aboard a containership is made. To be clear, the only background of interest is what interferes with fissile material measurement. Gamma background lines of concern are only those around important energies such as 2615 keV and 1001 keV. Conversely, due to their continuous energy spectrum, neutrons of all energies will have to be considered.

^{232}U does not occur in nature and therefore poses no threat of interference; however, the natural decay chain of thorium poses a problem because its daughter products match those in a weapon as shown in Table 5-1. While natural uranium is responsible for the 1001 keV line and occurs in both the environment and weapon, its intensity is so low that the line is not usually seen in terrestrial measurements. Natural thorium emits a 2615 keV gamma, which interferes with weapon gammas from ^{232}U . While ^{232}U and ^{232}Th have different parent nuclides, their daughters past ^{228}Th are identical as seen in Table 5-1. The difference at the top of these two decay chains will prove useful and is explained in detail below in section 5.3.4.2 and Appendix A. After an extensive search, including hundreds of possible medical and industrial isotopes, it is safe to conclude that no other naturally occurring isotopes or expected cargo materials, beyond thorium and uranium, directly interfere with the 2615 keV and 1001 keV lines.

Table 5-1: Decay series comparison

Thorium Series	²³⁶Pu/²³²U Series
Th-232 (α)	
Ra-228 (α)	Pu-236 (α)
Ac-228 (β^-)	U-232 (α)
Th-228 (β^-)	Th-228 (β^-)
Ra-224 (α)	Ra-224 (α)
Rn-220 (α)	Rn-220 (α)
Po-216 (α)	Po-216 (α)
Pb-212 (β^-)	Pb-212 (β^-)
Bi-212 (β^- 0.6496) (α 0.3504)	Bi-212 (β^- 0.6496) (α 0.3504)
Po-212 (α)	Po-212 (α)
Tl-208 (β^-)	Tl-208 (β^-)
Pb-208 (stable)	Pb-208 (stable)

Some mention of the types of radioactive materials potentially in cargo is necessary. While not the focus of the ship-based system, the system will likely detect dirty bomb materials and some of the radioactive cargo might interfere with that signal. It is also necessary to look at these medical and industrial isotopes as a check to be sure that no other interfering gammas are present. As a reference for customs personnel, the IAEA provides the list in Table 5-2 of radioactive isotopes commonly shipped for medical and industrial purposes [IAEA, 2002].

The gamma energies of these isotopes show no interference and are given for reference in Appendix B. While spontaneous fission yields of ²³⁸Pu and ²⁵²Cf could potentially interfere with measurement, they are rarely transported via containership and in most circumstances do not occur in large quantities. Moreover any shipment of these neutron-producing isotopes would be on the shipping manifesto. Other common background isotopes that might have been included by the IAEA report are ⁴⁰K (1460 keV), which is common in concrete, fruits and kitty litter, ⁸⁷Rb (no gammas) and ¹³⁴Cs (604 keV). None of the isotopes in Table 5-2 interfere with important gammas from the weapon.

Table 5-2: Common medical and industrial radionuclides

Most Common Medical and Industrial Radionuclides		
Sodium-22	Yttrium-90	Barium-133
Phosphorus-32	Technetium-99	Cesium-137
Calcium-47	Technetium-99m	Promethium-147
Cobalt-58	Ruthenium-106	Iridium-192
Cobalt-60	Palladium-103	Mercury-197
Gallium-67	Indium-111	Thallium-201
Selenium-75	Iodine-123	Radon-222
Krypton-81m	Iodine-125	Radium-226
Yttrium-88	Iodine-129	Plutonium-238
Strontium-89	Iodine-131	Californium-252
Strontium-90	Xenon-133	

There are many possibilities requiring attention when characterizing the expected background, especially considering the wide range of potential cargo materials. Having briefly mentioned benign background, a thorough discussion of potentially interfering background follows, which will lead to a quantification of expected neutron and gamma background rates.

5.2 Neutron Background

Fortunately, the neutron background on sea-going vessels has been measured by several groups and is already well characterized. There are limitations to this data, as they apply to containerhips full of cargo; however, the limitations will be minimal due to the extreme rarity of naturally occurring neutron sources in cargo. For this initial assessment of neutron fluxes, published measurements will be taken as a very good approximation.

5.2.1 Neutron Sources

Neutrons from terrestrial sources are almost non-existent. The vast majority of neutron background comes from cosmic events in the atmosphere. Cosmic ray muon interactions in the upper atmosphere cause a cascade of particles, a percentage of which are neutrons

[Kudryavstev, 1999]. Cosmic neutrons can be detected directly or can interact with other nuclei in spallation events. Due to spallation, an increase in the neutron population near dense, high atomic number objects is commonly seen and several groups have measured this phenomenon.

The background neutron flux from natural sources will increase at the detector due to the “ship-effect”. The effect was studied and described in detail by O’Brien, et al. who report up to twelve times the natural flux due to spallation from cosmic neutrons interacting with the heavy metals composing the hull of the ship [O’Brien, 1978]. Due to interest in the increased flux around high atomic number materials, the ship-effect has been studied extensively. A detailed survey of ship-effect literature has produced a fairly comprehensive measurement of neutron populations on sea-going vessels. Most of these measurements were made on U.S. Navy ships and can be considered good approximations as to what might be seen on a containership. The extrapolation of an increased flux due to the addition of spallation events with iron, steel and aluminum in the cargo is not significant since the vast majority of cargo materials do not have a high enough mass number to allow more than a negligible addition of events; however, to stay conservative, some accounting for spallation in the cargo is assumed.

The complete and detailed study of neutron fluxes near various interfaces, carried out by O’Brien, et al., has been summarized in Table 5-3 [O’Brien, 1978].

Table 5-3: Expected neutron background

Neutron Background including Ship Effect			
Interface	Neutrons/(cm²*sec)	Neutrons/(m²*2 weeks)	Weighting factor
Air/Ground	0.0064	77,414,400	0.00
Air/Seawater	0.0031	37,497,600	0.10
Air/Iron	0.0770	931,392,000	0.25
Air/Aluminum	0.0210	254,016,000	0.15
Air/Air	0.0052	62,899,200	0.50
Weighted Average	0.0127	153,634,804	

Taking the interface numbers a step further to estimate the effect of the steel cargo containers and an overestimation of aluminum in cargo (to err on the conservative side), weighting factors were postulated to calculate a weighted average. The weighting factors were rather arbitrarily assigned and are only intended to be rough estimates of the neutron population throughout the complicated geometry and composition of the ship and cargo. The postulated range is between 10 million and 1 billion neutrons incident on the detector due to natural background over a two-week voyage.

Another comprehensive study aboard the USNS Regulus characterizes the ship effect [Kernan, 2003]. A key bit of information, not addressed elsewhere is the vertical variation of neutron flux within the ship. Neutrons will be quickly moderated in the seawater, lowering them below spallation energy thresholds, such that the flux of neutrons below sea level will be lowered. Because of the complex nature of ocean wave patterns and container depths on the ship, the analysis of vertical variation of neutron background within the containership is not discussed here. Rather, it is merely stated that backgrounds will follow the general trend of decreasing flux with height. For detection limit analysis, the higher top deck numbers will be assumed in the interest of conservatism. The lower background fluxes below sea level are mentioned only for completeness.

5.2.2 Neutron Background Quantification

Data from the Regulus agrees within statistical and reasonable measurement error with that of O'Brien quoted above. Other sources corroborate the O'Brien numbers as well, for instance, similar results were obtained by Sheu, et al. in their study of neutron fluxes near interfaces [Sheu, 2002]. And from an integration of MCNP modeled spectra produced by Frank, et al., a total flux of just below 10^{-3} neutrons $\text{cm}^{-2} \text{sec}^{-1}$ was calculated [Frank, 2001].

Since there are virtually no neutron sources in common cargo, the quantification of neutron background will rely on the data reproduced from O'Brien above, which is heavily corroborated. The measured fluxes form a much better estimate than calculation and a reliance on experiment produces the weighted average flux from Table 5-3, 1.54×10^8 neutrons per square meter per two weeks. This number will be adopted as the benchmark for neutron detectability calculations

5.3 Gamma Background

The characterization of gamma background is straightforward when considering contributions from the ocean and ship, but an assessment of the gamma background from cargo depends largely on the assumed constituents. A description of backgrounds due to the ship and ocean as well as a description of potential backgrounds from cargo follows.

As discussed above, natural thorium and uranium, ^{232}Th and ^{238}U , contribute the only significant gamma energies that could interfere with measurement. It follows, then, that the number of 2615 keV and 1001 keV counts seen in the background will be directly proportional to the concentration of thorium and uranium in the ocean, ship and cargo. An effective way to deal with variations of thorium and uranium laden cargo must be postulated. For the remainder of this thesis, a concept termed "potential background" will be used. This term refers to the prospective background in the cargo due to products with high thorium and uranium concentrations. The concept is necessary because of the high variability of such a limited set of thorium and uranium rich items. More directly, the statistical approach of finding an average concentration of thorium on a containership would be ineffective since the standard deviation would be much larger than the mean. Furthermore, finding the average would likely be a time prohibitive endeavor, requiring careful documentation of millions of cargo materials and their respective thorium and uranium concentrations. Therefore the potential background concept is employed and introduced as what could potentially be in the cargo that would cause an increase in gamma background.

5.3.1 Gammas from the Ocean

One constant contributor to the gamma background is that of thorium and uranium in the ocean. Thorium entering the ocean is preferentially attached to sinking particulates, which causes extremely low concentrations near the surface [Ivanovich, 1982]. Lawrence Berkeley National Laboratory estimates concentrations of thorium in seawater are on the order of 10^{-7} milligrams per liter ($4 \times 10^{-3} \text{ Bq m}^{-3}$). As compared to the expected concentration of thorium on the earth's surface of $11,000 \text{ Bq m}^{-3}$, more than a million-fold reduction in background from thorium is achieved at sea [LBL, 2005].

More quantitatively, measurements have been made of thorium concentrations in several relevant parts of the Pacific and Atlantic Oceans are reproduced in Table 5-4. The total number of 2615 keV gammas is also calculated for a vast volume of ocean surrounding the containership. As seen in the fourth column of Table 5-4, a calculation of total thorium grams in a "relevant volume" of water surrounding the ship is used to characterize the total 2615 keV flux. The relevant volume is taken to be a square mile of ocean surface area projected 10 meters deep into the water, which is likely an overestimation of source boundaries for gammas. Taking into account the surface area of the relevant volume, $5.24 \times 10^6 \text{ m}^2$, the flux/ m^2 is also tabulated.

Table 5-4: Thorium concentrations in the ocean

Thorium Concentrations in the Ocean					
Location	Concentration (gm/liter)	Concentration (gm/m ³)	Total grams in relevant volume	2615 keV gammas/sec	2615 keV Flux/m ² aboard ship
North Atlantic	6.40E-10	6.40E-07	16.58	9	1.65E-06
Caribbean	6.40E-10	6.40E-07	16.58	9	1.65E-06
North Pacific	3.30E-10	3.30E-07	8.55	4	8.50E-07
Pacific	1.60E-09	1.60E-06	41.44	22	4.12E-06

Clearly, there is no significant contribution of 2615 keV background from the ocean water, even with a large volume taken into consideration. The 2615 keV gamma is basically non-existent. A similar calculation can be made of the background contribution

of the 1001 keV line from uranium in the ocean water. It would be redundant to reproduce the calculation here, but since every part of the thorium calculation is linear with concentration, a simple scaling can be applied. Uranium is present in the ocean in concentrations approximately four orders of magnitude higher than thorium (it does not attach to sinking particulates as well) [Ivanovich, 1982; LBL, 2005]. Not even accounting for the low relative intensity of 1001 keV gammas per ^{238}U decay, a four order division of column six of Table 5-4 shows that the 1001 keV background contribution from the ocean is still negligible. The above calculation illustrates the huge advantage for detection of weapons concealed on cargo ships coming at sea as opposed to land based detection such as at ports or at border crossings.

5.3.2 Gammas from the Ship

The possibility exists that thorium and uranium might be found in various material constituents of the ship. Some construction materials and heavy metals will have small concentrations of thorium and uranium and the number of background gammas from the ship must be considered. While characterizing the neutron ship effect aboard the Regulus, gamma measurements were made with high-purity germanium detectors. The ship was parked at dock so that some 2615 keV flux is expected from the docked side of the Regulus. Hour long measurements netted 3 and 13 counts of the 2615 keV gamma (no distinguishable 1001 keV peaks were present). This translates into the fluxes shown in Table 5-5.

Table 5-5: 2615 keV gamma background from the ship

2615 keV Gamma Background from Ships	
Measured 2615 keV Counts/hour	2615 keV Flux ($\text{m}^{-2}\text{s}^{-1}$)
3	0.001
13	0.004

Making the conservative assumption that none of these gammas originated from the land or dock, the above fluxes are low and likely negligible for all practical purposes.

Some concern has been raised in various settings about the radioactivity of the containership's engine fuel. The thought is that excess uranium might be present in the large volume of engine fuel and would therefore increase the background of 1001 keV lines. Measurements made aboard the Regulus were specifically designed to address this concern. The activity of ^{226}Ra , a ^{238}U daughter, was measured and the results indicated no increased flux near the engine fuel [Kernan, 2003].

5.3.3 Gammas from the Cargo

It has been quite easy to characterize the contribution of gamma background from the ship and ocean, but contributions from the cargo are not so straightforward. As such, a considerable amount of work has been devoted to potential ways to quantify natural background in the cargo.

The most concentrated source of thorium and uranium in cargo exists in objects made of rock and in particular, granite and marble. Almost all forms of commercial granite and marble have some concentration of thorium and uranium. A few relatively rare types of granite and marble have high concentrations of thorium, especially those originating from Brazil and India, where huge deposits exist; however, most granites and marbles contain very little thorium and uranium [Tzortzis, 2003]. Other relatively rare, but non-negligible sources of thorium in cargo include ceramic tiles and kitty litter. Sources of thorium that will be considered negligible (due to both the rarity of the item and low activity) are lantern mantles, camera lenses and welding rods [Smith]. There is also little concern for other sources of uranium that have much lower activities than granite and marble such as ceramic glazes (fiesta ware), dental ceramics and polishing powders, especially considering the low emission rate of the 1001 keV gamma [IAEA, 2002].

A first step towards characterizing the potential background is to calculate thorium concentrations in various granites and marbles. Concentrations of thorium in marble and granite are approximately equal, so to minimize redundancy the calculation will be constrained to granite [Tzortzis, 2003]. This might also be considered a time prohibitive task; but fortunately, the work has already been carried out for other purposes. Tzortzis, et al. completed two studies on the specific activities of many different type of granite and their results are shown in Table 5-6 at the end of this section. Also shown is the number of interfering 2615 keV gammas per second per kilogram for each type of granite.

The average density of granite is 2.7 gm/cm^3 and the average concentration of thorium in granite is 15 parts per million [Sachs, 2003; Tzortzis, 2003]. Using these numbers, 9.0×10^{20} thorium atoms per kilogram of granite are expected, which correspond to around 14 Bq/kg. Assuming secular equilibrium and taking into consideration the number of 2615 keV gammas per decay of ^{232}Th , this concentration equates to a specific activity of around one 2615 keV gamma per kilogram per second of granite on average. One interfering gamma for each kilogram of granite is not a significant problem considering that the specific activity of 2615 keV gammas from the weapon at 100 parts per trillion ^{232}U is $54,783 \text{ kg}^{-1} \text{ sec}^{-1}$.

An imaging system measures specific activity, not just activity, and it is clear why this capability is necessary. Consider that a large slab of average granite (say, for a large commercial countertop) is on board with dimensions of 5 meters x 2 meters x 10 centimeters, which weighs on the order of 2700 kilograms and would have around 2700 2615 keV gammas. The entire slab of granite would show up on the image as a distributed background of 2700 gammas per full solid angle, spread over an imaged surface area of 10 m^2 , while the weapon would show up as an imaged point source (effective surface area of $1/100 \text{ m}^2$) with 54,783 gammas per full solid angle. Not accounting for self-shielding of the slabs, it would take twenty 2700 kg countertops of granite stacked one behind the other just to equal the number of counts from the weapon, but the specific activity would still pale in comparison, hence the value of imaging.

To quantify the effect and advantage of imaging as well as justify the low false alarm rate from granite in the cargo, an intensity factor, $R_{SpecificActivity}$, is employed. The intensity factor is a simple ratio of specific activities.

$$R_{SpecificActivity} = \frac{(A/m)_{weapon}}{(A/m)_{granite}} = \frac{SA_{weapon}}{SA_{granite}} \quad (5-1)$$

where A is the activity, m the mass, and SA the specific activity. The intensity factor is also shown in Table 5-6.

Table 5-6: Intensity factor for granite

Commerical Name	Specific Activity in Granite		Intensity Factor
	Specific Activity (Bq kg ⁻¹)	2615 gammas kg ⁻¹ sec ⁻¹	SA(Weapon)/SA(Granite)
Bianco Perla	37	2.6	20728.7
Santa Cecilia	85	6.1	9023.1
Blue Paradise	92	6.6	8336.5
Blue Pearl	77	5.5	9960.5
Verte Brazil	121	8.6	6338.5
Upatuba	21	1.5	36522.0
Verte Eukalptos	26	1.9	29498.5
Red Africa	113	8.1	6787.3
Tropical Japorana	17	1.2	45115.4
Astudo	32	2.3	23967.6
Baltic Brown	136	9.7	5639.4
Rosso Balmoral	490	35.0	1565.2
Rosso Porino	172	12.3	4459.1
Giallo Penere	82	5.9	9353.2
Nero Africa	0	0.0	N/A
Rosa Beta	69	4.9	11115.4
White Arabesco	146	10.4	5253.2
Saint Tropez	40	2.9	19174.1
Kinawa	101	7.2	7593.7
Multi-Colour	82	5.9	9353.2
Capao Bonito	190	13.6	4036.6
New Imperial	273	19.5	2809.4
Juparana	265	18.9	2894.2
Prand Paradisso	51	3.6	15038.5
Café Brown	906	64.7	846.5
Rosa Ghiandone	89	6.4	8617.6
Jacaranda	147	10.5	5217.4
Colibri	155	11.1	4948.1

Even for the worst case scenario, a slab of Café Brown (product of Brazil) with a specific activity of 906 Bq kg^{-1} , the number of counts per unit area from a weapon is still 846 times higher than that of the granite.

5.3.4 Reducing False Alarms

While unlikely given the analysis above, an alarm condition from granite or marble is conceivable and some course of action should be in place as a safety net. There are several ways of further distinguishing the difference between granite and a weapon. These include both cross-references with shipping manifestos and with other isotopic measurements.

5.3.4.1 Shipping Manifesto Cross-Reference

Per implementation of U.S. Customs Office policy, all shippers are required to report the contents of their sealed containers at least 24 hours prior to loading at the foreign port. This information could be used as a way to pre-empt false alarms by simply cross-referencing the containership's manifesto. Any major shipments of granite, while still unlikely to cause a false alarm, would be known in advance and would therefore be used to adjust expected backgrounds.

5.3.4.2 Spectroscopic Source Identification

5.3.4.2.1 The Use of ^{238}U Gammas

Another way to reduce the possibility of a false alarm condition is to reference measurements of the 1001 keV gamma from ^{238}U with the 2615 keV gamma from ^{232}Th . Uranium is commonly present in granite with a ratio of about 1:3 (U:Th), but the ratio of ^{238}U to ^{232}U is vastly higher in the weapon. In practice, it is very difficult to find a 1001 keV peak when taking environmental measurements and granite spectra produced by Tzortzis fail to distinguish the peak after lengthy measurement [Tzortzis, 2003]. The

reason for this difficulty is that the relative intensity of the 1001 keV gamma is low and accounts for just over half of a percent of total gammas from ^{238}U . Conversely, a look at the WgU spectrum shown in Figure 4-3, where ^{238}U makes up nearly 7 atom percent and ^{232}U is only 100 ppt, gives a rough ratio of 1001 keV to 2615 keV gammas at about 1:1. Clearly, the combination of a nearly 1:1 1001 keV to 2615 keV ratio would indicate a weapon and a spectrum showing only (or mostly) the 2615 keV peak would indicate only a benign slab of granite.

5.3.4.2.2 The Use of ^{228}Ac Gammas

The concept of using other gammas to confirm source origin can be extended and further strengthened by looking for the 911 keV peak from ^{228}Ac . A brief glance at the decay chain of both the ^{232}Th from natural sources and the ^{232}U from the weapon reveals some distinguishing thorium daughters (see Table 5-1).

Note that the spectra of daughters below ^{228}Th will match exactly, but there remains an important distinction between the two decay chains. The five radionuclides atop the chain offer a way to distinguish between the origins of the ^{208}Tl gammas. ^{232}Th , ^{228}Ra , ^{236}Pu and ^{232}U are not exceptionally active and emit mostly low energy gammas; however, the contribution of ^{228}Ac is significant. ^{228}Ac emits penetrating gammas with energies at 911 keV, 969 keV, 965 keV, 795 keV, and less intense but more energetic, 1631 keV and 1459 keV. These ^{228}Ac lines, especially 911 keV, are readily visible on a spectrum of granite and account for 41.2% of the activity of the entire thorium series. A more detailed quantification of the actinium procedure and suggested background reduction techniques are provided in Appendix A.

In much the same way as the 1001 keV line can be used to confirm the presence of fissile material relative to benign granite, the presence of a 911 keV line can be used to confirm benign quantities of granite relative to fissile material. Simply put, a measurement of 2615 keV gammas accompanied by 1001 keV gammas indicates the presence of fissile

material, while a measurement of 2615 keV gammas accompanied by 911 keV gammas indicates the presence of natural thorium in granites and marbles.

5.3.5 Gamma Background Quantification

After consideration of gamma contributions from the sea, ship and cargo, a quantification of potential background can now be approximated based on reasonable and conservative assumptions. The quantification of background from the sea and ship is straightforward and explicitly stated in Tables 5-4 and 5-5, but a potential background from cargo is not so easy to determine. Further complicating quantification is the above demonstrated background reduction due to imaging and source distinguishing algorithms from 1001 keV and 911 keV lines. As such, four potential backgrounds will be stated: one worst-case scenario, where no imaging capability is assumed and Café Brown granite in large quantity is aboard; two average scenarios, where an average amount of granite in the field of view is assumed both with and without imaging; and one best-case scenario, where imaging is assumed and no granite or marble is present. To stay conservative, the inclusion of spectroscopic source identification is not assumed in any scenario.

The best and worst case scenarios are unlikely, but serve to bracket background potential. The worst-case scenario assumes 1000 tons of Café Brown granite in the detector's field of view and the two average scenarios assume 5 tons of average activity granite. The average, no imaging estimate represents the expected background if just a large detector is placed in the container. The average, with imaging scenario represents a best estimate of the most likely gamma background seen by the ship-based system without any credit for source distinction algorithms using uranium and actinium lines. With imaging capabilities, the background directly in front or behind the weapon's effective surface area is considered. That is, only the projection of granite cast through the surface area of the weapon is taken into account. This entails simply dividing the average, no imaging cargo flux by the average intensity factor (11,637) from Table 5-6 above. Quantification proceeds through Table 5-7 by simple addition of contribution.

Table 5-7: Expected 2615 keV gamma background

Expected 2615 keV Gamma Background				
(all units in gammas m⁻² s⁻¹)				
Case	From the Sea	From the Ship	From the Cargo	Total
1000 tons of Café Brown	2.07E-06	2.22E-03	6.47E+07	6.47E+07
Average, no imaging	2.07E-06	2.22E-03	5.10E+04	5.10E+04
Average, with imaging	2.07E-06	2.22E-03	4.38E+00	4.38E+00
No granite aboard	2.07E-06	2.22E-03	0.00E+00	2.22E-03

Because imaging capabilities are expected to easily distinguish between the distributed granite and concentrated point source, the expected background will fall much closer to the average, with imaging scenario than to the average, no imaging scenario. Allowing no credit for spectroscopy and accounting for background for the portion of the image directly behind the weapon a conservative estimate of 2615 keV gamma background flux is around 4.38 2615 keV gammas per square meter per second. It must be restated that this number is only an estimate, but is as conservative and accurate as possible given the entirety of the above discussion. For the detectability calculations to follow, the number of 2615 keV gammas over the 2 week voyage is 5.3×10^6 per square meter.

5.4 Detectability

The motivation for the above discussion of background is to quantify detectability. Accurate characterization of background is a necessary ingredient in statistical analysis for stating positive detection confidence intervals. False positives are not only costly because they would disrupt commerce, but also because they would tend to devalue the perceived effectiveness of the ship-based approach. It is common practice in the isotope identification industry to quote a 95% confidence limit before claiming detection, but much more stringent standards are necessary for this application. An at sea interdiction of a containership resulting in a false positive is unacceptable and it is therefore necessary to absolutely minimize the number of false positives due to background interference. This minimization cannot result in 100% confidence because of inherent statistical constraints; however, the false positive rate can be pushed so far as to remain practically negligible.

A good benchmark for negligible false positive detections should be set at less than 1%. The IAEA makes similar recommendations for guards at border crossings [IAEA, 2002]. The target number adopted for this thesis will take an even more conservative approach and demand that the false positive rate not exceed 0.3% (this target corresponds to a 3σ detection, which will be explained below). The detectability limit is set such that if 1,000 nuclear devices were concealed in containerships, the system would produce only 3 false interdictions, a negligible disruption of commerce. Similarly, the system will detect all but three of 1,000 concealed weapons and the chances of finding one weapon are 99.7%.

In order to achieve the target minimization of false positives, statistical analysis has been carried out with the intent of quoting a minimum number of counts over background. This is done in the following manner. A Gaussian distribution of counts is assumed as

$$G(x) = \frac{e^{-x^2/2}}{\sqrt{2\pi}} \quad (5-2)$$

The 0.3% confidence level occurs at $x = \pm 3$ so that a 3σ standard deviation corresponds to the required number of counts above background.

Defining the variables P as the peak counts, B as the background counts, w_p as the region of interest width around the peak and w_b as a region of interest width in the background, the standard deviation of the peak with background contribution can be simplified to

$$\sigma_p \approx \sqrt{P + \left(1 + \frac{w_p}{w_b}\right) B} \quad (5-3)$$

One major radiation detection equipment manufacturer [Gedcke, 2004] derives an expression for the detection limit, P_{DL} , and concludes that

$$P_{DL} \approx (2)(3\sigma_p) = 6\sqrt{\left(1 + \frac{\eta_p}{\eta_b}\right)} B \quad (5-4)$$

The ratio $\frac{\eta_p}{\eta_b}$ is a function of the background reduction software, but a normal estimate is to set $\eta_p = \eta_b$ so that the term in parenthesis becomes 2 [Gedcke, 2004]. Using the backgrounds derived for neutrons in section 5.2.2 and gammas in section 5.3.5, the 3σ , or 99.7% confidence, detection limit can be calculated. The results are shown in Table 5-8.

Table 5-8: Three-sigma detectability limits

Detectability			
	2615 keV Gammas/(m²*sec)	2615 keV Gammas/(m²*2 weeks)	99.7% Confidence Detection Threshold
Gammas	4.38	5.30E+06	19,531
	Neutrons/(m²*sec)	Neutrons/(m²*2 weeks)	
Neutrons	0.083	1.54E+08	105,300

The detection threshold represents the minimum number of counts needed to claim a positive detection. As presented in Table 5-8, the threshold is conservative in its assumptions in that a high-A cargo for increased spallation events in the cargo was assumed and an absolutely no credit was given for spectroscopic source identification and reduction. In the presentation of simulation results (Chapter 7), these numbers will be constantly referenced and are a key component to the analysis of system capabilities.

Chapter 6: Cargo Characterization

Characterization of common cargo on the containership is one of the key components requiring detailed attention during the modeling process. It is necessary to properly and accurately describe the cargo that lies between the weapon and the containerized detection units because the attenuation and path of the radiation directly depends on the intervening material properties. More directly, the elemental composition and bulk density of various cargo will affect the gamma signal and the isotopic composition and bulk density will affect the neutron signal. It is therefore vital to the accuracy of the simulation, and indeed the results presented in this thesis, that the cargo is appropriately and accurately characterized.

The model described here was created as input for simulation with MCNP (Monte Carlo N-Particle Transport Code). In the academic community, the code is considered the gold standard of radiation transport and the Monte Carlo method of simulation is well established. Developed by Los Alamos National Laboratory for other applications, the code has evolved through several iterations, constantly improving its accuracy. Specifically, the version used in this simulation was MCNP5 and was run directly on personal computers, not on parallel processors.

6.1 Importance of Cargo Constituents and Density

Any simulation of radiation transport that does not accurately model the intervening material is essentially useless. A thorough literature search and discussion with various field experts does not yield a detailed and accurate model. All attempts encountered have adopted a single density, single material, homogenized representation of cargo. This single material model has severe drawbacks that depart greatly from reality as will be described below.

The isotopic composition of the materials between the weapon and the detectors attenuate the radiation signal exponentially. For photon transport, the exponent not only depends on the thickness of material, but also depends on both the density, ρ , and atomic number, Z ; and for neutron transport, the exponent depends on both ρ and mass number, A . For photons, the fraction of measured to source intensity at a given thickness, x , of a material is

$$\frac{I}{I_o} = e^{-(\mu x)/\rho} \quad (6-1)$$

where μ is the mass attenuation coefficient, defined in many ways, but depending on cross sections for Compton scattering, Rayleigh scattering, pair production and photoelectric effect [Turner, 1995]. The dependence on the number of electrons, Z , in these cross sections is firmly established. For neutrons, there is negligible interaction with electrons, thus the attenuation dependence on mass number A , not Z . Signal reduction is not as well defined for neutrons because of multiple scattering events and due to inaccuracies in calculation, neutron transport is generally simulated on a computer. The dependence of mass number on neutron slowing down and the vast variation in capture cross section with isotope is also well known.

Due to the non-linear nature of signal attenuation and wide variation in densities of common materials, the characterization of intervening cargo is the most important facet of the entire MCNP model; therefore, a significant portion of the time allotted for this thesis was spent characterizing and modeling common cargo.

To date, it appears that the vast majority of attempts to characterize cargo have made the approximation of condensing the entire set of possible materials into one container. This has been done either by physically placing a single material inside a container for subsequent measurement or by making some sort of average density approximation in a computer model. Most attempts have been made with the goal of describing a “typical” container with the constituents often chosen to demonstrate the particular strengths of one

method (i.e. low Z for gammas and high A for neutrons). A typical container is not sufficient for this application; rather, the model requires a statistical distribution of cargo in many containers.

One of the underlying contentions of this thesis is that these models are wholly unreasonable and vastly inaccurate due to the existence of randomly oriented pathways of air [Wagner, 2004].² That is, in reality, cargo is not evenly distributed and much of the volume between the weapon and detector is air, effectively creating random pathways for eased radiation transport. In an average density approximation, these pathways of air do not exist and aggregate transport will be significantly lower. This is why, for example, shielding is designed with an average density, often a solid block of material, not a block with drilled holes. Many of these pathways exist throughout each container; some will occur because of packing inefficiencies and some will occur because of the physical geometry of the cargo.

It is the relative nature of exponential attenuation in common material and essentially $1/r^2$ solid angle intensity loss in air that provides the difference in radiation transport of a uniform and lumped density model. Presented below is a new approach to the characterization of a large number of possible materials, which is more accurate than a simple average density approximation.

6.2 Modeling of Cargo for MCNP

Almost any industrial product or good that can fit into a container could potentially find its way between the weapon and detector. Most common applications of radiation transport have only a few possible materials to model; even human dose calculations are often limited to a few major constituents of tissue. A completely accurate model of cargo requires literally millions of material compositions and densities. It is both time prohibitive and likely impossible to perfectly characterize and model every type of

² Rich Wagner, of Los Alamos National Laboratory, first suggested this idea, termed the “pinhole effect”, through personal correspondence in 2004.

shipped good. Moreover, the computing power needed for simulations including millions of materials likely comprising billions of surfaces and cells is not at present available. Therefore, an optimization of practicality and accuracy was made.

The first, and most obvious, approximation limited the number of cargo types considered. Lumping together materials with common attributes, such as beverages or woods, immediately reduced the number of materials needed in the model. For instance, soft drinks, juices, wines, and drinking water have similar compositions and densities, so all were combined into one “beverages” material. Likewise, all woods were taken to have the same elemental composition and were combined into one material. Taking the woods a step further, however, wood density varies greatly from balsa to oak, so an average density was calculated for the model. Unfortunately, this average density approach within some materials tends down the path just argued against; however, the discrepancy in attenuation between similar materials such as various woods is not nearly as great as the discrepancy between, say, metal and air. Where applicable, similar lumping of materials occurred.

A second approximation was a geometric condensing of the materials. It is both computationally impractical and time prohibitive to model the geometry of even lumped materials. For example, all the various types of furniture could be exceedingly difficult to model. Further, MCNP runtime is proportional to the number of surfaces defined and detailed modeling of things like furniture, let alone farm machinery, is not practical.

Each material composition was carefully researched. Isotopic concentrations were generally limited to abundances greater than a tenth of a percent, but a few impurities of lower concentration were added to ensure realistic simulation.

6.2.1 Redistribution of Density

Instead of modeling detailed geometry, the materials were lumped into cubes with their densities kept constant. The cube approximation requires both explanation and

justification. Simply put, the approximation removes any air from the volume that the cargo displaces and redistributes the air in the volume surrounding the material. Continuing with the furniture example, the volume that a single-piece wooden chair takes up in each container does not have an even density distribution. Rather, there is a certain percentage of the volume that is just air with a density of around 0.001 gm/cm^3 and a certain percentage of the volume that is wood with a density of, say, 0.55 gm/cm^3 . The cube approximation simply accounts for only the wood, so that a cube of 0.55 gm/cm^3 wood is made with a reduced volume (still constant density) and the remainder of the volume is left for air. This, of course, changes the volume that the chair would take up in reality. To account for the extra volume, air surrounds the cube of wood. In a sense, all that has happened is a redistribution of density. Figure 6-1 illustrates the concept.

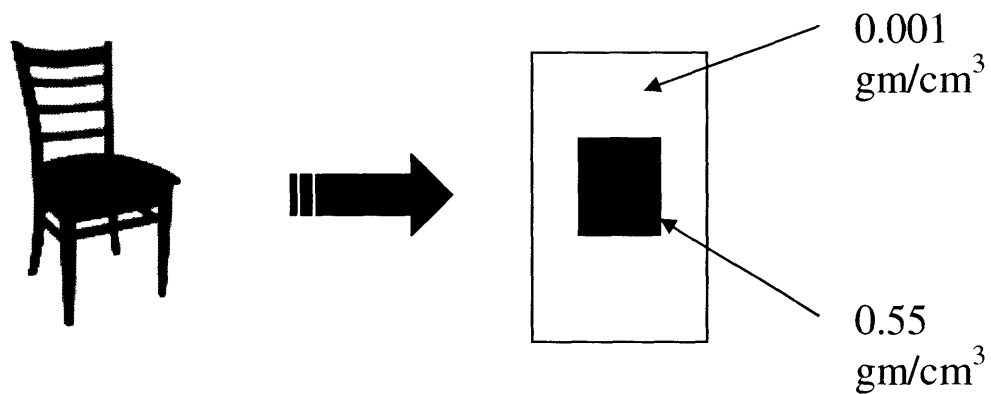


Figure 6-1: Cargo Density Redistribution

Each material was approximated in the same way. In this manner, every material was essentially made into a cube of constant density corresponding to the material surrounded by a volume of air.

The question of how much volume to choose for the wood and how much to choose for the air immediately follows. Fortunately, most seaports publish the imported tonnage of various cargo and commodities, which, when combined with known shipping volumes (generally quoted in twenty foot equivalent units, TEU), respective densities and frequencies, can be used to calculate the volume of each material.

6.2.2 Cargo Materials

As might be expected, the type and volume of materials imported varies by point of origin. It is therefore necessary to reference not just one shipment, but rather to reference at least a year of shipments to a major port so that individual fluctuations of materials are minimized. As such, the Port of New York/New Jersey was chosen because of its large number of port calls and because it receives shipments from all over the world. Cargo tonnage data categorized by material and imported by the Port of New York/New Jersey in 2002 is provided in Appendix G [Harlingen, 2002].

After lumping the material types, Table 6-1 shows the 33 materials selected for the MCNP model.

Table 6-1: Material for MCNP model

Material	Tonnage
Crude Fertilizers/Minerals	7,441,496
Organic Chemicals	3,231,415
Beverages	2,721,911
Vehicles	2,139,004

Machinery	1,377,754
Paper & Books	1,373,404
Vegetables	1,358,524
Plastics	1,350,073
Furniture	1,236,492
Iron/Steel	1,196,708
Fruits	1,061,098
Stone	1,024,583
Iron/Steel Bulk	898,939
Ceramics	875,203
Animal/Vegetable Fats/Oils	867,002
Apparel	772,932
Cocoa	723,678
Wood	720,008
Coffee	681,737
Electric Machinery	585,960
Inorganic Chemicals	569,990
Edible Preparations	529,901
Sugars	498,905
Toys	476,707
Glass	457,304
Cereals	451,862
Rubber	444,504
Fish/Meat	366,262
Dairy	348,738
Copper	309,682
Aluminum	199,502
Cereals	167,071
Others	3,202,039
Total	39,660,388

For reasons outlined above, a large portion of work was allotted such that a careful description of the density and elemental composition of each material was obtained. When lumped (as in the beverage example), a tonnage-weighted average of densities and compositions was calculated. Needing to set a tonnage cut-off at some point, the “others” entry above is the sum of all other materials imported with a weight less than the 150,000 tons annually. A composition and density approximation was employed for this miscellaneous material that consisted of an average over the above materials. As expected this miscellaneous material was mostly organic, with a small percentage of iron and aluminum.

6.2.3 Air Percent by Volume

The combination of tonnage and density is still not enough to completely model the cargo, because it would only be a guess as to what percentage of air is in each type of container. For example, “toys” might have a large portion of air (picture a plastic doll house), while fertilizer will have very little air. Also, the arrangement of packaging could increase or decrease the amount of air remaining. For instance, “fruit” might be packed in a simple cubic or a body cubic centered fashion. Moreover, the packaging of boxes inside the cargo container varies depending on the space available. See below for examples of various recommended packaging arrangements in 40-foot containers [TIS, 2005].

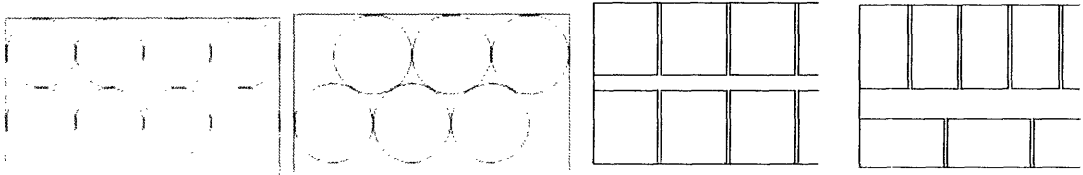


Figure 6-2: Container Packing Examples

It is clear that any guess at air volume percentage would not be consistent. Fortunately, there is a way to constrain the problem that provides an answer without any assumptions.

The average density of cargo shipped into the United States is available with a quick calculation by using the total weight of cargo shipped into the U.S. ports and the total number of TEU [Palmer, 2003]. The density calculation is shown in Table 6-2.

Table 6-2: Average density of cargo

Average Density Calculation							
Trade Origin	Tonnes/TEU	TEU Imported (yr⁻¹)	Origin weighting factor	Tonnes/TEU weighted contribution	gm/TEU	Density gm/cm³	Density weighted contribution
Africa	10.95	70000	0.0072	0.0789	10950000	0.2861	0.0021
Far East	6.04	4734000	0.4873	2.9432	6040000	0.1578	0.0769
Latin America	9.22	1299000	0.1337	1.2328	9220000	0.2409	0.0322
Mediterranean	9.21	706000	0.0727	0.6693	9210000	0.2407	0.0175
Middle East	8.5	31000	0.0032	0.0271	8500000	0.2221	0.0007
North America	9.77	23000	0.0024	0.0231	9770000	0.2553	0.0006
North Europe	8.73	1406000	0.1447	1.2634	8730000	0.2281	0.0330
Oceania	12.84	117000	0.0120	0.1546	12840000	0.3355	0.0040
South East Asia	7.06	1329000	0.1368	0.9658	7060000	0.1845	0.0252
Totals/Averages	82.32	9715000		7.3584			0.1923
Weighted Average Tonnes/TEU	7.3584						
Weighted Average (gm/cm³)	0.1923						

The average density, $\rho_{avg_container} = 0.1923 \text{ gm/cm}^3$, can now be used to derive the relative volume of air. The procedure will be to find an average material density, $\rho_{avg_material}$, specifically *not* including the contribution of air. Once calculated, the material density will be constrained by the average density, $\rho_{avg_container}$, specifically including the air, to set an equation that will give the volume of air per unit volume of material. The entire calculation is provided for each material in Table 6-3 at the end of this section.

Not yet including the contribution of air, the remaining 33 material masses, m_i , were assigned volumetric probabilities, $P(V_i)$, by dividing through by the respective material densities, ρ_i ,

$$V_i = \frac{m_i}{\rho_i} \quad (6-2)$$

such that the probability of finding material i in an average containership volume is

$$p(V_i) = \frac{\frac{m_i}{\rho_i}}{\sum_{i=1}^{33} \frac{m_i}{\rho_i}} \quad (6-3)$$

The next step involves a calculation of average material density, specifically not including the air. To calculate the average density of just the cargo materials, each volume in equation 6-3 must be weighted by its density so that a probability of finding density $p(\rho_i)$ can be found.

$$p(\rho_i) = p(V_i)\rho_i \quad (6-4)$$

The sum of these $p(\rho_i)$ then gives the average density of just the cargo materials, not including the air

$$\rho_{avg_material} = \sum_{i=1}^{33} p(\rho_i) \quad (6-5)$$

As can be seen in Table 6-3, the average density of just the cargo materials, $\rho_{avg_material}$, is 0.7931 gm/cm³. Once an average density of the 33 materials is known, the above referenced average cargo density, $\rho_{avg_container}$, of 0.1923 gm/cm³ can be used as a constraint to give the relative volume of air required per unit volume of material. With $\rho_{air} = 0.001$ gm/cm³ and using a unit volume of material, a simple algebraic expression can be set up as

$$\frac{\rho_{air} V_{air} + \rho_{avg_material} \cdot 1}{V_{air} + 1} = \rho_{avg_container} \quad (6-6)$$

and inserting the numbers for clarity

$$\frac{0.001V_{air} + 0.7932}{V_{air} + 1} = 0.1923 \quad (6-7)$$

where the left and right hand sides are both the average densities in a unit volume. The different representation on the left hand side is simply a breakdown of density weighting by volume. Solving for the volume of the air needed,

$$V_{air} = 3.1611 \quad (6-8)$$

The volume fraction of air can now be stated as

$$\frac{V_{air}}{V_{air} + 1} = 0.7596 \quad (6-9)$$

where the 1 in the denominator represents the volume of a unit cell of material. So that 75.96 percent of the volume in an average cargo container is air. It is crucial to the believability of this percentage to point out that the calculation been constrained only by the *known* numbers, $\rho_{avg_container}$, $\rho_{avg_material}$, and the reported tonnages and import volumes.

The more than three quarters fraction might be surprising at first, but when visualizing things like solid wooden chairs or plastic doll houses, the percentage is not so startling.

For example, an examination of the chair in Figure 6-1 clearly reveals that a large percentage of the volume needed for the chair in a container is air. By inspection of Figure 6-1, it appears that the volume percent of wood is significantly less than $\frac{1}{4}$. Perhaps further examples are necessary because it is non-intuitive to accept that $\frac{3}{4}$ of the volume is air. For instance, consider that a box of Christmas ornaments, commonly shipped from Southeast Asia, has very little material per unit volume. It might be instructive to picture what a box of Christmas ornaments might look like if completely flattened by a truck. Only a small volume of flat material would be left and the rest of the original volume would be air. Similarly, a trash compactor typically condenses large volumes of garbage into small cubes for disposal by simply removing all the air (which is a rather good analogy to the cube approximation outlined above). It is essential to the simulation results presented in Chapter 7 that the $\frac{3}{4}$ air volume is accepted and it might be important to reiterate that the percentage is extracted purely from known shipping data; there are no assumptions in the calculation.

With the air comprising 76 percent, the rest of the materials make up the final 24 percent. Combining the air percentage with the known probabilities of cargo an absolute list of volumetric probabilities with corresponding densities was created for simulation and is shown in the last column in Table 6-3.

6.3 Pixel Approach

Given the above assigned probabilities, it remains to model the cargo. This was done by setting up an array of cargo “pixels” between the weapon and detector. Each pixel had easily variable dimensions in the model, but for the simulation results presented in this thesis, pixels were 1.0 meters x 1.0 meters x 1.5 meters. The longer pixel dimension extends along a line between the detector and weapon (see Figure 6-3).

Table 6-3: Material volume probability calculation

Material	Mass (MT)	Density (gm/cm ³)	Volume (cm ³)	p(Volume)	p(Density)	Absolute Probability
<i>Equation Reference</i>	<i>known</i>	<i>known</i>	(6-2)	(6-3)	(6-4)	
Fertilizers	7,441,496	1.29	5,768,602	0.1154	0.1488	0.0277
Organic Chemicals	3,231,415	0.984	3,283,958	0.0657	0.0646	0.0158
Beverages	2,721,911	1.01	2,694,961	0.0539	0.0544	0.0130
Vehicles	2,139,004	7.3	293,014	0.0059	0.0428	0.0014
Machinery	1,377,754	7.8	176,635	0.0035	0.0276	0.0008
Vegetables	1,358,524	0.4	3,396,310	0.0679	0.0272	0.0163
Plastics	1,350,073	0.927	1,456,389	0.0291	0.0270	0.0070
Furniture	1,236,492	0.55	2,248,167	0.0450	0.0247	0.0108
Paper & Books	1,373,404	1.201	1,143,550	0.0229	0.0275	0.0055
Iron/Steel	1,196,708	7.8	153,424	0.0031	0.0239	0.0007
Fruits & Vegetables	1,061,098	0.641	1,655,379	0.0331	0.0212	0.0080
Stone	1,024,583	1.65	620,959	0.0124	0.0205	0.0030
Iron/Steel Bulk	898,939	2.5	359,576	0.0072	0.0180	0.0017
Ceramic	875,203	2.4	364,668	0.0073	0.0175	0.0018
Animal/Vegetable Fats/Oils	867,002	0.952	910,716	0.0182	0.0173	0.0044
Apparel	772,932	1.314	588,228	0.0118	0.0155	0.0028
Cocoa	723,678	0.593	1,220,368	0.0244	0.0145	0.0059
Wood	720,008	0.55	1,309,105	0.0262	0.0144	0.0063
Coffee	681,737	0.432	1,578,095	0.0316	0.0136	0.0076
Electric Machinery	585,960	7.8	75,123	0.0015	0.0117	0.0004
Inorganic Chemicals	569,990	2.5	227,996	0.0046	0.0114	0.0011
Edible Preparations	529,901	1.4	378,501	0.0076	0.0106	0.0018
Sugars	498,905	0.721	691,963	0.0138	0.0100	0.0033
Toys	476,707	0.9247	515,526	0.0103	0.0095	0.0025
Glass	457,304	1.55	295,035	0.0059	0.0091	0.0014
Cereals	451,862	0.79	571,977	0.0114	0.0090	0.0027
Rubber	444,504	1.522	292,053	0.0058	0.0089	0.0014
Fish	366,262	1.04	352,175	0.0070	0.0073	0.0017
Dairy	348,738	1.025	340,232	0.0068	0.0070	0.0016
Copper	309,682	8.93	34,679	0.0007	0.0062	0.0002
Aluminum	199,502	2.7	73,890	0.0015	0.0040	0.0004
Cereals	167,071	0.6	278,452	0.0056	0.0033	0.0013
Others	3,202,039	0.1923	16,651,269	0.3330	0.0640	0.0800
Total	39,660,388		50,000,976		0.7932	
Air						0.7597
<i>Equation Reference</i>					(6-5)	(6-9)

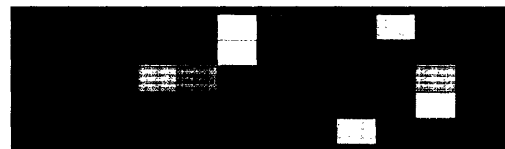
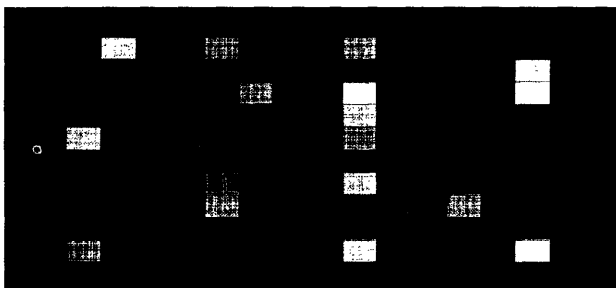


Figure 6-3: Pixel array example, top-down view (left) and side view (right)

There are a total of 700 pixels in the 3-dimensional array, 10 across the long side of the weapon container, 5 vertically stacked and 14 deep. Varying shades represent different materials. The weapon can be seen as a small circle inside its container on the top-down view.

A theoretical detector was set in each pixel to measure the flux of neutrons and photons at different distances. Each detector is essentially a ghost, not filled with any material so that a detector in one pixel would not affect results in an adjacent detector. In this way, literally hundreds of measurements could be made with one simulation. Note that, in practice, only one detector would be available, but there is no way of knowing, *a priori*, which direction the weapon will be located relative to the detector. In a sense, the problem has been turned around so that there is one weapon location and many detector locations. Of course, it is the distance between the weapon and detector that matters and the use of several detectors is only a time minimizing convenience that produces, in one simulation, an entire 3-dimensional map of the flux throughout the whole volume.

Using the probabilities in Table 6-3, each pixel was assigned a material. The pixels were filled with a material by generating a random number and matching it with corresponding probabilities. The process of generating the distribution of materials was carried out in Microsoft Excel. Using the random number function, 700 random numbers between 0 and 1 were generated and referenced to the probability of each material appearing. A series of nested IF/THEN test functions were used to assign materials.³ A typical array of materials is shown in Figure 6-4. The materials, along with corresponding densities, were then transferred directly to the cell definition cards in the MCNP input deck.

³ As the adept Excel user will note, the maximum number of nested IF/THEN functions is seven, but there are 33 materials. To circumvent this problem, random numbers not yet assigned a material were reprinted to a different worksheet and a new test was run. This included five iterations before all materials were accounted for.

Table 6-4. Example of a random array of materials, side view (see Figure 6-3, right).

Plastics	Air	Air	Miscellaneous	Beverages	Iron/Steel Bulk	Miscellaneous	Beverages	Air	Air	Miscellaneous
Coffee	Air	Air	Air	Edible Preparations	Air	Fertilizers	Air	Air	Air	Air
Plastics	Air	Air	Vegetable	Air	Iron/Steel	Vegetable	Coffee	Air	Furniture	Air
Air	Vegetable	Air	Furniture	Fruits & Vegetables	Air	Air	Vehicles	Air	Air	Air
Vegetable Fats/Oils	Vegetable Fats/Oils	Air	Miscellaneous	Vegetable Fats/Oils	Plastics	Air	Air	Air	Air	Air

6.4 Discussion of the Pixel Approach

The pixel approach is an approximation. As such, it has deficiencies; however, the pixel approach is a much better model of actual cargo than the commonly used average density approach. One way to quantify the improvement is through the concept of resolution as it applies to lumped density. Defining resolution, R , as

$$R = \frac{\text{Pixels}}{\text{Container}} \quad (6-10)$$

The resolution of the average density approach is 1, while the resolution of the pixel approach proposed here is 102. There are 102 pixels composing each container. A two order of magnitude improvement in resolution (and an invaluable increase in accuracy) is gained by using this method. An optimization between computer runtime and number of pixels was made and ultimately limited the resolution. An improved resolution would provide even more accurate results, however, the major advantage of the pixel approach is already attained with any resolution above 1 due to the lumping of densities and inclusion of air.

Another approximation made by the pixel approach is the loss of detailed geometry. Remembering that space is linear (in non-relativistic terms), there is no difference in

number of counts between a geometry where an attenuating medium is near the source or near the detector for an unscattered particle. Figure 6-4 illustrates the two cases.

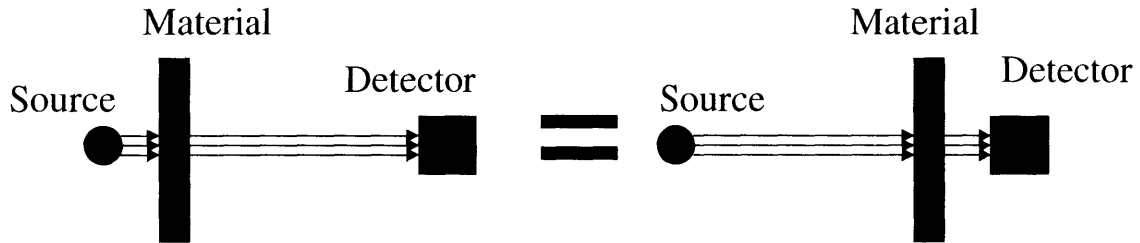


Figure 6-4: Linearity of space

The model's divergence from reality appears when scattering is considered. If part of the geometry actually extends closer to the source than the pixel approximation assumes, there is a chance of lost counts due to low-angle scattering events. An illustration of this concept is provided below in Figures 6-5 and 6-6.

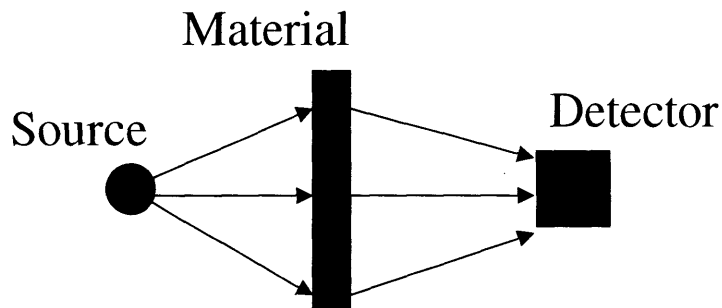


Figure 6-5: Extra low angle scattering events into the detector

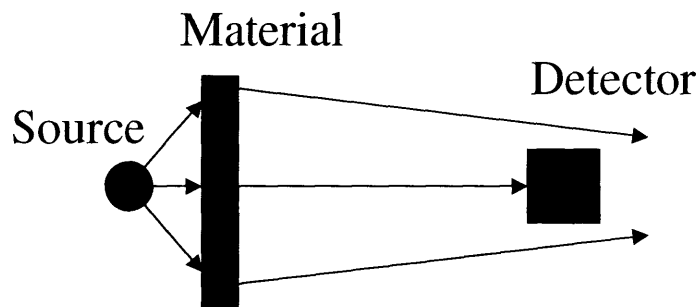


Figure 6-6: Loss of low angle scattering events due to pixelized geometry

Similarly, moving the material closer to the detector will lose some events otherwise counted.

Because of the large energies (2615 keV) and the forward biased (non-isotropic) nature of scattering cross sections involved in the process, only low angle scatter will contribute significantly to the number of counts. This contribution will be maximized for materials with densities concentrated in the center of each container as their geometry provides the largest range of low scattering angles still able to reach the detector.

The geometric effects on the pixel approximation are discussed only for completeness. In fact, the divergence of model and reality is minimal and likely negligible. This can be easily shown by studying change in energy seen in low angle Compton scattering and comparing it to the energy resolution of the detector. The change in energy due to Compton scattering is

$$E - E_0 = \frac{EE_0}{mc^2}(1 - \cos \phi) \quad (6-11)$$

where E is the incident energy, E_0 is the outgoing energy, and ϕ the angle of scatter. As ϕ exceeds a few degrees, given the geometry of the pixel array, the change in energy is larger than the resolution of the detector. The counts would fall into the Compton continuum on the measured spectrum. Thus, a negligible number of counts are lost due to the geometry effect from the pixelized approach. Moreover, counts lost due to the pixel geometry effect might be regained if the modeled pixel happens to fall in the center of a container that in reality has cargo stacked at its edges. The bottom line is that there are competing negligible gains and losses depending on the difference between the model and reality and as resolution increases, these divergences disappear.

6.5 Cargo Model Summary

The most important part of any radiation transport model is the accurate characterization of intervening materials that attenuate the signal. Because signal attenuation in air depends essentially on only solid angle and attenuation in matter depends on much higher exponents, a significant gain in radiation transport is likely with a lumped density model. Pixelizing the cargo allows for quantification of air volumes, calculated from known shipping tonnages and material densities. The inclusion of air redistributes the modeled cargo into lumped densities, which are more representative of real cargo. The new pixel approach in combination with probabilistic density distribution improves the accuracy of existing models.

Chapter 7: Results and Discussion

This chapter presents the results of MCNP simulations, which directly characterize the capabilities of the ship-based approach. To increase confidence in the results and quantify the effects of varying parameters, 38 different simulations were made based on the three pixel arrays. The simulation and subsequent data processing of all 38 input files was time intensive and despite the advantage of running more cases, a cut-off had to be set. Three different arrays were run as controls while variable parameters changed. Variables include fissile material, fissile mass, gamma energy and shielding. Also, average cargo density runs were made for each of the above variables as a comparison to other current projects adopting this model. Clearly, there is an incentive to continue the simulation for more than three different random arrays where more reasonable best and worst case scenarios might be statistically established. Only two arrays were in the original set of input decks, but third array was chosen for its concentration of dense materials in one location. The intent was to demonstrate the limitations of the system in the rare case that several containers worth of dense material are concentrated in one part of the ship. The results of all 38 simulations are presented in this chapter in graphical form.

7.1 Control and Variable Description

To set the stage for presentation of results, it is important to delineate the different input decks with the intent of describing postulated radiation source and shielding scenarios. In previous sections (4.1 and 6.2), the detailed model of the weapon and cargo was described for a standard case. It remains to outline the motivation for changing the radiation source variables.

There is no way of knowing, *a priori*, what type of weapon might be smuggled in a containership, especially given the nature of the enemy and the consequences of being caught with a stolen nuclear weapon. It is therefore crucial to plan for and be able to detect all possible scenarios. While it is safe to assume that WgU or WgPu will be in the

weapon, it is not at all clear how much will be there. The control model given by Fetter, et al., assumes a uranium content of 12.2 kg or a plutonium content of 4 kg. A study of weapon design is far out of the scope of this thesis, but one obvious thought is that a terrorist group might not be as efficient as a state and would therefore require more fissile material. Not at all suggesting any design considerations and to study the effect of an increased fissile mass, some simulations were run with 50 kg of WgU and others with 12 kg of WgPu. This was done with the intent that a thorough review would be made by qualified individuals and the MCNP model could then be rescaled such that different amounts of fissile material would be present. It is important to stress that no calculations or other considerations were made and the 50 kg and 12 kg numbers were quite arbitrarily chosen. Only a rescaling of dimensions occurred to account for the extra material. All other thicknesses were kept constant. Some perhaps surprising results exist when comparing fissile mass variations.

Another parameter varied was shielding. There are literally thousands of possible ways that the terrorist might package the weapon. To conceal the device, it is assumed that some normal packaging or cargo will also be present in the container; however, this still allows ample room for a multitude of shielding options. Simple radiation protection principles apply and the group would likely choose to use the most effective shielding possible to minimize their chances of being caught. As such, an optimal shielding, within reason, has been assumed for both photons and neutrons. In models with WgU, the shielding assumed is an encompassing sphere of lead 2 centimeters thick. For neutrons, two shields were considered, one 5-centimeter sphere of water equivalent and one 20-centimeter sphere of polyethylene. Also, as side interest and not at all practical, in one simulation the entire container was filled with Portland concrete to see what effect it had on long-term neutron transport.

A quick comment concerning the limitation of 2 centimeters of lead as an optimal configuration for the terrorist group is necessary. Clearly, one would achieve an optimal shielding by filling the entire container with lead or some other high-Z material, but this is not practical. The extra weight of adding large amounts of lead, even on the order of a

few centimeters, might cause an alarm condition at the port of origin due to the increase in expected weight and balancing offset during loading. Additionally, it is likely that in the near future, some cargo will be x-rayed at the port of origin. A large amount of lead would signal an alarm, especially when the shipping manifesto would indicate less dense material. Even if only a small number of containers were x-rayed at the port of origin the thought is that due to the risk of failure, there would be enough of a deterrent against the use of exorbitant amounts of lead.

Finally, the gamma energy for uranium models was switched between 2615 keV and 1001 keV. Of course, this was done to measure the distance of confident ^{232}U detection relative to confident ^{238}U detection. Also, the entire spectrum of ^{232}U and daughters was input to better understand the transport of all gammas (see Appendix D for energies and intensities). To save on computational time and improve the statistical reliability of the results, all simulations other than the spectral ones were run with monochromatic sources. That is, some runs were made with only 2615 keV and some with only 1001 keV gammas at later rescaled for branching and intensity.

7.2 Number of particles

The sheer number of decay gammas per second makes the simulation of two weeks worth of radiation computationally prohibitive. Rather, only several minutes of radiation can be simulated without exceeding the MCNP stride. Stride refers to the ability to generate truly random numbers and once it has been exceeded, the sequence begins to repeat and no real useful information is gained. Statistically, the stride is the limiting upside for the number of particles. Two source strengths were considered for these simulations. The number of ^{232}U decay gammas over a two minute period for the assumed model is 1.1228×10^9 for 12 kg of uranium and the number of spontaneous fission neutrons is over a 30 second period is 1.320×10^7 for the 4 kg case. A scaling of branching ratios and absolute intensities was made during data processing. Most importantly, the time was scaled up for a two-week voyage. The logic that time is, of course, linear and once statistically significant, it is not physically problematic to scale time from two minutes to two weeks.

7.3 Model Dimensions

Some dimensions for the MCNP model have been outlined in Chapters 4 and 6, but for completeness the rest are given here. The weapon sits in a regular 40-foot container. The dimensions of the container are 6.058 meters long, 2.438 meters wide and 2.591 meters high. Container walls are normally corrugated, but the model here is flat and assumed 0.27 centimeters thick. The weapon is situated in the center of its container and the distance from the center of the weapon to the end of the pixel array is 22.28 meters.

7.4 Additional MCNP Modeling Comments

This brief section is included with the intent of describing miscellaneous parts of the MCNP model for the purpose of completeness. Anywhere that open spaces exist in the model (for instance in the center of the weapon), an air fill was used. The radiation source in the fissile material was given a power law distribution, which allows for an accurate representation of average ^{232}U concentration in a hollowed sphere. Also, MCNP's built-in function for the spontaneous fission neutron spectrum in ^{240}Pu was utilized for plutonium problems. While the tamper consisted of depleted uranium, no additional 1001 keV gamma source was included in the simulation because there is no guarantee that a terrorist would utilize a depleted uranium tamper instead of tungsten or another dense material. The gamma simulations made measurements using discrete energy bins, each 10 keV wide, ranging from 0 to 3000 keV. It is probably not necessary to state, but the entire spectrum of neutrons was tallied in one energy bin.

7.5 Distance to Threshold

One of the most important numbers presented in this section is the distance to threshold. The definition of "distance to threshold" is the distance from the weapon's core at which the flux falls below the three-sigma detectability limits calculated in section 5.4. Likewise, the average distance to threshold is an average distance over all measured

fluxes in a particular case that fall below the three-sigma detectability limit. A tabulated summary of all distance to threshold cases is shown in Table 7-1 at the end of this chapter.

7.6 Energy resolution

Because simulations do not consider actual counts by a detector, there is no statistical or electronic peak broadening. The peaks produced by MCNP are therefore broadened only by bremsstrahlung and parts of the Compton continuum. There are some advantages and disadvantages to this representation. As in any model, it is impossible to precisely reproduce the physical world. In this case, the departure from the real world comes in the form of double and single escape peaks, electrical noise, pulse shaping and general engineering irregularities. The model is not without advantage as it gives an absolute number of gammas that will cross the detector's surface area at a certain energy and discounts real world inconsistencies for the purpose of physics quantification. The engineering aspects such as inefficiencies can be addressed at a later time.

Typically, the way that data processors account for peak broadening is to define an energy range in their multi-channel analyzer. Any gamma falling within that energy range is then counted and a continuous spectrum is formed by approximation and extrapolation. The total number of counts attributed to a peak is then calculated by discrete summation over a specified full-width half-max (FWHM) which corresponds, in part, to the detector's energy resolution. Fortunately, the discretization of energies is exactly what MCNP does when it creates energy "bins". If a gamma falls into a user-specified energy range, it is counted and in this way MCNP models an MCA very well. There are two opposing forces at play: one physical process (electrical noise, pulse shaping, etc.) that tends to broaden discrete gamma energies thus making them continuous and one analytical process (MCA) that discretizes the continuum. MCNP does not account for the physical broadening but does discretize the energies. Therefore, all results presented below have a defined energy range encompassing a tall, thin peak and with a very fine energy resolution. Unlike a real world detector, the model allows for a

narrow energy range to be defined and all the expected contributions from that discrete gamma energy will be counted. For example, in many of the results quoted below, a small energy range of 20 keV (two 10 keV bins) was defined around the 2615 keV peak and all gammas were counted. In the real world, a range of perhaps 100 keV or more would be necessary to account for all the gammas. Either way, both the MCNP model binning and the real world MCA binning theoretically count the same gammas; the real world simply has a wider range to count.

7.7 Simulation Results

The following section presents some of the most important conclusions of this thesis and serves to quantify the capabilities of the ship-based system. The graphs presented here consist of flux estimates based on surface tallies in MCNP. It is important to note that these numbers are fluxes, not counts. Some degree of detection efficiency and dead-time losses will have to be taken into account. Efficiency losses should account for no more than a factor of 4-6 reduction. Detectability limits are also quoted from section 5.4 in terms of flux so that a direct comparison can be made without taking into consideration any efficiency losses. The flux across all weapon-facing surfaces was measured using the MCNP tally surface-segmenting feature.

7.7.1 Spectral Simulation

It makes sense to begin the presentation of simulation results by looking at the spectral attenuation of the signal as it propagates through both the weapon and cargo. To accomplish this, the intensities of the entire litany of ^{232}U decay gammas (see Appendix D) were input and measured at various interfaces. To quantify the effects of self-shielding, measurements were made within the weapon at surfaces directly outside the core, reflector, tamper and high explosives. Surface measurements were also made at several pixel interfaces to show why, even through air, low energy gammas offer little to no value for detection of fissile material from any practical distance. The following charts

represent the entire series of spectral flux measurements and it is important to keep in mind that each peak will be broadened during detection due to counting statistics and interactions within the crystal. The first plot presented, Figure 7-1, is the spectrum of radiation coming out of the weapon core.

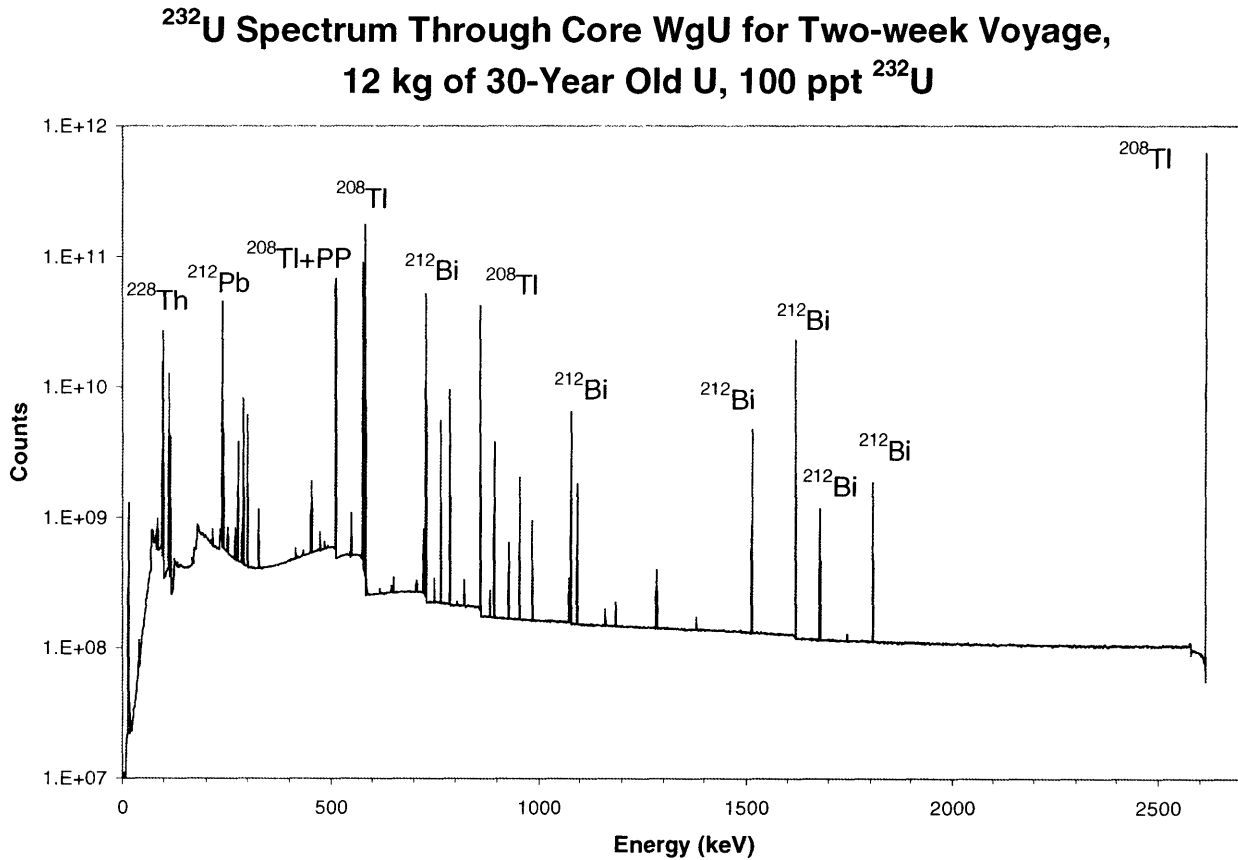


Figure 7-1: ^{232}U spectrum through core

The key interest is to search for peaks with high energy, which will have better transport and lower background. Several major peaks have been identified, but the large difference in counts and background of the 2615 keV peak is obvious and clearly the most attractive for detecting uranium. The ^{212}Bi peaks are of interest because of their high energy and low background; however, they are all orders of magnitude less intense than the 2615 keV peak.

Moving outward through the weapon, Figure 7-2 shows the spectrum through the reflector.

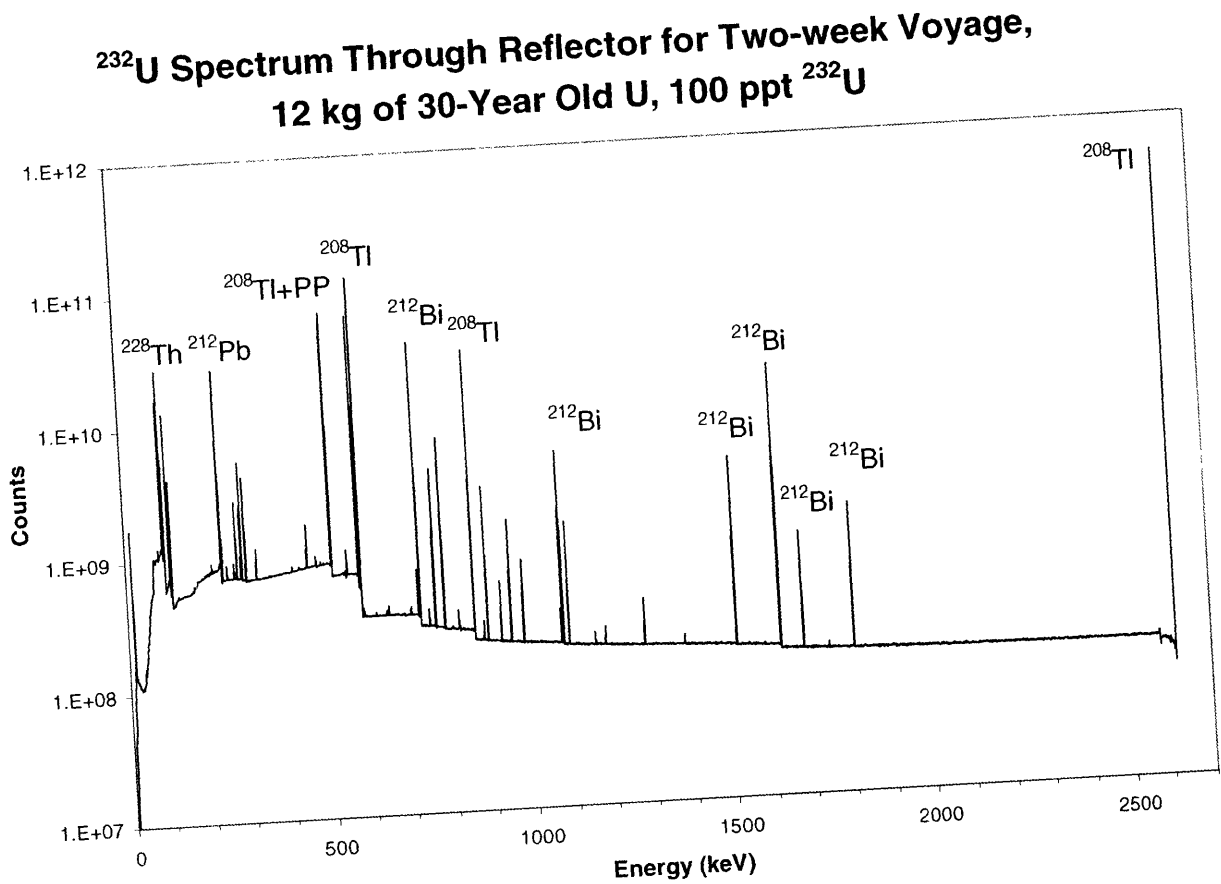


Figure 7-2: ^{232}U spectrum through reflector

Not much difference is seen as the radiation travels through the relatively thin reflector, but a slight attenuation is occurring at low energies. For the most part, photons leaving the core also travel through the reflector. Figure 7-3 shows the spectrum through the depleted uranium tamper. Recall that the depleted uranium was not considered another source and no contribution to the spectrum was simulated for the tamper.

**^{232}U Spectrum Through Tamper for Two-week Voyage,
12 kg of 30-Year Old U, 100 ppt ^{232}U**

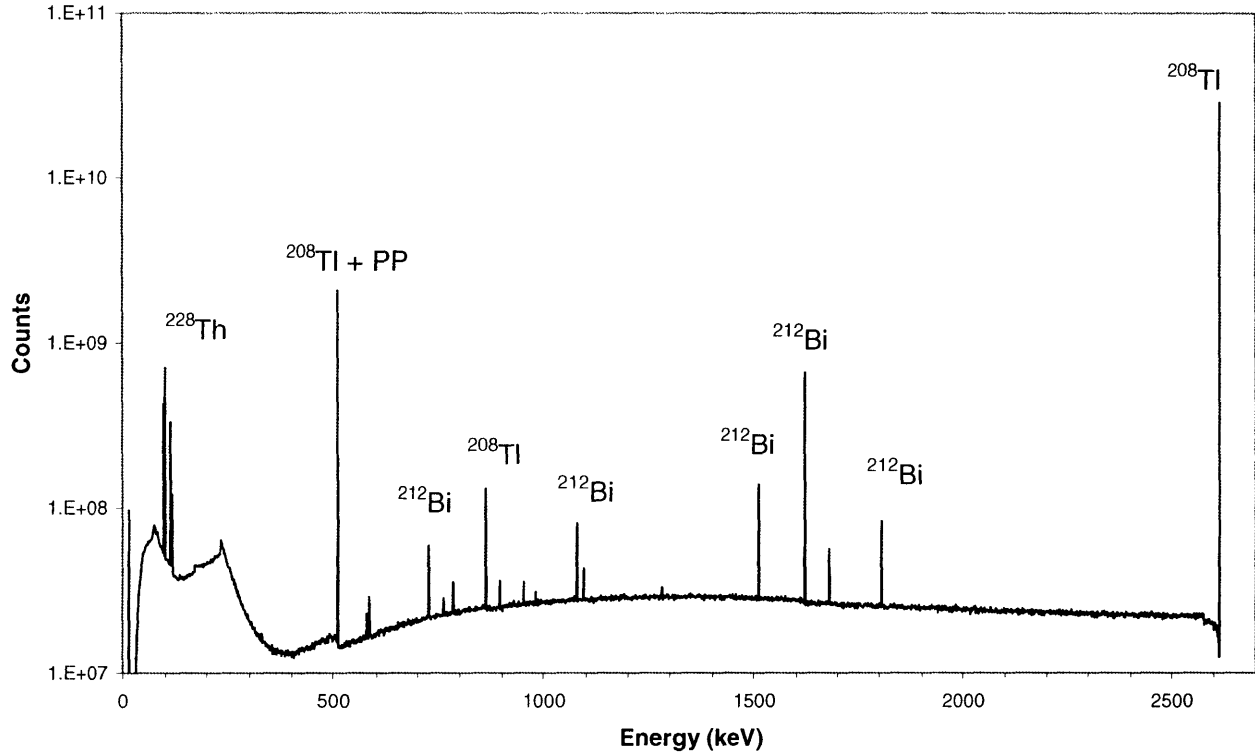


Figure 7-3: ^{232}U spectrum through tamper

A significant attenuation of low energy gammas occurred through the dense, high-Z tamper. The higher energy bismuth and thallium gammas still transport well, although more than an order of magnitude drop in each peak occurred. The next measurement was made at the edge of the high explosives, which essentially gives the spectrum of gammas from ^{232}U leaving the weapon and is shown in Figure 7-4.

^{232}U Spectrum Through High Explosives for Two-week Voyage, 12 kg of 30-Year Old U, 100 ppt ^{232}U

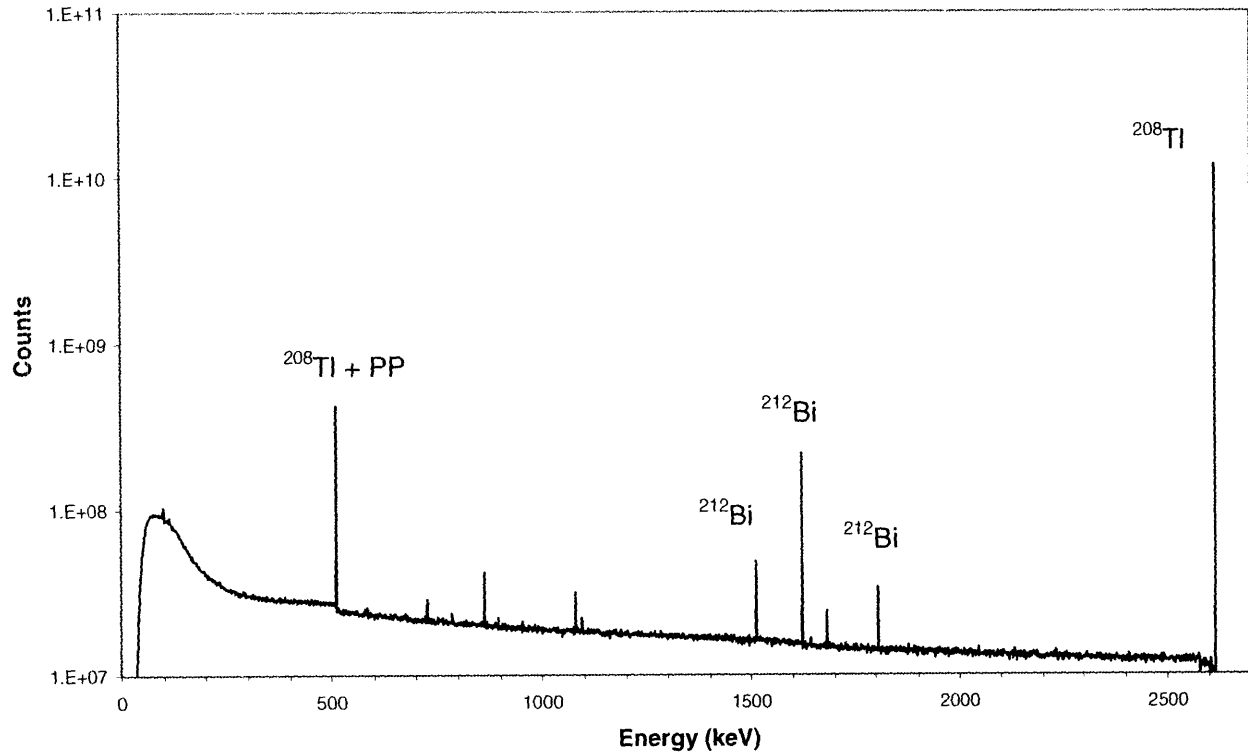


Figure 7-4: ^{232}U spectrum through high explosives

More attenuation occurred through the thick high explosives as several peaks have begun to vanish. The bremsstrahlung continuum can now be plainly seen superimposed over the Compton continuum in the low energy regime. Only four major peaks of interest still exist—three bismuth and one thallium—once the radiation has left the weapon and self-shielding has occurred. The next series of charts tracks the attenuation of radiation after it has left the weapon and once it is traveling through the cargo. No pixilated cargo is present; instead, a uniform density has been used so that the attenuation of lower energy gammas can be plainly seen.

Figures 7-5 through 7-8 show the evolution of the spectrum as it travels through the *uniform density* cargo. Uniform density was chosen for the spectral simulation to eliminate ambiguity as is meant only to show relative attenuation, not represent real cargo. Distances measured at the surface of each pixel are given in the chart title (the uneven distances are due to the width of the cargo container).

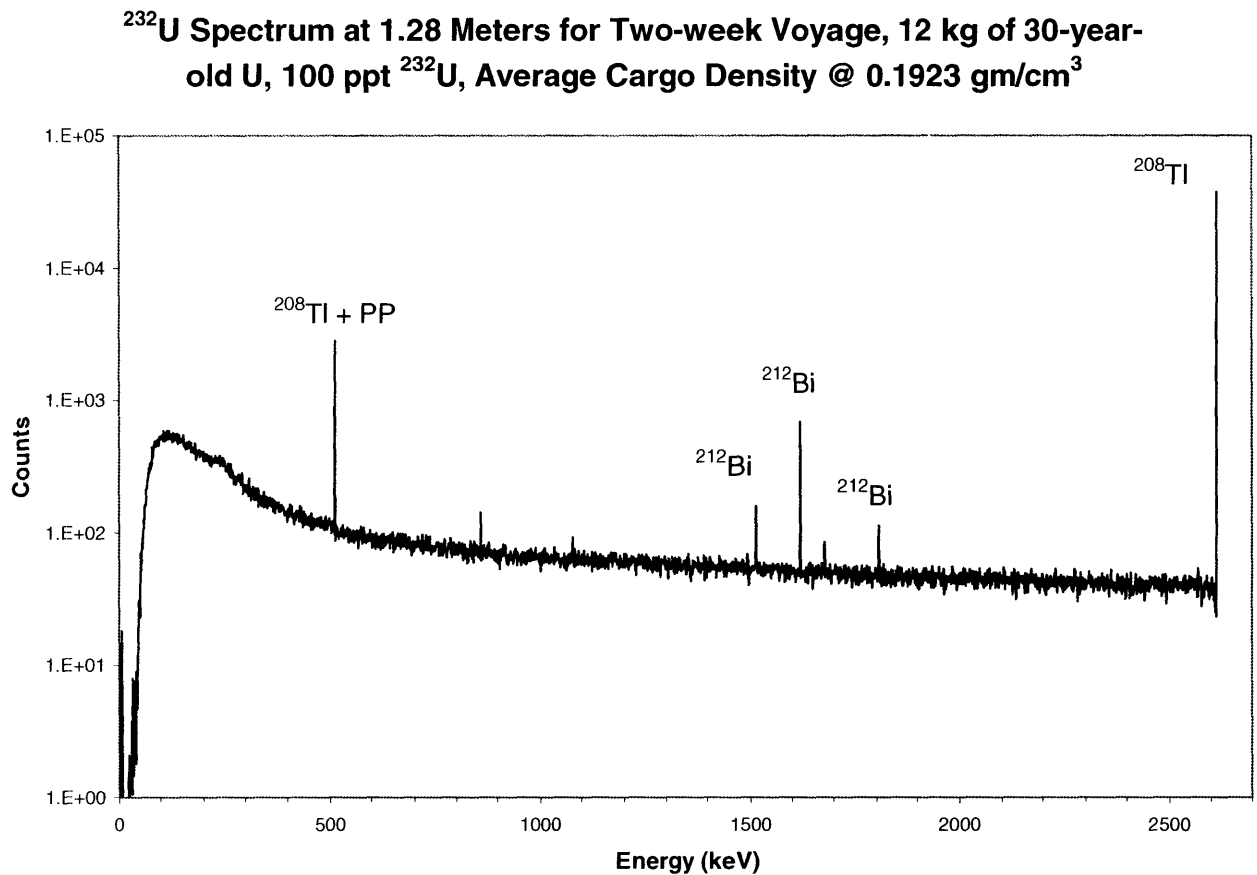


Figure 7-5: ^{232}U spectrum at 1.28 meters

^{232}U Spectrum at 2.78 Meters for Two-week Voyage, 12 kg of 30-year-old U, 100 ppt ^{232}U , Average Cargo Density @ 0.1923 gm/cm³

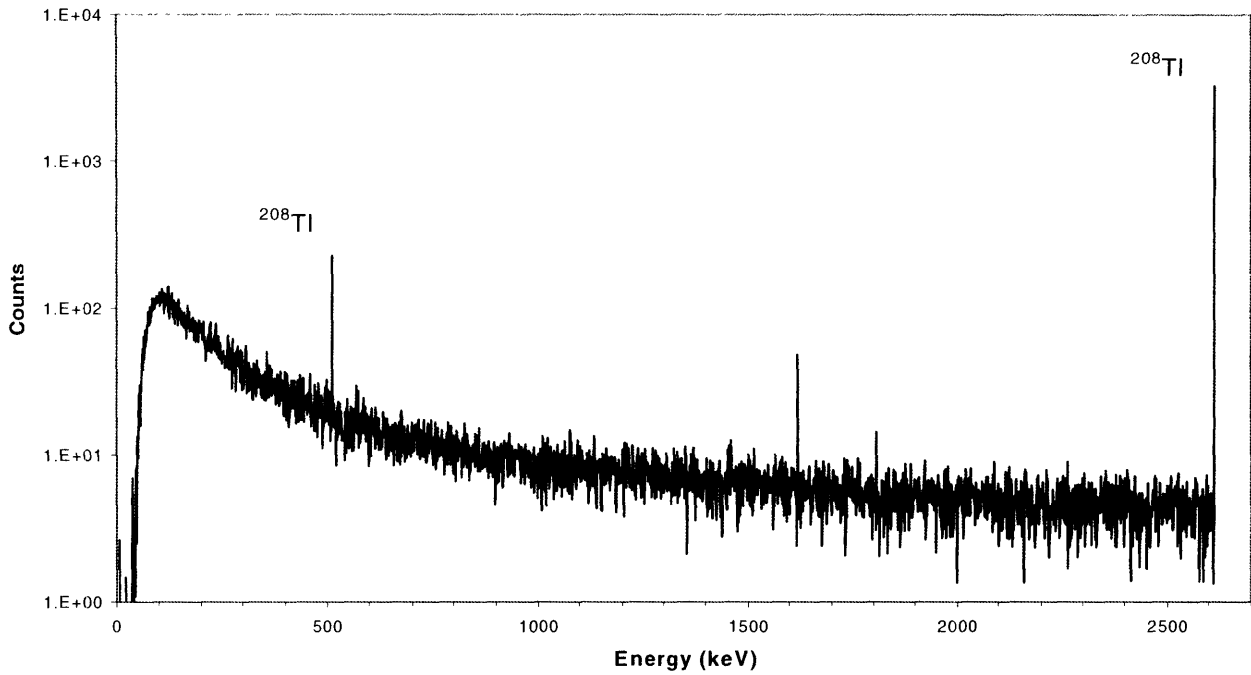


Figure 7-6: ^{232}U spectrum at 2.78 meters

^{232}U Spectrum at 4.28 Meters for Two-week Voyage, 12 kg of 30-Year Old U, 100 ppt ^{232}U , Average Cargo Density @ 0.1923 gm/cm³

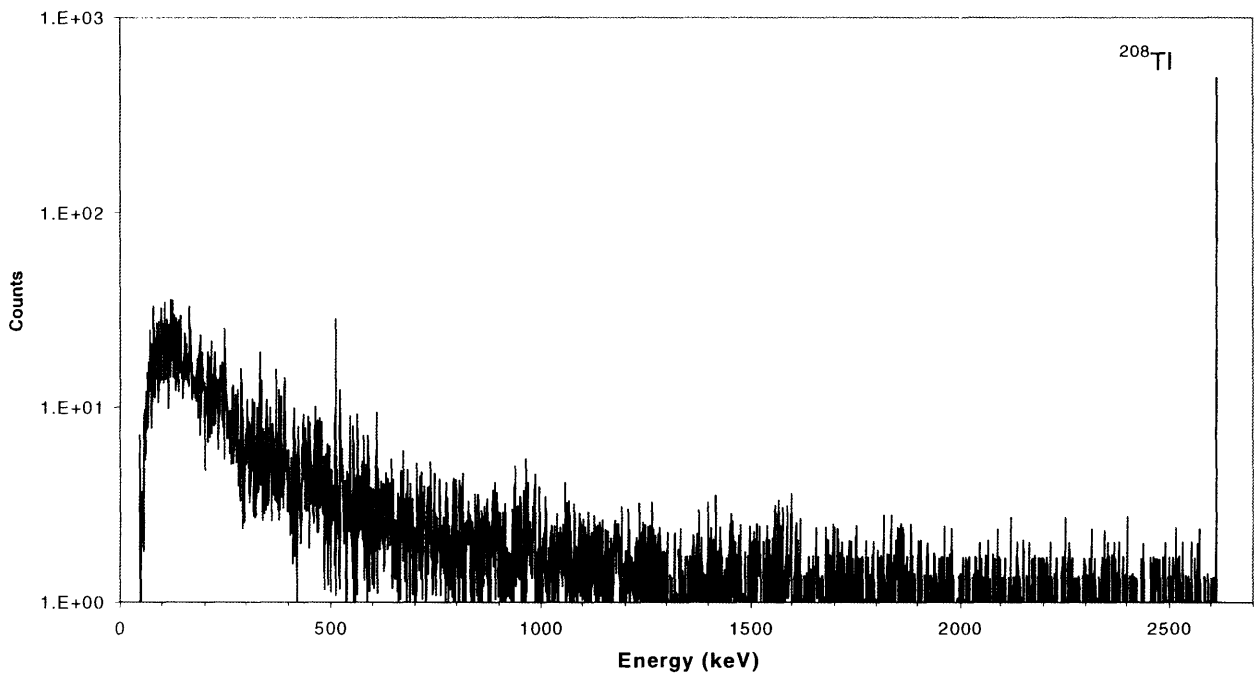


Figure 7-7: ^{232}U spectrum at 4.28 meters

After around four meters of *uniform density* cargo, all except the 2615 keV peak have fallen into the background. The ^{208}Tl signal still remains on the order of 1,000 particles above the background continuum.

7.7.2 Signal Attenuation in Air

In this section, simulation results are presented that measure the amount of attenuation in air. The inclusion of these elementary results might at first seem superfluous, but the intent is to build a visual contrast between the model of radiation transport in air, the model of radiation transport in a uniform density (presented in 7.7.3) and the model of radiation transport in the pixel model which will fall between air and uniform density. As will be a common theme throughout this chapter, there are four cases presented here, one with 12.2 kg of WgU, one with 50 kg of WgU, one with 4 kg of WgPu and 12 kg of WgPu.

The 3-dimensional surface plot will be used to present many of the subsequent results. Each point is defined by the flux measured on the weapon-facing side of each pixel. Three dimensions are required to present two-dimensional variations, so that presenting the flux over the three-dimensional MCNP model would demand an inaccessible fourth dimension. To circumvent this problem, the vertical direction has been suppressed by averaging fluxes from all five pixels stacked on top of each other into one flux. The following surface plots then represent both the east-west and north-south directional variations but an average over all the up-down variations. This manner of presentation actually improves the accuracy of the results because it takes into account all five up-down pixels in one plot, thereby reducing the variance. In a simpler way, it may be useful to just think of an array of pixels in just the east-west and north-south directions and what is plotted in Figure 7-8 is the variation of flux through a 2-dimensional pixel array.

The variation of gamma signal in air as it propagates through the pixel array is plotted in the following figures and represents the best-case scenario for radiation transport. Figures

7-8 through 7-11 can be thought of as a ceiling for the maximum fluxes possible after self-shielding by the weapon, but with no cargo present.

**2615 keV Flux per m² for a 2 Week Voyage, 12 kg of 30-year old U,
100 ppt ²³²U, in Air**

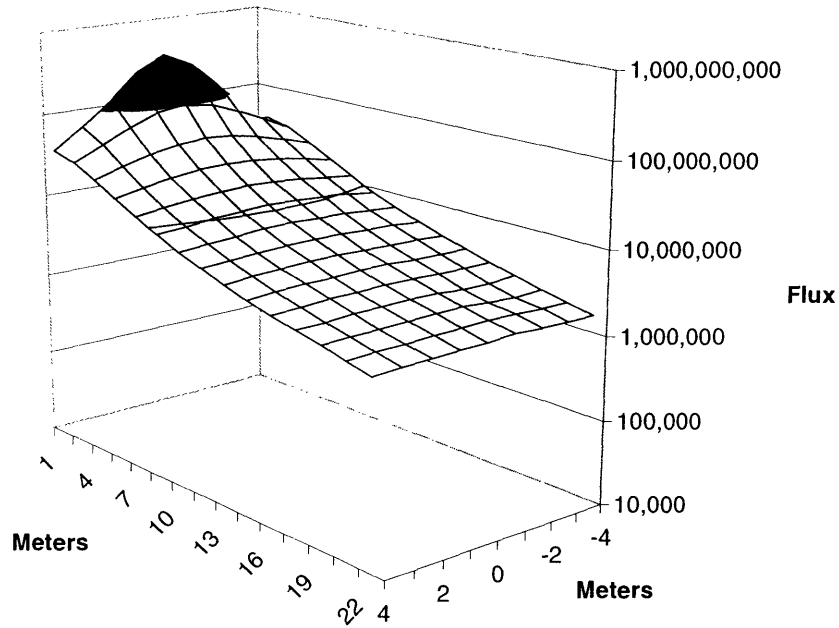


Figure 7-8: 2615 keV flux 12 kilograms of uranium in air

As expected, the essentially $1/r^2$ attenuation of signal due to solid angle is seen and very little, if any, attenuation occurs due to Compton scattering or pair production. Figure 7-9 shows the case with 50 kg of uranium.

**2615 keV Flux per m² for a 2 Week Voyage, 50 kg of 30-year old U,
100 ppt ²³²U, in Air**

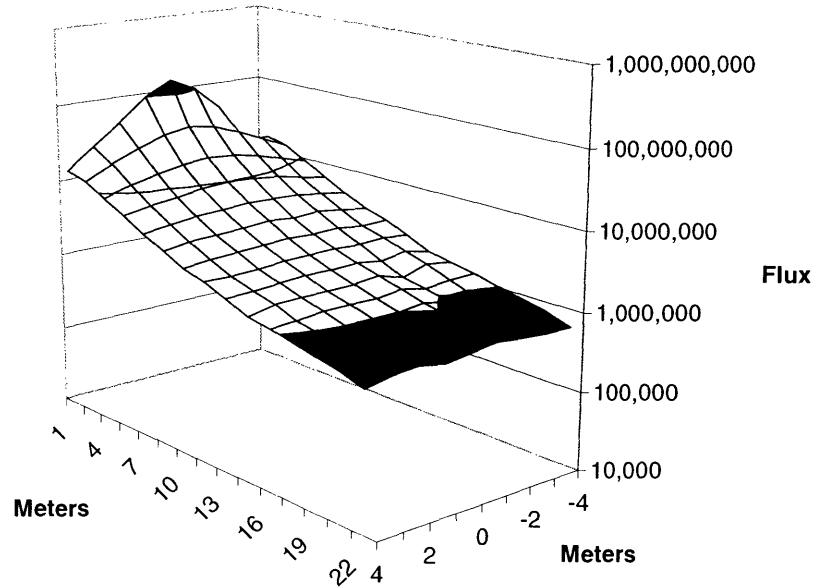


Figure 7-9: 2615 keV flux 50 kg U in air

The same linear drop is seen with 50 kg of uranium as expected. One important and unexpected phenomenon can be seen here. As a result of the thicker core, the effects of the weapon self-shielding have caused enough attenuation to bring flux levels below the 12 kg model. The distribution of source particles throughout the core has been held constant, but a significant portion of inward lying particles do not make it out. More quantitatively, the distribution of source particles falls off as $1/r^2$ with distance, while r is in the exponent of signal attenuation. For the 50 kg case, a back-of-the-envelope approximation shows the expected effect that the signal should be reduced by roughly 1/3, which was measured (see Appendix E for the calculation).

Figures 7-10 and 7-11 show the 4 kg and 12 kg of plutonium models in air. The linear behavior on the log plot shows the expected decay of neutron signal. Also of note is the extremely flat plane, which indicates that uniform scattering has occurred.

Neutron Flux per m² for 2 Week voyage, 4 kg Pu,
in Air

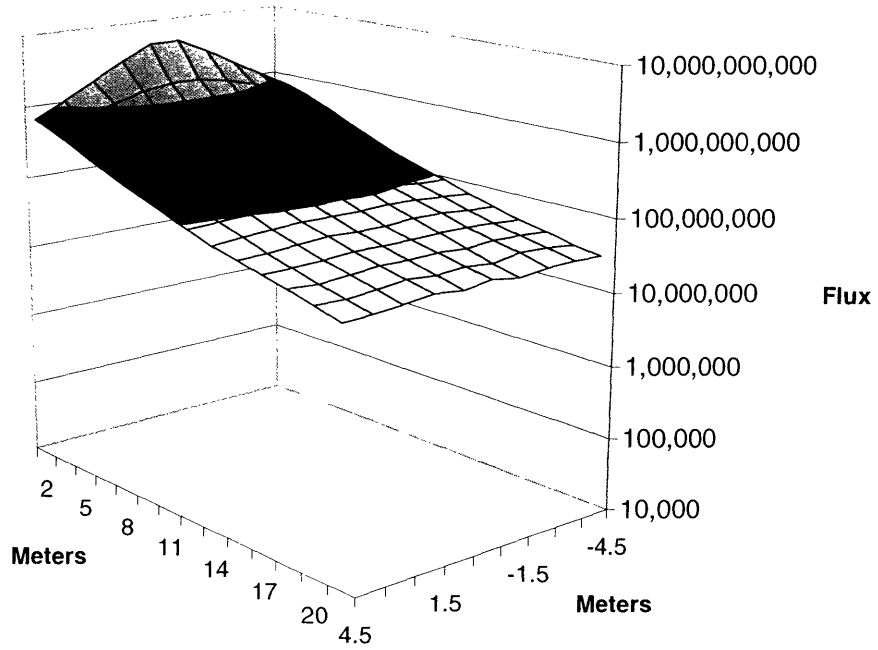


Figure 7-10: Neutron flux 4 kg of Pu in air

Neutron Flux per m² for 2 Week voyage, 12 kg Pu,
in Air

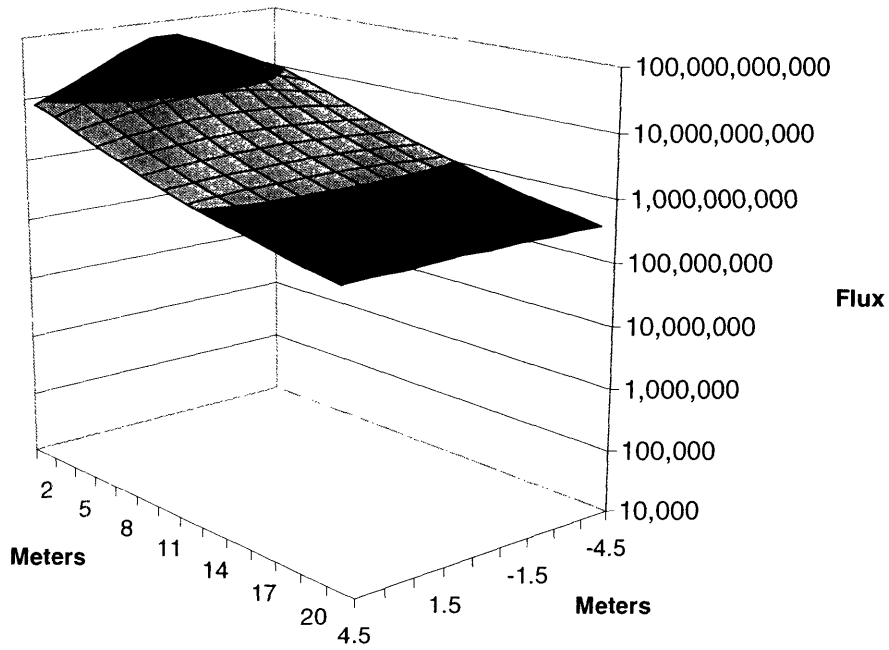


Figure 7-11: Neutron flux 12 kg of Pu in air

7.7.3 Signal Attenuation in a Uniform Density Model

Using the uniform density model commonly adopted in current practice, five more simulations were carried out. Four of the five cases correspond to the air models run above and an additional case is run for the 1001 keV gamma. The uniform density model assumes the 0.1923 gm/cm^3 calculated in section 6.2.3 across the entire array of pixels. Additionally, a common composition was chosen to represent an average cargo. Isotopic composition for the uniform density material was based on a weighted average of other cargo materials. As expected, this consisted mostly of organics with some iron and aluminum. The intent of this section is to give a worst-case scenario where no free air pathways are allowed. It is also meant to match simulations run elsewhere with a uniform density model. One of the basic themes of this thesis lies in the comparison of results from this section and subsequent sections, which present a more accurate pixilated cargo model.

Each surface plot lower range has been truncated at 10,000 counts because anything below this level falls well into the noise and is below detectability limits. There exists a potentially erroneous inference that a flux of 10,000 particles is seen at this level due to the flat floor of the graph; but that is not the case, in fact the surface plot falls well below the defined floor. Figure 7-12 shows the flux plot for the 12 kilogram uranium weapon in the uniform density model.

The lower-bound case of Figure 7-12 shows a significantly steeper gradient than the air models. In this case, the flux drops below the detectability threshold of $\sim 20,000$ at around 10 meters, which corresponds to about four total containers (three with cargo, one corresponding to the weapon/detector) worth of linear coverage. The 50 kg model follows in Figure 7-13 for comparison.

2615 keV Flux per m² for a 2 Week Voyage, 12 kg of 30-year old U,
100 ppt ²³²U, Uniform Density @ 0.1923 gm/cm³

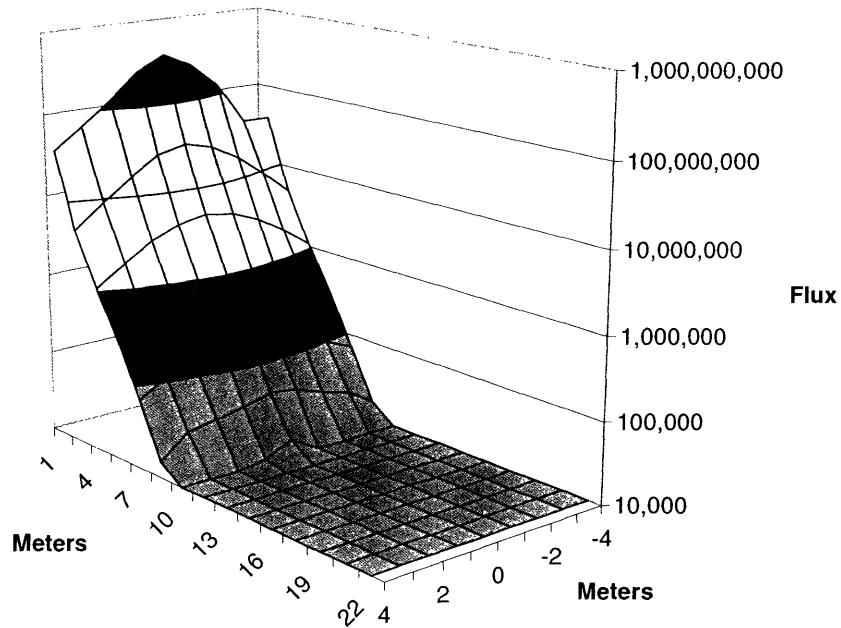


Figure 7-12: 2615 keV flux 12 kg U, uniform density model

2615 keV Flux per m² for a 2 Week Voyage, 50 kg of 30-year old U,
100 ppt ²³²U, Uniform Density @ 0.1923 gm/cm³

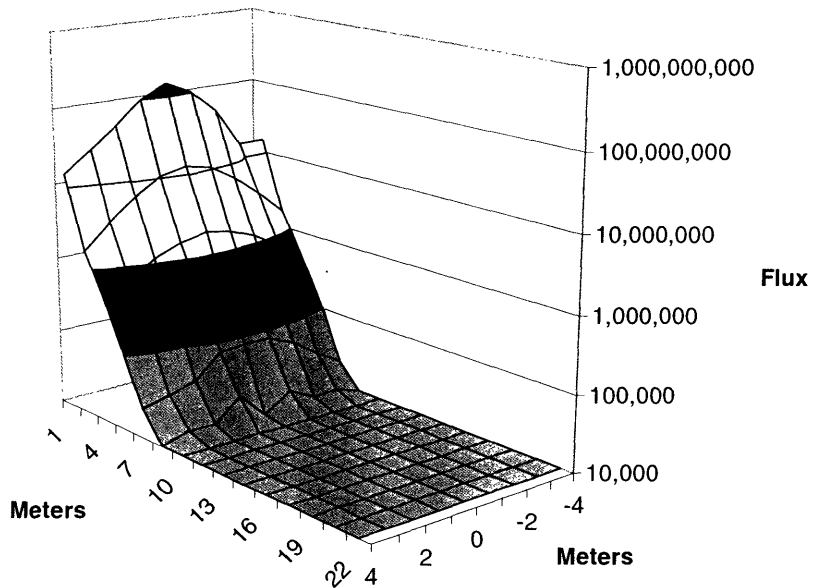


Figure 7-13: 2615 keV flux 50 kg U, uniform density model

Not much difference is seen between the 50 kg model and the 12 kg model, although the lower flux out of the larger core is seen in this case as well. The signal drops below the three-sigma limit at around 8.5 meters, an additional 1.5 meters less than the 12 kg simulation.

To set a basis for estimation of the 1001 line, an exact replica of the 12 kg model presented above was simulated except the gamma energy was changed. The results are shown in Figure 7-14.

**1001 keV Flux per m² for a 2 Week Voyage, 12 kg of 30-year old U,
100 ppt ²³²U, Uniform Density @ 0.1923 gm/cm³**

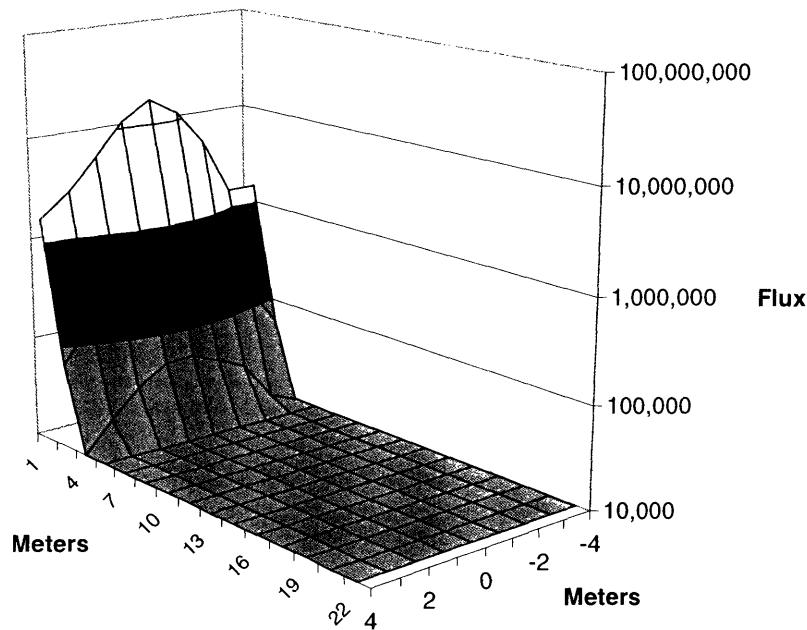


Figure 7-14: 1001 keV flux 12 kilograms uranium, uniform density model

There is clearly a significant difference between the 1001 keV transport and the 2615 keV transport. The 1001 line will not be seen above detectability threshold past about 4.5 meters in the uniform density model.

Neutron transport was also simulated using the uniform density model to establish a lower bound for plutonium detection as well. Shown in Figure 7-15 is the 4 kg case.

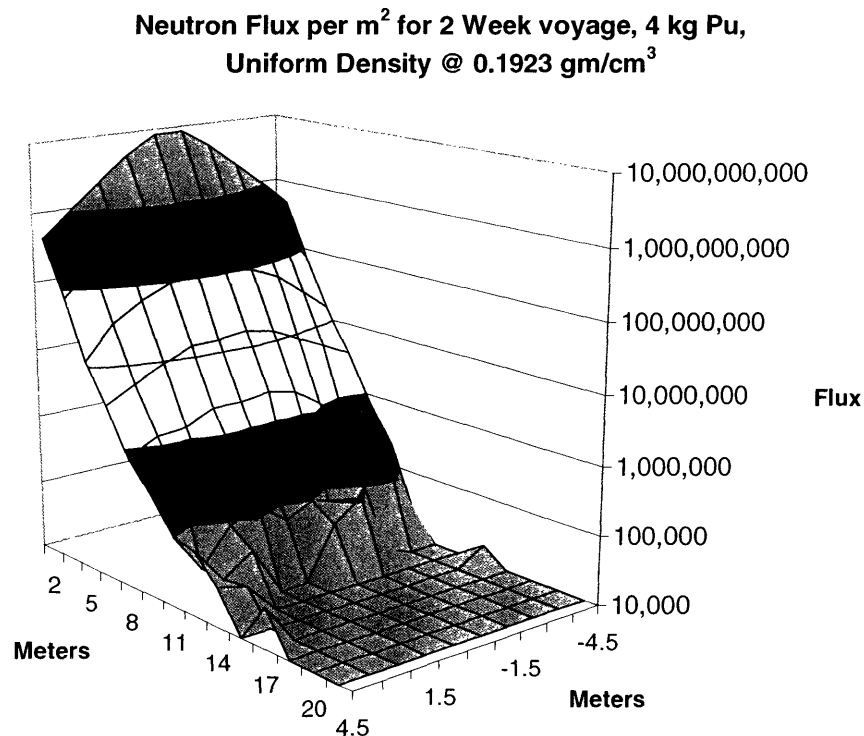


Figure 7-15: Neutron flux 4 kg Pu, uniform density model

Neutron transport through uniform density is actually rather significant. Recall the detectability threshold for neutrons was just over 100,000. This means that 4 kg of plutonium can be seen through around 10 meters of material in the uniform density approximation. Some additional counts and a jagged plane are seen below the detectability limit, but can be attributed to statistical noise since scattering should still be fairly uniform with a uniform material. The 12 kg version is presented in Figure 7-16.

Unlike the gamma situation for increased fissile material, three times as much plutonium leads to a significant increase in distance of confident detection. The detectability threshold is not reached until about 12 meters in this case. The difference in gamma and

Neutron Flux per m² for 2 Week voyage, 12 kg Pu,
Uniform Density @ 0.1923 gm/cm³

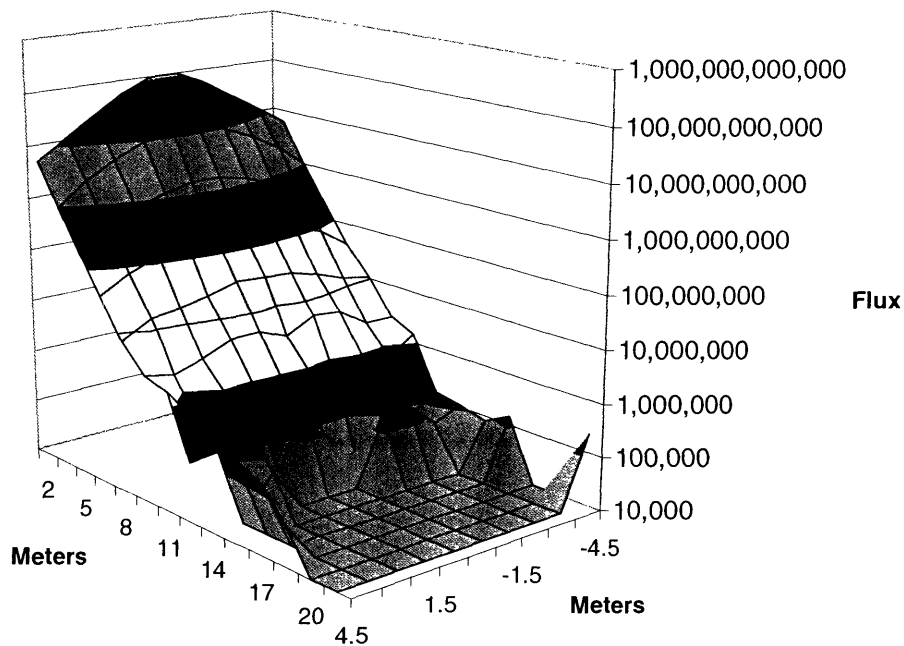


Figure 7-16: Neutron flux 12 kg Pu, uniform density model

neutron transport with increasing fissile mass should be apparent. Additional self-shielding severely affects the gamma signal because of its dense, high-Z material; while the extra fissile material hardly serves to slow down neutrons. Also, as explained in more detail in section 7.7.4.3.2, the extra neutron multiplication due to a large geometry (less leakage) is evident.

7.7.4 Results with Pixelized Cargo

The pixelized model of cargo is a more accurate construct for radiation transport. The relative merit of the approach was discussed in detail in section 6.4, but an adjustment of perception can now be more concretely understood in the context of the air and uniform density models presented above. The air model is an upper bound, while the uniform

density model represents a lower bound and the pixel model, a mixture of air and cargo, should fall somewhere in between.

Three different pixel arrays were chosen and each of the five cases was simulated to better characterize the distance to threshold. The three arrays of materials, including 700 pixels each, are relegated to Appendix F for reference. Again, it is essential that the $\frac{3}{4}$ air by volume cargo model is based on known shipping quantities and no assumptions are built into the volume calculation. The results quoted below are the very substance of the entire thesis and everything discussed to this point has been both a preparation and justification for these results, which are based on reasonable, but conservatively biased assumptions.

7.7.4.1 2615 keV Transport

7.7.4.1.1 12 Kilograms of Uranium

2615 keV gamma radiation transport is shown in Figure 7-17 for the base case of 12 kilograms of uranium, implosion-based weapon with 100 parts per trillion ^{232}U over a two-week voyage.

Studying Figure 7-17, it should be clear that the more accurate model, allowing pathways of air for partially unimpeded signal propagation, gives results of great significance. The detectability limit of $\sim 20,000$ particles is only breached in a couple of locations at distances less than 22 meters. More importantly, an order of magnitude over the threshold is seen in some places past 22 meters. The average distance to threshold can be extrapolated out to around 25 meters. As shown by Broderick, the distance of 20 to 22 meters is important because large decreases in number of containerized detectors needed to cover a ship at these ranges are seen (details will follow in Chapter 8) [Broderick, 2004]. The deployment of the ship-based approach is practical for a much lower distance to threshold than 25 meters and the results suggested by the surface plot of Figure 7-17 are extremely encouraging.

**2615 keV Flux per m² for a 2 Week Voyage, 12 kg of 30-year old U,
100 ppt ²³²U, Pixel Array #1**

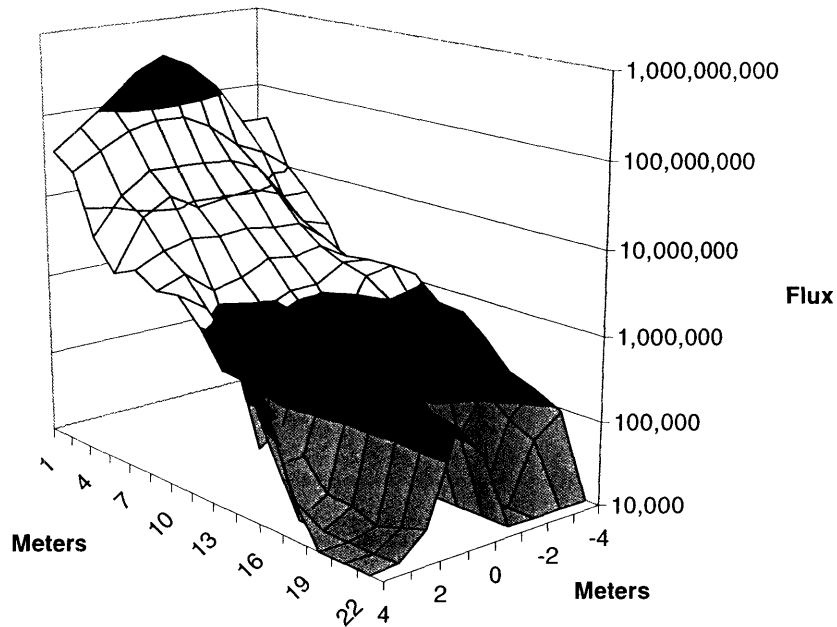


Figure 7-17: 2615 keV flux 12 kg U, pixel array #1

It may be important at this point to reproduce the above plot with a different scale. It is quite non-intuitive that any radiation would make it through 22+ meters of material because the tendency is to rely on the exponential signal decay equation. However, this reliance should not mask the larger picture, which points precisely the advantage of sensitivity with the ship-based approach. The fact that 2 weeks of count time is available for measurement and that there are a large number of source particles produced during that time should not be underestimated. To better illustrate this point and alleviate over-reliance on intuition, Figure 7-17 is reproduced in Figure 7-18 which is scaled in terms of flux per source particle.

**2615 keV Flux per Source Particle per m², 12 kg of 30-year old U,
100 ppt ²³²U, Pixel Array #1**

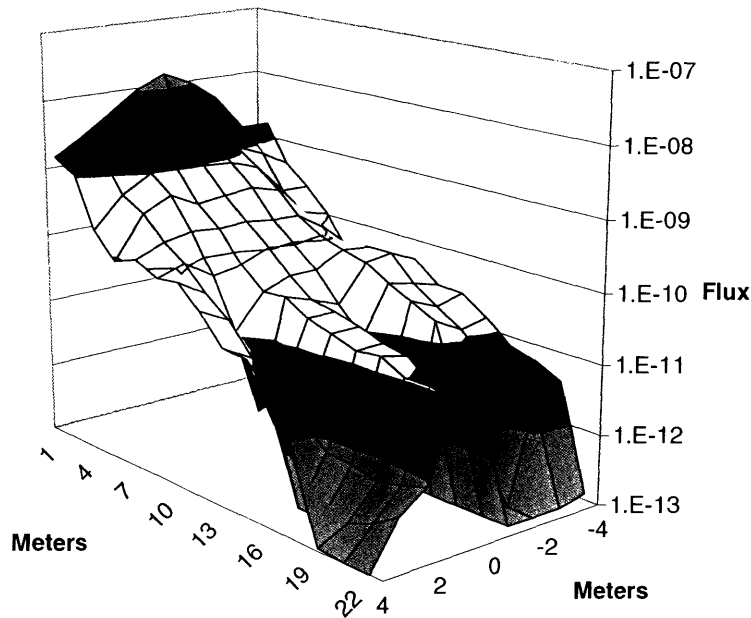


Figure 7-18: 2615 keV flux per source particle, 12 kg U, pixel array #1

It is notable that on average only around 1 in 10^{12} particles are reaching the detector at 22+ meters; but this low transmission rate is well over detection limits during the two week voyage. This should solidify the case that a reliance on radiation transport intuition is not pertinent to the situation. It is unlikely that many experiments are carried out such that only 1 in 10^{12} particles are actually seen so that there is no basis for intuition in this case.⁴ The end result is that fluxes of 10,000-100,000 particles still reach detectors at 22+ meters due to the long count time for a 2-week voyage.

The above and following graphs are interesting from another perspective in that they are not smooth. The bumpiness seen is due to the discontinuous nature of the pixelized cargo and it is clear that some pixels significantly attenuate the signal and some pathways of air

⁴ An acknowledgement of the scientists looking for neutrinos is necessary here since they are dealing with a much smaller number of detection events per particle.

lend themselves to extremely good transport. It is an interesting exercise to match the pixel materials to the gradients seen in these graphs. For instance, a look at the pixel located 2 meters off center and around 13 meters deep in Figure 7-17 appears to have significantly affected the signal relative to surrounding pixels. After cross-referencing the pixel array, it turns out that some steel and iron and fertilizer occurred in significant quantities at this location. Pixel array #2 is presented in Figure 7-19 for the same weapon model.

**2615 keV Flux per m² for a 2 Week Voyage, 12 kg of 30-year old U,
100 ppt ²³²U, Pixel Array #2**

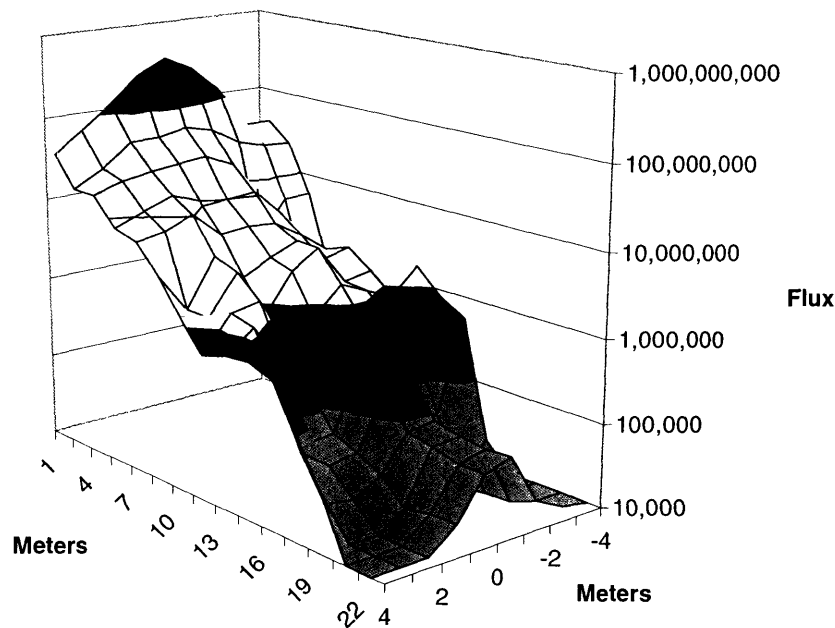


Figure 7-19: 2615 keV flux 12 kg U, pixel array #2

It appears that the random array output for pixel array #2 consists of slightly more attenuating material deeper in the array. As compared to array #1, both fluxes drop below one million around the 11-12 meter range, but array #2 drops rather quickly to below 100,000 particles by 16-17 meters. Even with the abrupt drop, the detectability threshold is not breached before 20 meters and fluxes near 100,000 are still seen in the end in the center. A good estimate of the average distance to threshold for pixel #2 is around 21 meters.

It was the original intent of this work to run all cases for two different pixel models as a first order check of accuracy. However, to worsen the uniform density approximation and see what might prevent the system from detecting a weapon, the random pixel generator was iterated extensively until a large grouping of dense materials ended up in one place. Using density probabilities from Table 6-3, the probability of finding a material greater than 1.0 gm/cm^3 is 0.068 in a pixel. In this third pixel model, the probability of having such an arrangement of dense materials (see Appendix F) is approximately 1 out of every 10,000 containerships (just over 1,000 containerships are in operation at any one time, which translates into approximately 1.7 such arrangements each year for the entire fleet). Clearly, the probability of having several adjacent and concentrated dense materials is exceeding low. This might represent the nightmare case where several cargo constituents like farm machinery and bulk copper are stacked between the detector and weapon in concentrated locations. Somewhat surprisingly, the results shown in Figure 7-20 are not so discouraging and if the detector happens not to be directly behind the dense arrangement, then the signal will easily propagate through (as seen on the left side of Figure 7-20).

**2615 keV Flux per m^2 for a 2 Week Voyage,
12 kg of 30-year old U, 100 ppt ^{232}U , Pixel Array #3**

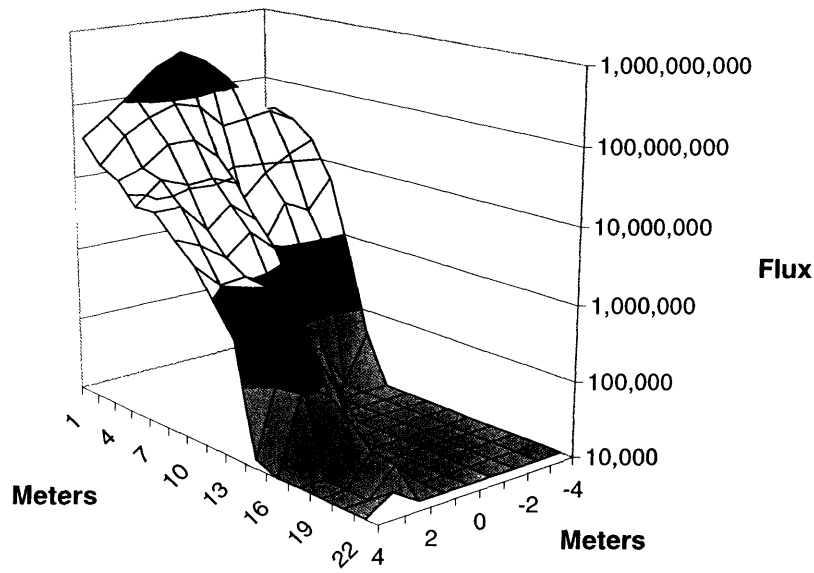


Figure 7-20: 2615 keV flux 12 kg U, pixel array #3

The effect of the concentrated and repeated high-density pixels is obvious on the right side of the graph. On the right side, the detectability threshold is breached at around 8 meters; and on the left side, it is not breached until after 20 meters. The results on the right are not so disappointing and look much like the uniform density model ranges seen above. Despite the concentrated dense materials, the same distance to threshold is attained because there are still limited pathways of air in this region, allowing some free transport. Even with the dense materials concentrated on the right side, the average distance to threshold over the whole array is still 13 meters.

7.7.4.1.2 50 Kilograms of Uranium

As another variation of transport, the effect of changing the amount of uranium was studied. The fissile mass of the weapon was changed to 50 kg and the same arrays used above were simulated. The results of pixel array #1 are shown for the 50 kilogram case in Figure 7-21. Some parts of the array allow for gamma transport above detectability limits past 22 meters and the average distance to threshold is around 20.5 meters. Consistent with the self-shielding discussed above, the fluxes are slightly lower for the 50 kilogram case.

The effect of increased uranium mass has been quantified in Figure 7-22 by calculating the ratio of fluxes from the 50 kilogram model to those from the 12 kg model. The ratio is constant at around 2.6 for most of the array, but diverges into a noisy region where some areas drop below the detectability limit. Figure 7-22 agrees to good approximation with the expected 3-fold increase in flux for the 12 kg model calculated in appendix E.

2615 keV Flux per m² for a 2 Week Voyage, 50 kg of 30-year old U,
 100 ppt ²³²U, Pixel Array #1

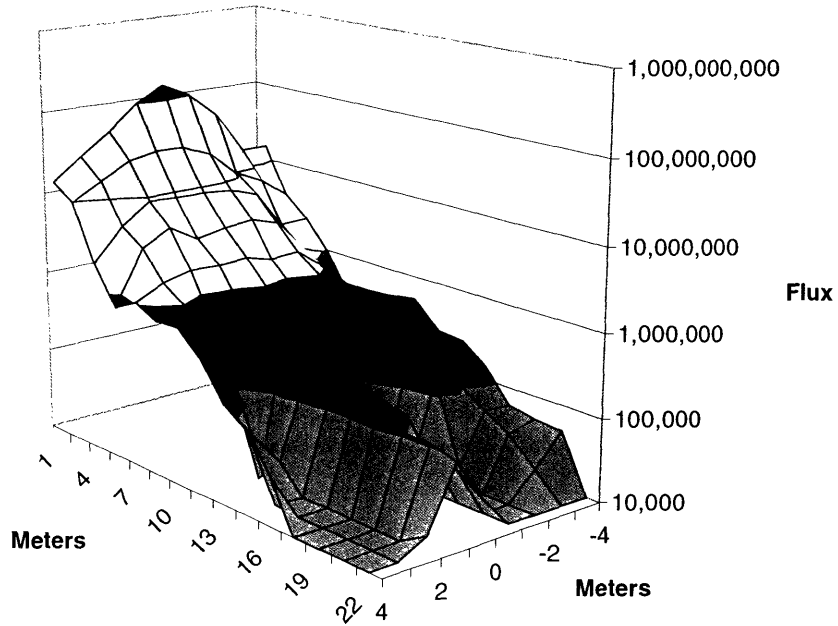


Figure 7-21: 2615 keV flux 50 kg U, pixel array #1

Fissile Mass Comparison, 12 kg/50 kg Flux, Pixel Array #1

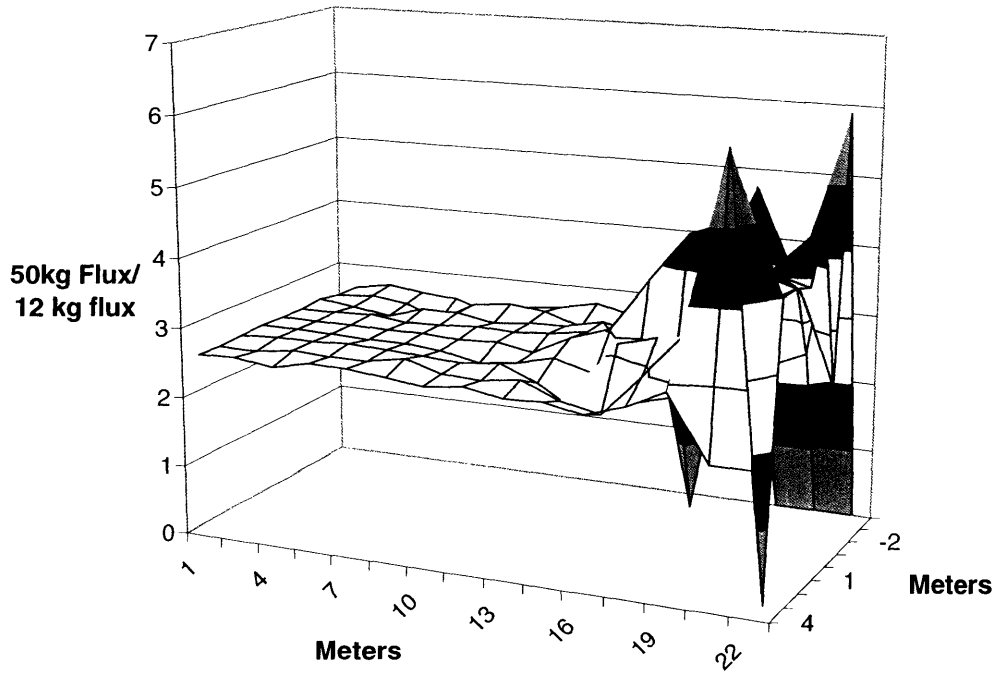


Figure 7-22: Ratio of 50 kg/12 kg fluxes, pixel array #1

The results of pixel array #2 are shown in Figure 7-23.

**2615 keV Flux per m² for a 2 Week Voyage, 50 kg of 30-year old U,
100 ppt ²³²U, Pixel Array #2**

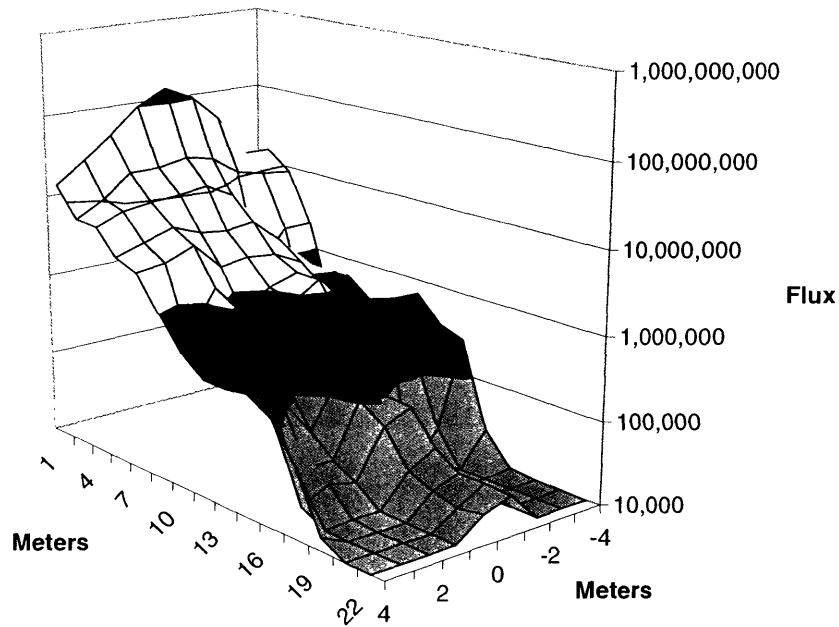


Figure 7-23: 2615 keV flux 50 kg U, pixel array #2

A similar pattern emerges with this pixel array. As in the 12 kg model for pixel array #2, gamma transport lowers the average distance to threshold, which in this case is around 19.5 meters. The ratio of 12 kg to 50 kg is extremely similar to Figure 7-22 above and is not shown to eliminate redundancy.

Pixel array #3, with the concentration of dense materials, is shown in Figure 7-24. As expected, the same effect as the 12 kg case is seen but with the detectability distances lowered. The average distance to detectability for this case is 12 meters.

**2615 keV Flux per m² for a 2 Week Voyage, 50 kg of 30-year old U,
100 ppt ²³²U, Pixel Array #3**

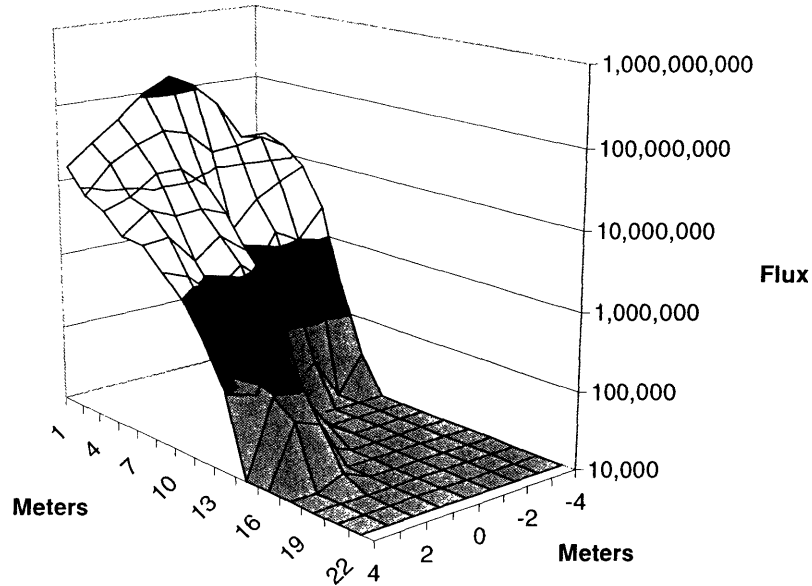


Figure 7-24: 2615 keV flux 12 kilograms uranium, pixel array #3

7.7.4.2 1001 keV Transport

To simulate the 1001 keV gamma from ²³⁸U, exactly the same pixel arrays and 12 kg weapon model were input and only the source energy changed. The following three simulations were run to quantify the flux of 1001 keV gammas through the pixelized cargo. Figure 7-25 shows pixel array #1.

The results are not as encouraging as the 2615 keV transport, but that is to be expected due to the much lower energy. Still, the detection threshold of ~20,000 is not crossed until 13-14 meters; and in the center, the flux stays above the limit until 17 meters. The average distance to threshold for this case is 15.5 meters, which is still a quite practical distance for detecting virgin uranium.

**1001 keV Flux per m² for a 2 Week Voyage, 12 kg of 30-year old U,
100 ppt ²³²U, Pixel Array #1**

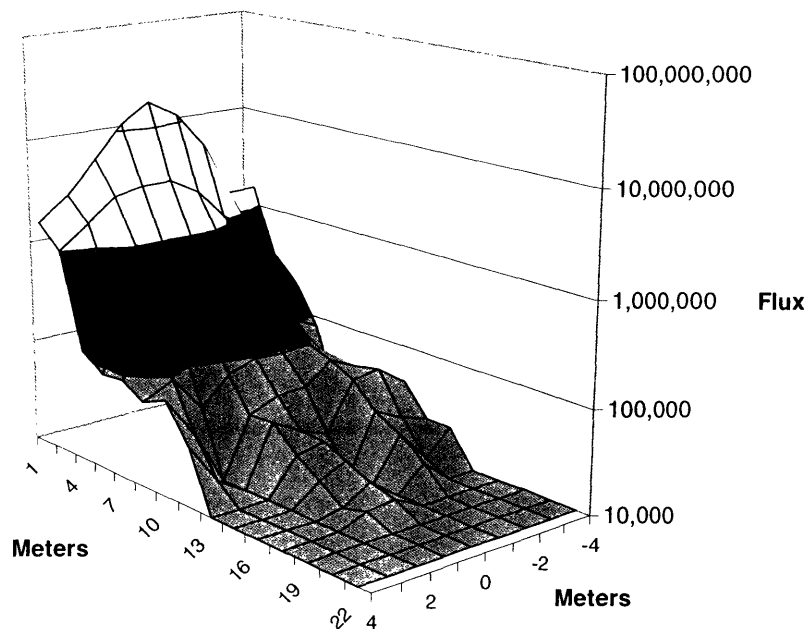


Figure 7-25: 1001 keV flux 12 kg U, pixel array #1

The discrepancy in transport between the two energies is precisely why no detectability credit was given for spectroscopic background reduction techniques (see section 5.3.4.2). No credit was clearly an overstatement because through at least 13 meters, some source verification using the 1001 keV line is not just possible, but practical. It should be noted that, while not explicitly simulated, the flux from the 911 keV gamma from ²²⁸Ac should be only slightly less than the 1001 keV graphs.

It may also be useful to point out that while the natural uranium tamper was not considered a source, the 1001 keV flux would be significantly increased if the terrorist would be careless enough to use it. The ~80 kg of extra ²³⁸U would produce a 1001 keV source increase by a factor of at least 6.

Pixel array #2 for 1001 keV transport is shown in Figure 7-26.

1001 keV Flux per m² for a 2 Week Voyage, 12 kg of 30-year old U,
100 ppt ²³²U, Pixel Array #2

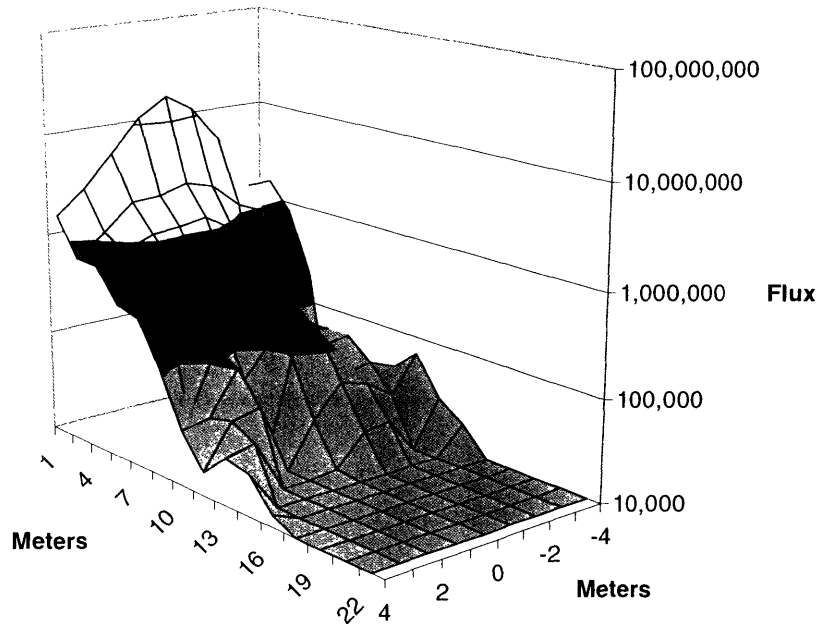


Figure 7-26: 1001 keV flux 12 kg U, pixel array #2

Different materials have different attenuation effects at different energies, which is why pixel array #2 as compared to pixel array #1 was relatively more transparent for the 1001 keV gamma than it was for the 2615 keV gamma. The sharp drop off is still seen around 16-17 meters, but there is more signal allowance from about 10-15 meters. Pixel array #2 is a little more convex in the center than pixel array #1 relative to the 2615 keV results because, at lower energies, Compton scattering is more prominent and pair production cannot occur (because $1001 \text{ keV} < 2m_e c^2$). The threshold for detectability here is on average around 13.5 meters.

The locally dense pixel array #3 is shown in Figure 7-27.

**1001 keV Flux per m² for a 2 Week Voyage, 12 kg of 30-year old U,
100 ppt ²³²U, Pixel Array #3**

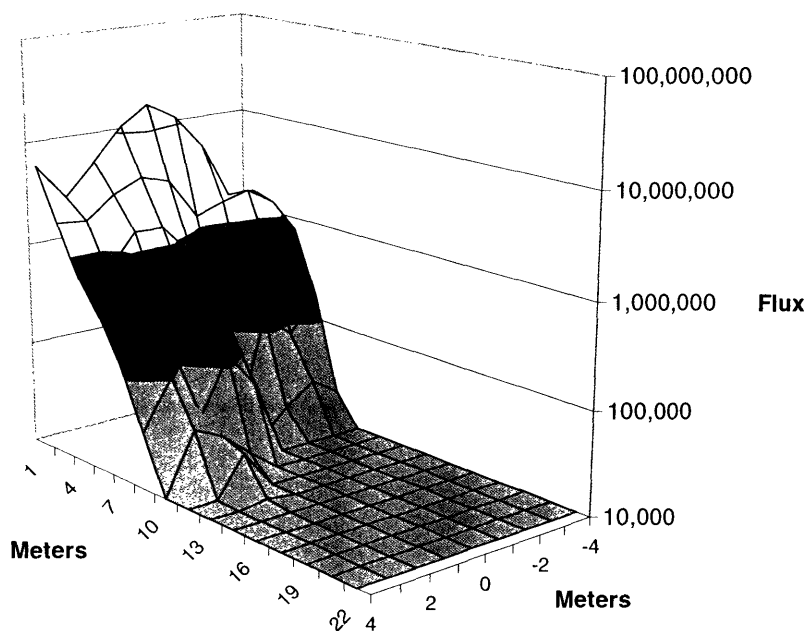


Figure 7-27: 1001 keV flux 12 kg U, pixel array #3

As expected, the flux falls rapidly near the 8 meters seen for the same 2615 keV case above. The average distance to threshold is around 9.5 meters.

7.7.4.3 Neutron Transport

All three pixel arrays were also subject to the built-in ²⁴⁰Pu spontaneous fission spectrum for fissile masses of 4 kg and 12 kg. The transport of neutrons through cargo is expected to be much different than photons with scattering events dominating such that the entire spectrum of neutrons was measured instead of discrete energy bins. If a neutron crossed a pixel's surface, it was counted regardless of energy. One other note on energy is that by the time the neutrons reach into the cargo, they have been well-thermalized and there is no need for a commonly used moderator surrounding the neutron detector, so no such material was built in to the simulation.

7.7.4.3.1 4 Kilograms of Plutonium

Figure 7-28 shows the expected flux throughout the pixelized cargo with a source of 56,000 spontaneous fission neutrons per kilogram per second for pixel array #1.

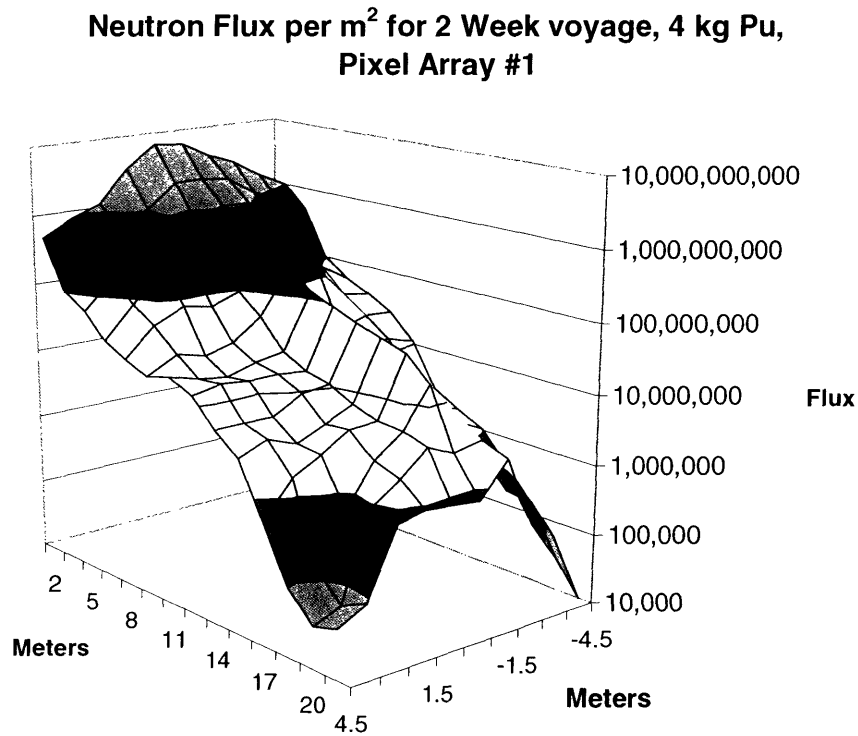


Figure 7-28: Neutron flux 4 kg Pu, pixel array #1

The surface is still bumpy, but somewhat smoother than the gamma plots, especially deeper into the cargo. The reason for this smoothing effect is of course that neutrons have been scattering in every direction, causing lateral and even backward migration throughout the cargo. The detectability threshold for three-sigma confidence is just over 100,000 and for pixel array #1, it is not breached on the corners until 20-22 meters. As with the gamma plots, some paths allow for fluxes out of the pixel array at greater than 22 meters that are significantly higher than the threshold. An extrapolation with similar

cargo might see the distance to threshold at somewhere around 25-26 meters for several pixels and an average distance would occur at around 23.5 meters. Needless to say, these results are extremely encouraging and will be cross referenced with thesis work from Broderick to show how many neutron detectors are required to adequately cover each type of containership (see Chapter 8).

The results of neutron transport simulation through pixel array #2 are shown in Figure 7-29.

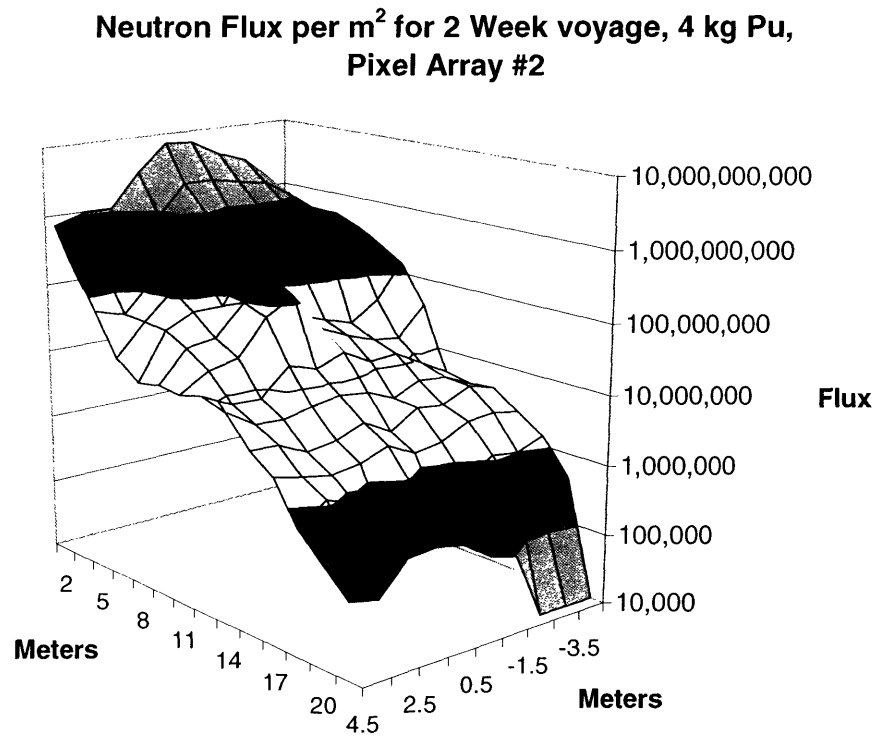
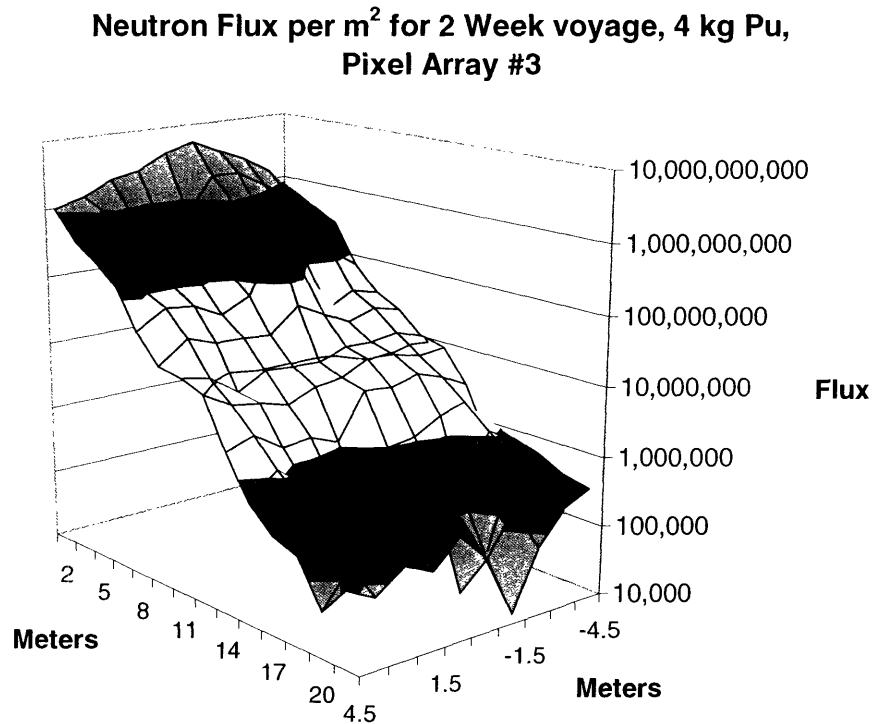


Figure 7-29: Neutron flux 4 kg Pu, pixel array #2

The flux pattern for pixel array #2 shows slightly poorer transport, especially in the middle. A fairly uniform signal attenuation occurs throughout the array, but a noticeable absorbing area is seen on the right from 8-11 meters. There are several materials in this area with higher neutron capture cross-sections. The distance to threshold extends slightly beyond the array except for the right side where threshold is met at around 21.5 meters.

An average distance to threshold might be postulated slightly below pixel array #1 at around 23-24 meters.

Pixel array #3 is shown in Figure 7-30.



Recall that pixel array #3 was chosen with a high concentration of dense material on the right side at around 8 meters. As expected, what is bad for photons is not so bad for neutrons and the concentration of high-Z material has little effect, allowing neutrons to travel through with less thermalization. In fact, it is hard to see any effect and pixel array #3 shows a smooth surface. Similar to the other arrays, it is not until the 20-22 meter range that detectability limits are breached. Again, in some cases an extrapolation of distance to threshold is necessary to postulate an average, which will be taken as 23.5 meters.

7.7.4.3.2 12 Kilograms of Plutonium

In this section, the 12 kg case is presented. Each pixel array was kept constant and the only difference between the results presented in that last section is the fissile mass of plutonium. Pixel array #1 is shown in Figure 7-31.

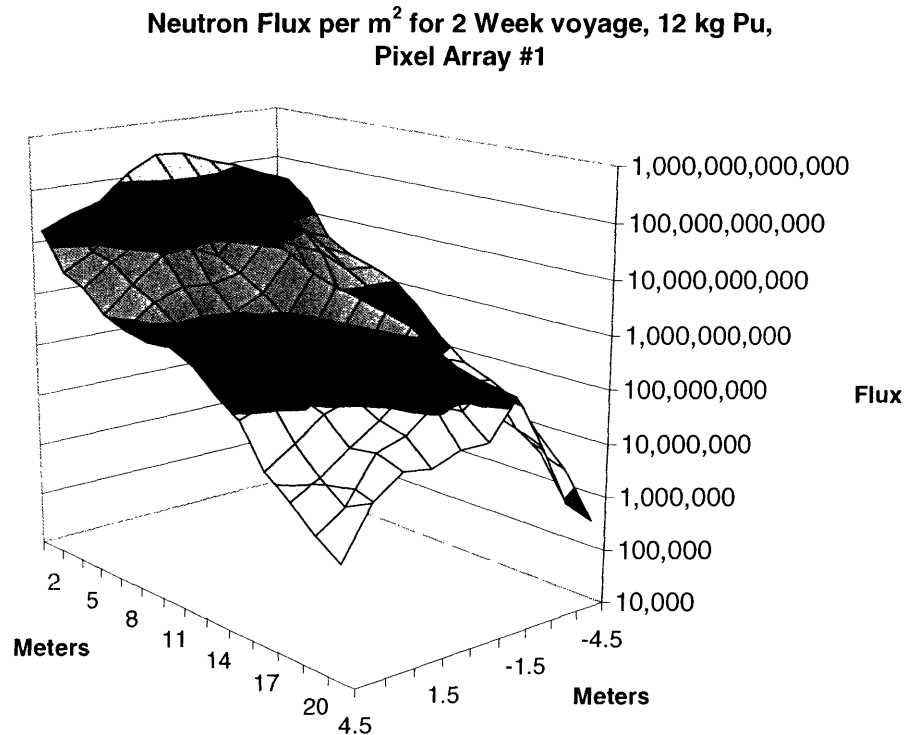


Figure 7-31: Neutron flux 12 kg Pu, pixel array #1

The increased flux of neutrons from the three-fold increase in source strength is readily seen above as compared to the Figure 7-28. Not a single point in the array falls below the detectability threshold. With many measurements at the end of the array showing 2 order of magnitude increase over the detectability limit, the extrapolated average distance to threshold is 29 meters.

A closer look at the data reveals an unexpected puzzle. Forming a ratio between the 4 kg flux and the 12 kg flux produces the surface plot of Figure 7-32.

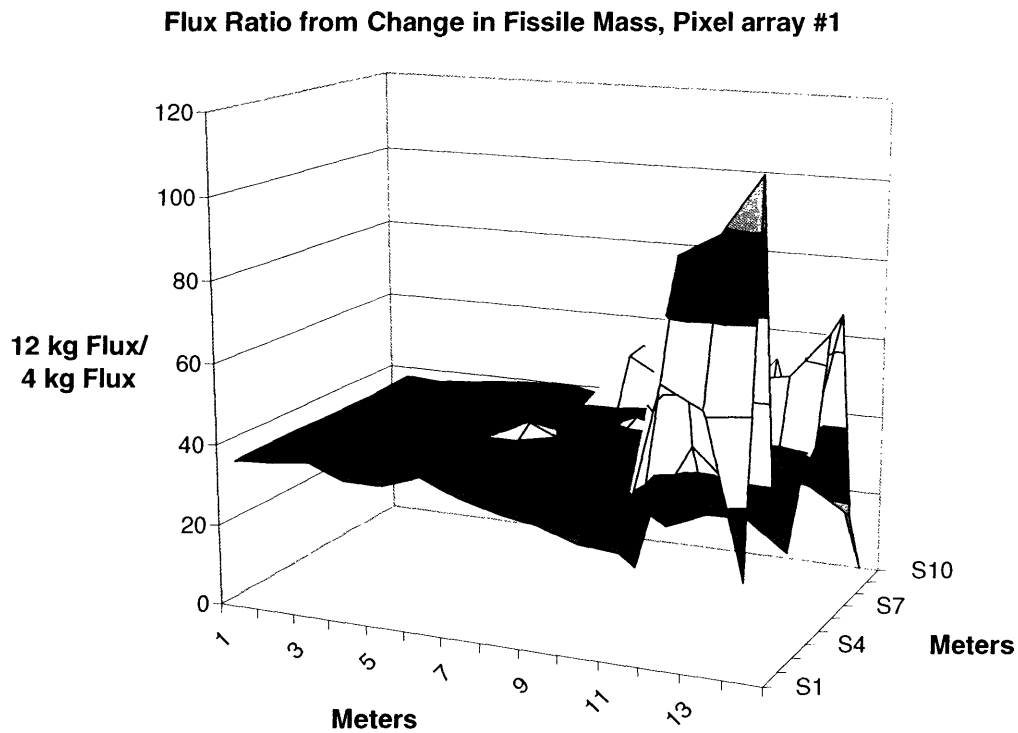


Figure 7-32: Ratio of 12 kg/4 kg Pu fluxes, pixel array #1

The ratio of fluxes stays nearly constant throughout 12 meters of the array, but then the lower fluxes near the end of the graph give rise to a degree of noise. The puzzle is that the ratio of fluxes exceeds the ratio of increased fissile mass, which should not be possible since there are only three times as many source neutrons. In fact, the large increase in flux from the extra fissile mass comes from increased internal neutron multiplication. Spontaneous fission neutrons can cause additional fissions, which multiply by the commonly known factor η , the number of neutrons per absorption. Additionally, increased multiplication occurs due to less leakage in the larger hollow sphere. Other reactions tend to multiply the number of neutrons including the (n, xn) process in the

reflector. MCNP keeps track of the total multiplication and prints the number as output. In the 4 kg case, the multiplication for all reactions was 1.608; while in the 12 kg case, the total multiplication was 6.096.⁵ The inclusion of increased photonuclear events and (n, xn) reactions, especially in beryllium, along with the factor of four in multiplication and the factor of three in fissile mass, makes clear the reason for the ~30-fold increase in flux seen in Figure 7-32.

Pixel array #2 for the 12 kilogram model is presented in Figure 7-33.

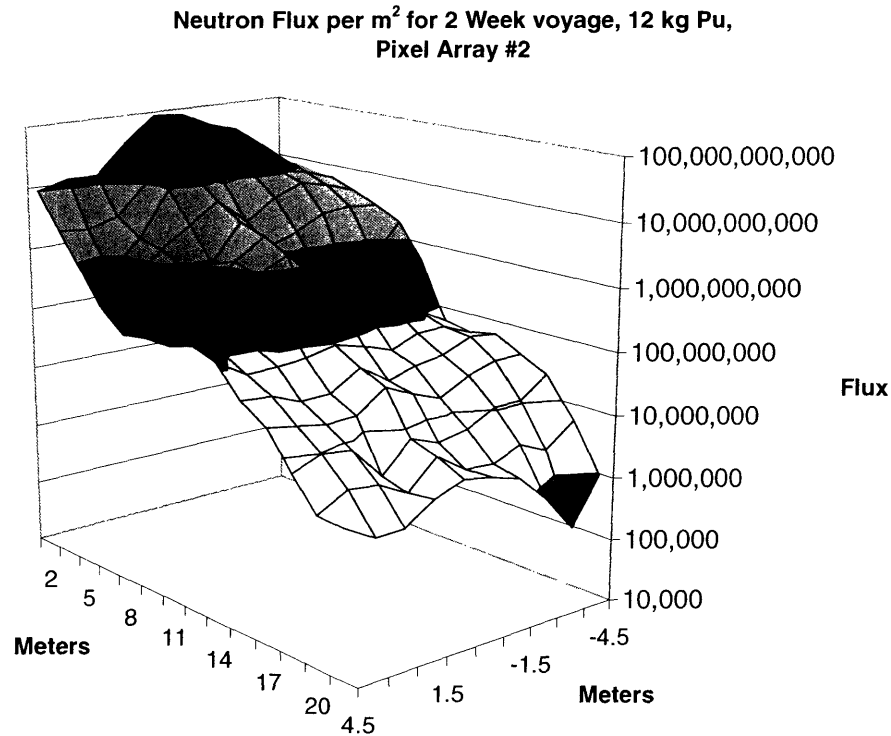


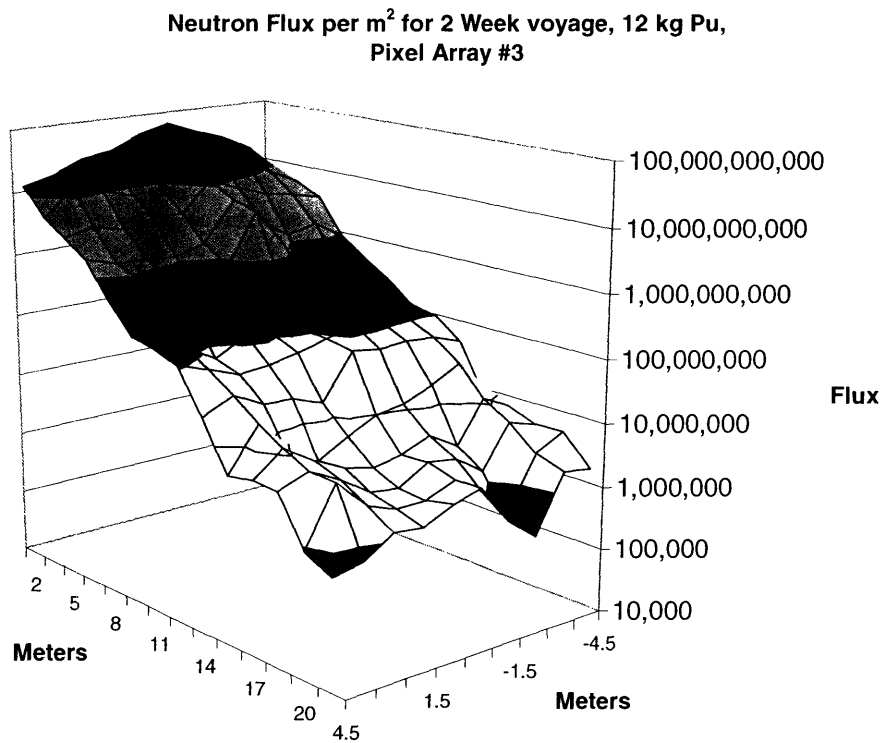
Figure 7-33: Neutron flux 12 kg Pu, pixel array #2

The increased flux from a 12 kilogram weapon model is very apparent here. By 22 meters, the flux still has not fallen below one million per m². The extrapolated average

⁵ The multiplication here is not k_{eff} ; rather it is the number of neutrons created per source neutron.

distance to threshold is 26 meters and in the center nearly 27 meters. The 30-fold increase in flux for the 12 kg case is seen in both pixel array #2 and #3, so the redundant charts corresponding to Figure 7-32 will not be shown.

Pixel array #3 is shown in Figure 7-35.



Again, the increased flux is easy to see. The extrapolated average distance to threshold is around 24 meters for this case. A summary of all average distances to threshold will be provided in the conclusion of this chapter, but there are several cases still to be characterized.

7.7.4.4 Shielded Gamma Transport

To this point, it has been assumed that no shielding was put in place around the weapon. The assumption may be unjustified because a terrorist group with the technical competence to build or procure a nuclear weapon will certainly take as many precautions as necessary to assure its delivery. It stands to reason that the group would attempt to shield the weapon to minimize the radiation signal. The above results are still valuable despite the likelihood of shielding. It is also quite possible that a terrorist group would attempt to conceal the weapon in common packaging to make it appear as benign cargo. For example, they might conceal the entire weapon, which less than a half-meter in diameter, as well as firing or booby-trap mechanisms inside a big screen television or common kitchen appliance such as a refrigerator or oven. While these items would be slightly heavier than expected, the weight of the weapon with no shielding, ~183 kg, might not raise any significant alarm, especially if shipped alongside other heavy cargo. If heavily shielded and still hidden inside a big screen television, the extra weight would be more than noticeable. The unshielded simulations thus correspond to a terrorist concealing a weapon alongside commonly shipped cargo, while the following shielded simulations correspond to a terrorist with sole access to a container that will not also include other cargo.

The way to shield gammas is through a dense, high-Z material, but by nature, these materials are heavy and thus more noticeable. The inclusion of a sufficiently thick lead shield surrounding the weapon would be easily distinguished due to its extra weight if the device were concealed in a large appliance. An optimization of shielding thickness is not carried out here due to the unknown variables of concealment and port/shipper scrutiny of cargo weights. Instead, a lead thickness of 2 cm is chosen because it doubles the weapon weight and may still be barely unnoticeable from simple weight aberration.

For neutrons, shielding is usually done with hydrogen rich substances such as water, concrete, polyethylene or paraffin wax. There is no weight constraint to the shield size

because all of these items would appear and weigh too much like typical cargo. As such, the shielding scenarios for neutrons include much more material. Several scenarios were considered for neutrons; the 4 kg case was shielded with 5 centimeters of a water-like substance, the 12 kg case was shielded with 20 centimeters of polyethylene. One final worst-case was considered where the entire container was backfilled with Portland concrete.

7.7.4.4.1 12 Kilograms of Uranium, Shielded

The following results are from exact replicas of the cases shown in Figures 7-17, 7-19 and 7-20 except a 2-centimeter thick sphere of lead surrounds the weapon. Pixel array #1 is shown in Figure 7-35.

**2615 keV Flux per m² for a 2 Week Voyage, 12 kg of 30-year old U,
100 ppt ²³²U, Pixel Array #1, Shielded with 2 cm of Lead**

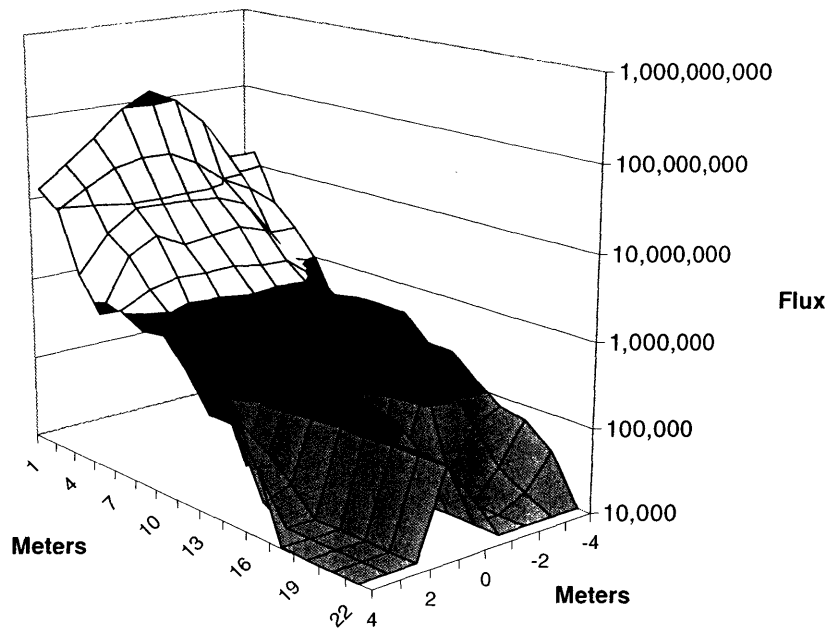


Figure 7-35: 2615 keV flux 12 kg U, shielded with 2 cm of lead, pixel array #1

The effect of lead shielding is surprisingly minimal, but not insignificant. There is still an above threshold flux at 20+ meters and the average distance to threshold is about 19.5 meters. Even with a heavy, 2 cm thick sphere of lead surrounding the weapon, the ship-based system can see through almost 20 meters of cargo on average. As compared to the base case, unshielded pixel array #1 shows better transport, but not by orders of magnitude. To quantify the effect of shielding, a simple ratio of the shielded case divided by the unshielded case was calculated and plotted in Figure 7-36.

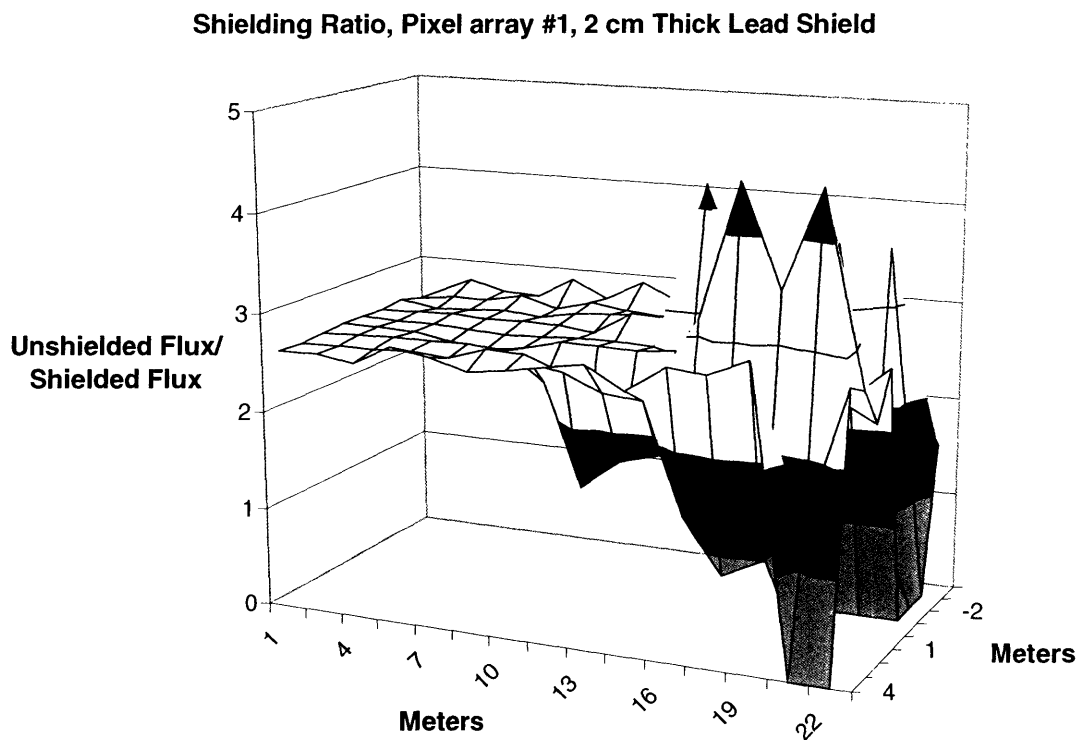


Figure 7-36: Ratio of unshielded/shielded flux 12 kg U, pixel array #1

The interesting thing to note about Figure 7-36 is that, except for some noise after 15 meters, there is only around a factor of 3 difference in the two cases. Even in the noise, there is no more than a factor of 5 reduction in flux. That is, a terrorist would have to be

willing to risk detection by excess weight to gain only a factor of 3-5 reduction in flux. It is not clear that the benefit of the lower flux is worth the extra risk for the terrorist, but this is pure speculation. It is, however, quite clear that the system will still detect their lead shielded weapon from around 20 meters with three sigma confidence.

The shielded version of pixel array #2 is shown in Figure 7-37.

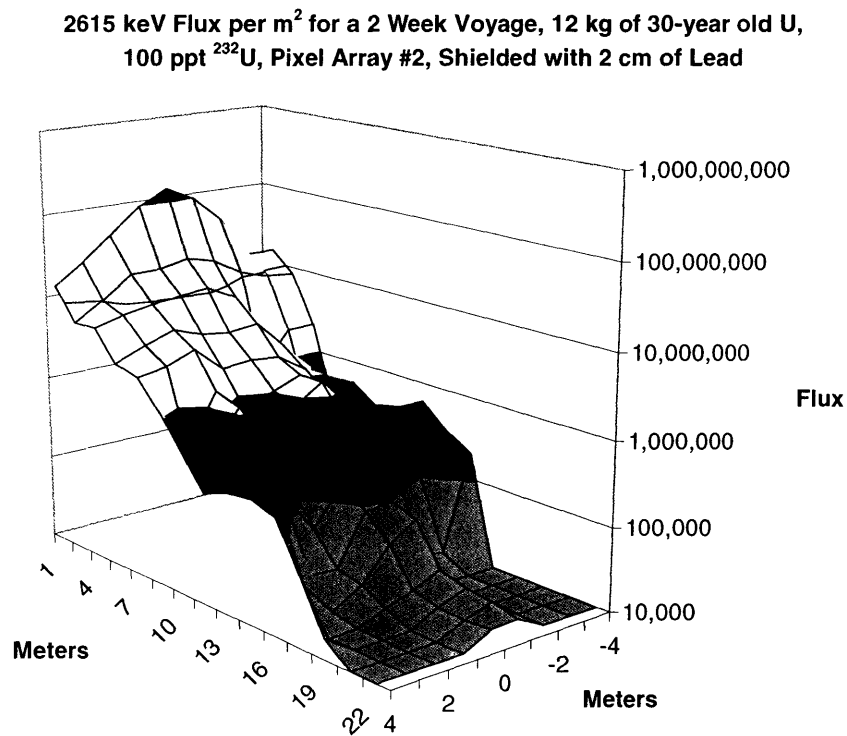


Figure 7-37: 2615 keV flux 12 kg U, shielded with 2 cm of lead, pixel array #2

The shielding case in pixel array #2 is slightly more limiting than pixel array #1 with distance to threshold over 22 meters only seen in the direct center, while an average distance is closer to 19 meters. The unshielded/shielded ratio for pixel array #2 is shown in Figure 7-38.

Shielding Ratio, Pixel array #2, 2 cm Thick Lead Shield

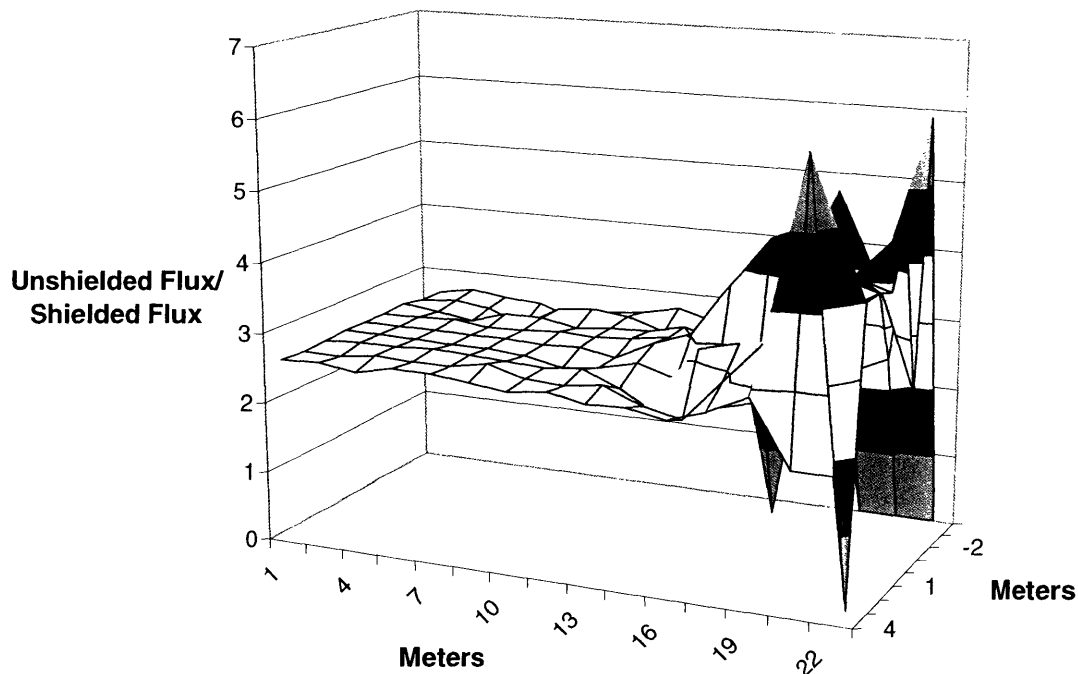


Figure 7-38: Ratio of unshielded/shielded flux 12 kg U, pixel array #2

An extremely similar plot is seen in pixel array #2, reinforcing confidence in the results presented for pixel array #1.

Continuing, pixel array #3 is shown in Figure 7-39. Just as in the normal case, the high-density concentration of cargo on the right side has taken its toll on the flux. For the shielded case, the detectability threshold is reached about a half-meter sooner, 7.5 meters, on the right side of the plot. A decent transport through the left side allows the average distance to threshold of the whole array to be around 10 meters. The shielded/unshielded ratio is shown in Figure 7-40 for pixel array #3.

2615 keV Flux per m² for a 2 Week Voyage, 12 kg of 30-year old U,
 100 ppt ²³²U, Pixel Array #3, Shielded with 2 cm of Lead

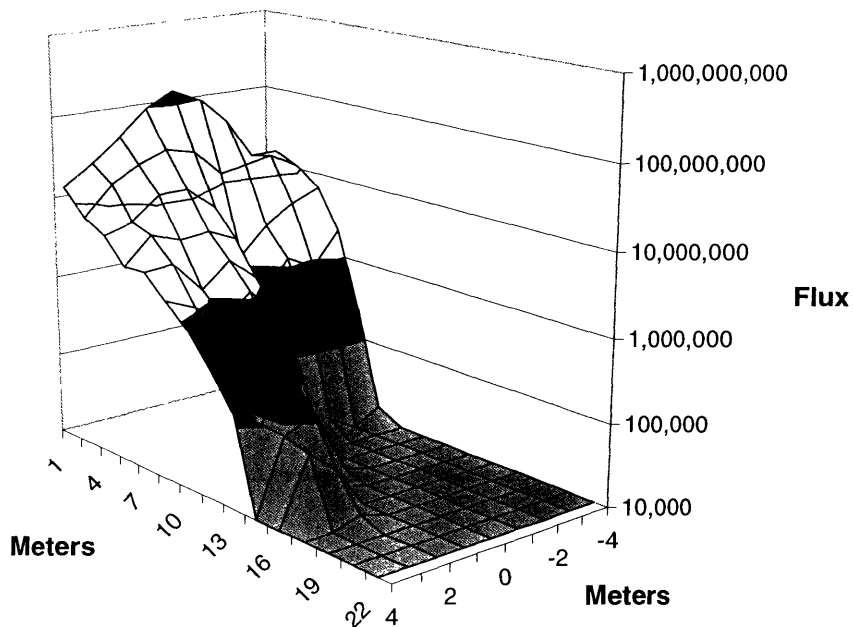


Figure 7-39: 2615 keV flux 12 kg U, shielded with 2 cm of lead, pixel array #3

Shielding Ratio, Pixel array #3, 2 cm Thick Lead Shield

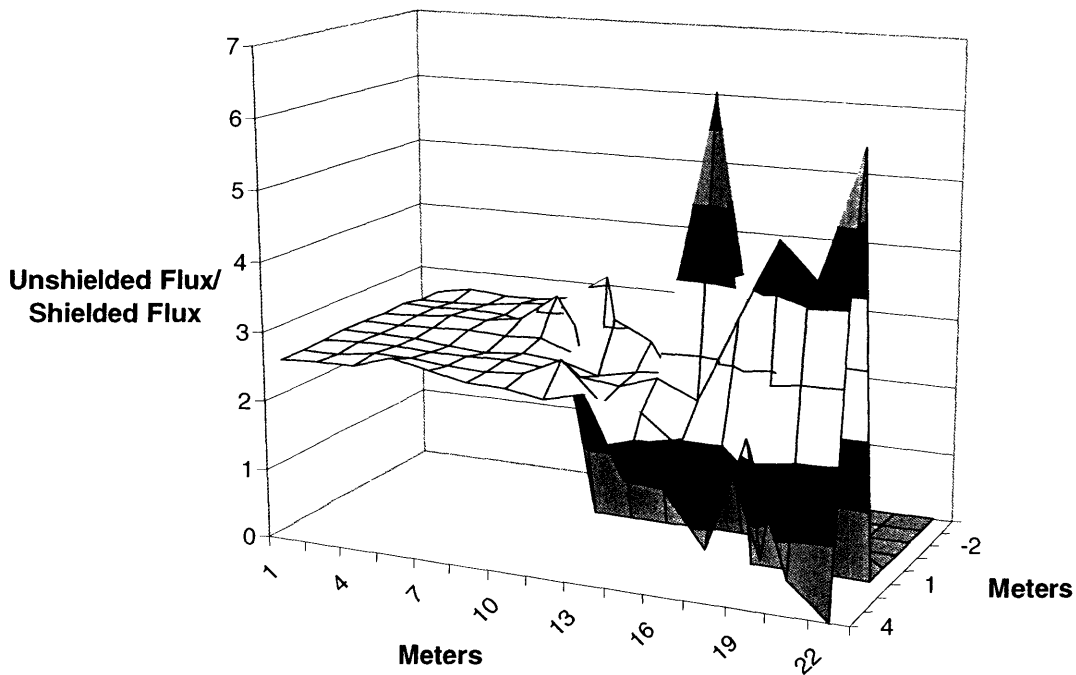


Figure 7-40: Ratio of unshielded/shielded flux 12 kg U, pixel array #3

Again, a similar result is seen in this array. The drop to zero on the left side is prominent because there is no flux to form the ratio in this location.

7.7.4.4.2 50 Kilograms of Uranium, Shielded

As in section 7.7.4.4.1, 2 centimeters of lead shielding was placed around the 50 kg weapon model and measurements were made for all three arrays. The results are shown in Figure 7-41 for pixel array #1.

**2615 keV Flux per m² for a 2 Week Voyage, 50 kg of 30-year old U,
100 ppt ²³²U, Pixel Array #1, Shielded with 2 cm of Lead**

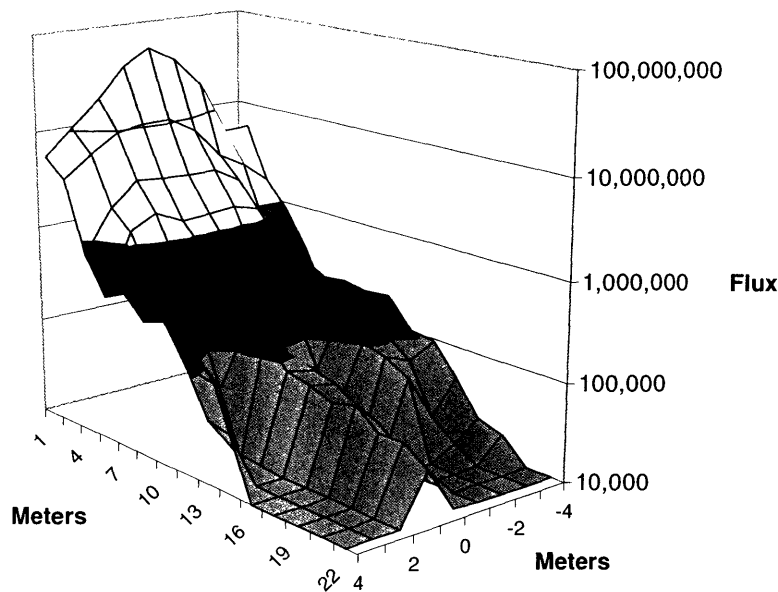


Figure 7-41: 2615 keV flux 50 kg U, shielded with 2 cm of lead, pixel array #1

The same ratio consideration applies in the shielded case of 12 kg/50 kg flux as the unshielded case. Fluxes are reduced to around a third of their 12 kg values. Still, a significant flux of gammas can be seen towards the back of the array. The average distance to threshold is around 18.5 meters in this case.

Shown in Figure 7-42 is the pixel array #2 case. The average distance to threshold for this case is 17.5 meters. The shielding ratios are similar to Figure 7-40 and are not shown.

2615 keV Flux per m^2 for a 2 Week Voyage, 50 kg of 30-year old U,
100 ppt ^{232}U , Pixel array #2, Shielded with 2 cm of Lead

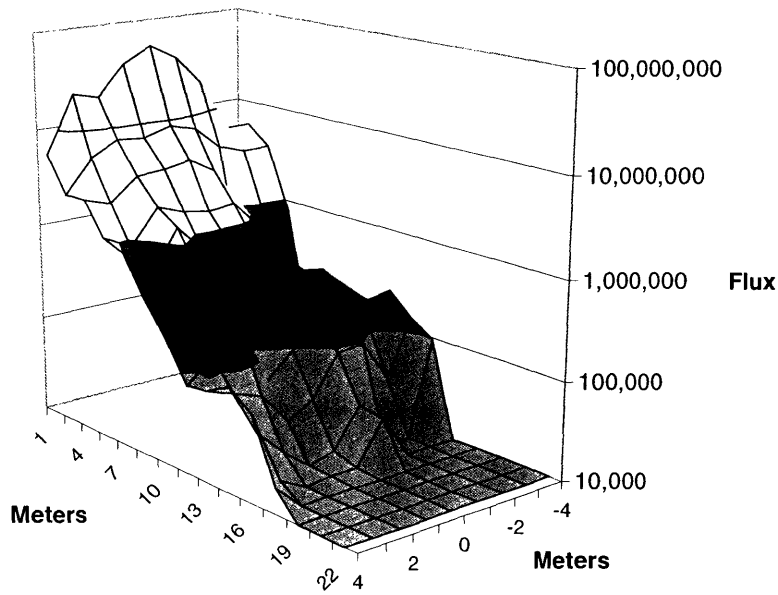


Figure 7-42: 2615 keV flux 50 kg U, shielded with 2 cm of lead, pixel array #2

2615 keV Flux per m^2 for a 2 Week Voyage, 50 kg of 30-year old U,
100 ppt ^{232}U , Pixel array #3, Shielded with 2 cm of Lead

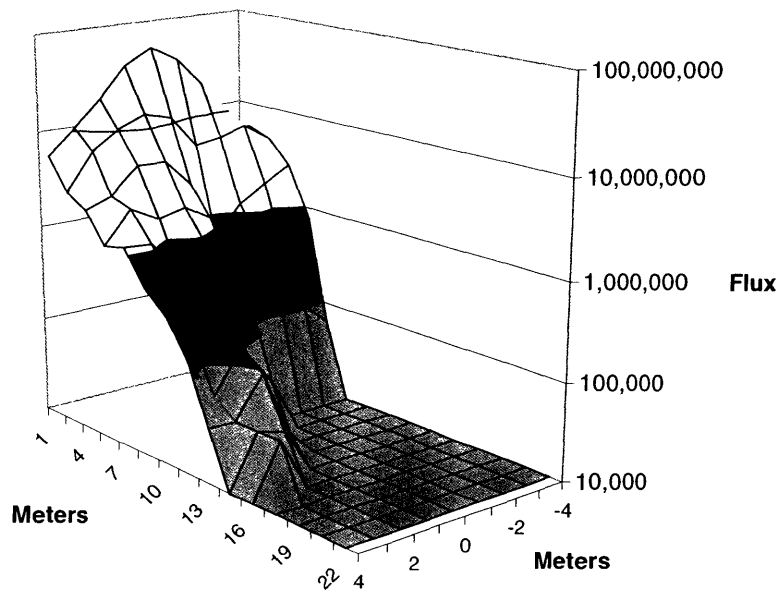


Figure 7-43: 2615 keV flux 50 kg U, shielded with 2 cm of lead, pixel array #3

Pixel array #3 is shown in Figure 7-43 for completeness. The additional attenuation results of pixel array #3 are very similar to those shown in similar cases. The distance to threshold is around 7.5 to 8 meters along the right side and the average distance for the whole array is around 11 meters.

7.7.4.5 Shielded Neutron Transport

7.7.4.5.1 4 Kilograms of Plutonium, Shielded

In a very similar fashion to the shielded gamma simulations, neutrons shielded with 5 centimeters of water equivalent are presented in this section for each of the three arrays. The shielded case for pixel array #1 is shown in Figure 7-44.

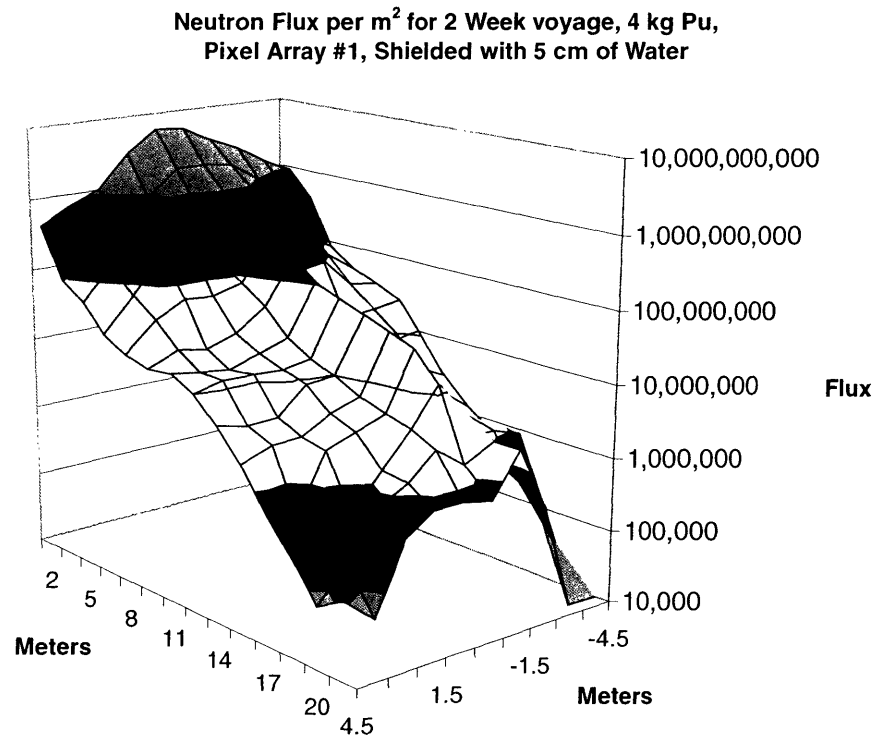


Figure 7-44: Neutron flux 4 kg Pu, shielded with 5 cm of water, pixel array #1

The above surface plot shows that the shielding has little effect on the neutron flux as compared to the unshielded case. The detectability threshold is not breached except in the corners and the extrapolated average distance to threshold is around 25 meters. There is very little difference between this case and the unshielded case. The unshielded/shielded ratio is plotted in Figure 7-45.

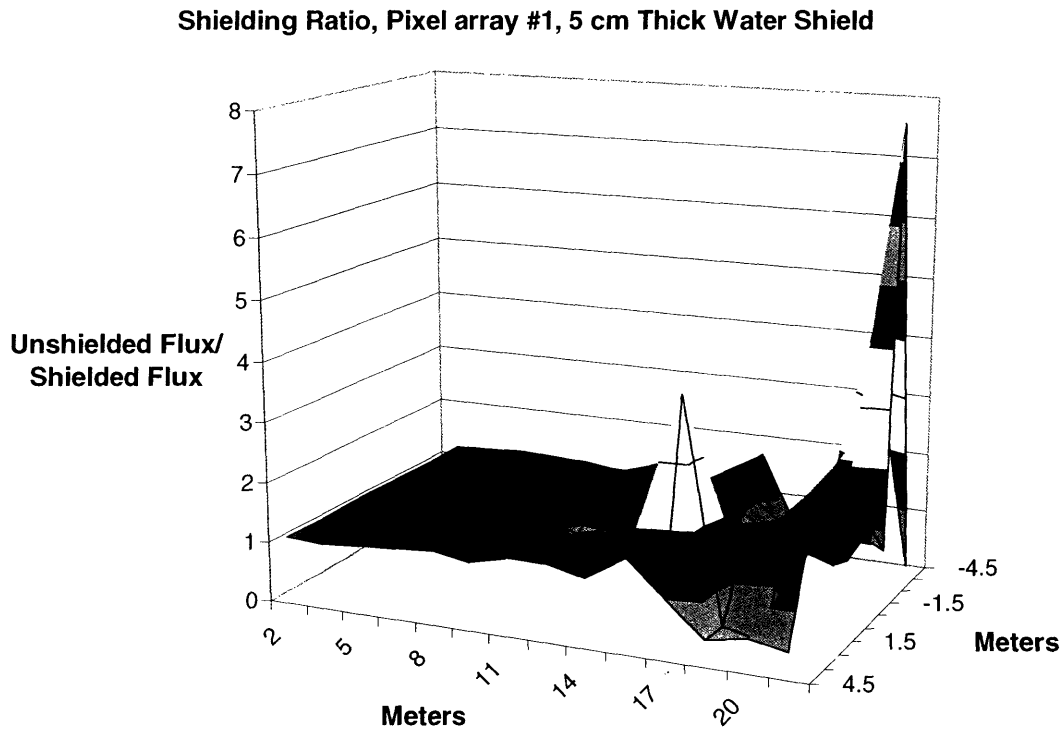
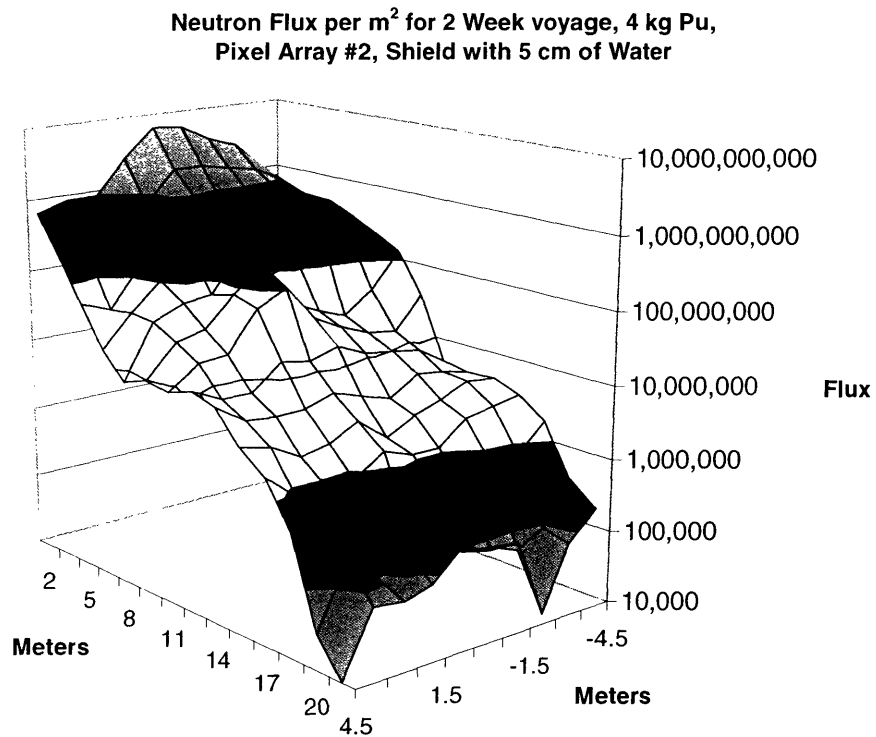


Figure 7-45: Ratio of unshielded/shielded flux 4 kg Pu, shielded with 5 cm of water, pixel array #1

The ratio is almost exactly one throughout most of the array. More noise is seen with neutrons as the scattering process is random and more directional variation presumably occurs near the end of the array where neutrons have undergone many, many scattering events. An interesting thing to note in the Figure 7-45 is that there is little to no effect on the flux at the front of the pixel array with the water-like shield in place as compared to the unshielded model (Figure 7-28). A faster thermalization of neutrons due to the shield

is occurring, but there is only a minimal amount of extra capture. Thermalized slightly more, neutrons have a higher chance of removal, but the above chart suggests that this effect is nearly negligible for the 5 centimeters of extra water-like material.

The graph in Figure 7-46 shows the results in pixel array #2.



The shielded case did not significantly alter the neutron transport. The unshielded/shielded ratio looks nearly identical to the one for pixel array #1 and the average distance to threshold is taken to be 25 meters. For completeness, pixel array #3 is shown in Figure 7-47.

**Neutron Flux per m² for 2 Week voyage, 4 kg Pu,
Pixel Array #3, Shielded with 5 cm of Water**

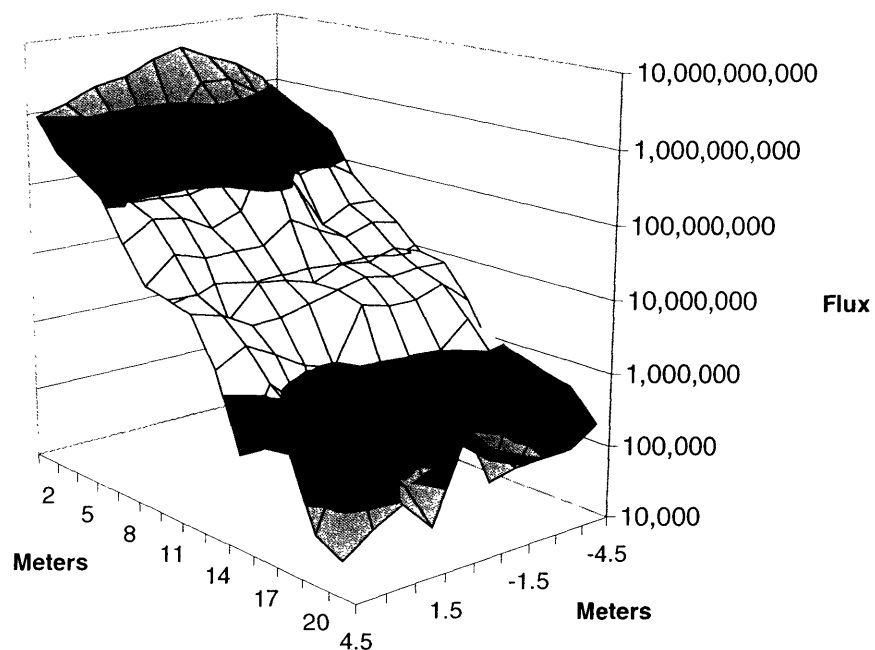


Figure 7-47: Neutron flux 4 kg Pu, shielded with 5 cm of water, pixel array #3

Again, little differs from the unshielded case. The distance to threshold is again beyond the edge of the pixel array, but an extrapolation gives a distance of around 24 meters. The unshielded/shielded ratio is also similar to array #1.

7.7.4.5.2 12 Kilograms of Plutonium, Shielded

In the same way that a 12 kilogram unshielded model was simulated in section 7.7.4.3.2, a 12 kilogram model with shielding was simulated using the three pixel arrays. Because the results of the unshielded, 12 kg/4 kg ratio was rather predictable and it would be redundant to show the exact same increase in flux as above, another variable was changed for the three subsequent plots. In this case, the shielding composition was

changed to 20 centimeters of polyethylene. The results of the change are shown in Figure 7-48 for pixel array #1.

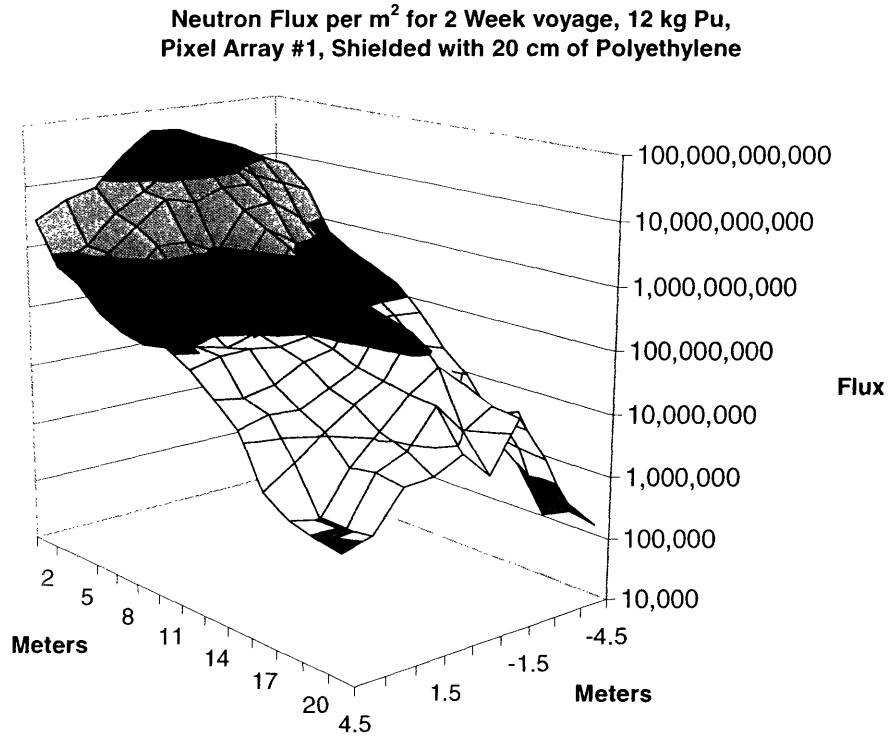


**Figure 7-48: Neutron flux 12 kg Pu, shielded with 20 cm of polyethylene,
pixel array #1**

A noticeable, but by no means restrictive, difference can be seen when comparing this surface plot to the 12 kilogram base case. The flux has dropped somewhat through the 20 centimeters of polyethylene, but still not one point on the chart is below detectability threshold. The average distance to threshold is taken to be around 24.5 meters and centerline fluxes might be above limits out to 26 meters. The ratio of the base case, unshielded 12 kg flux to the 20 cm shielded flux is shown in Figure 7-49.

Shielding Ratio, Pixel array #1, 20 cm Thick Polyethylene Shield

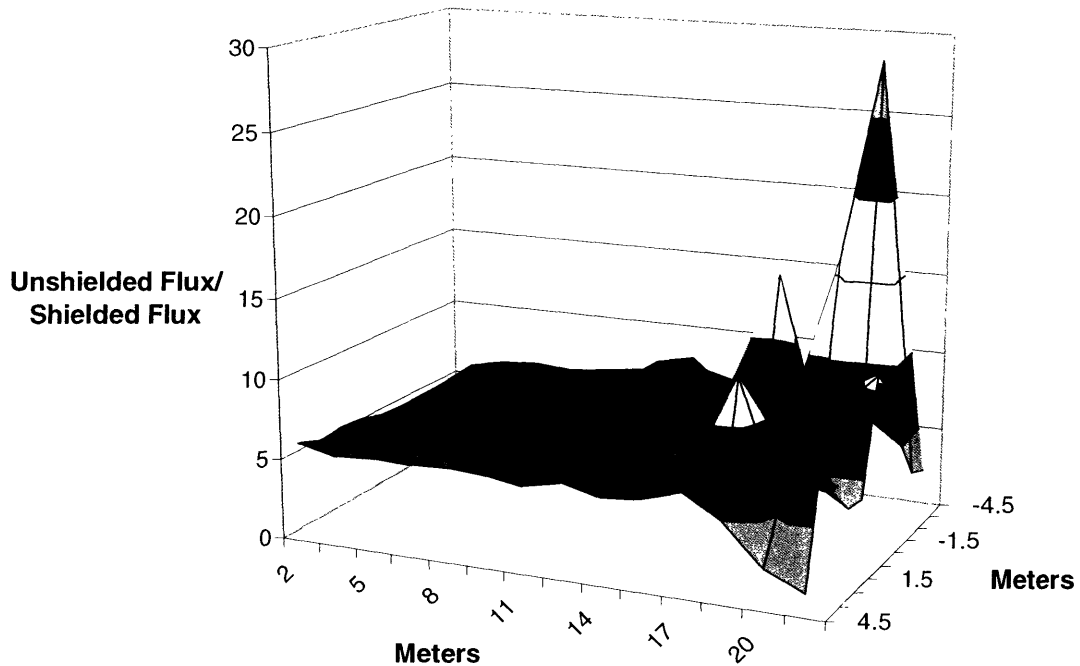


Figure 7-49: Ratio of unshielded/shielded flux 12 kg Pu, shielded with 20 cm polyethylene, pixel array #1

The drop off in flux for a 20-centimeter sphere of polyethylene is around a factor of five. This is a significant improvement in shielding, but still not enough to appreciably affect the distance to threshold.

The results of the shielded pixel array #2 case are shown in Figure 7-50. The effect of the 20-centimeter shield is seen above and has turned the flux at 21 meters almost uniformly below one million particles. In this case, the average distance to threshold is 23.5 meters, slightly lower than in pixel array #1. A plot very similar to Figure 7-49 is not shown.

Neutron Flux per m² for 2 Week voyage, 12 kg Pu,
Pixel Array #2, Shielded with 20 cm Polyethylene

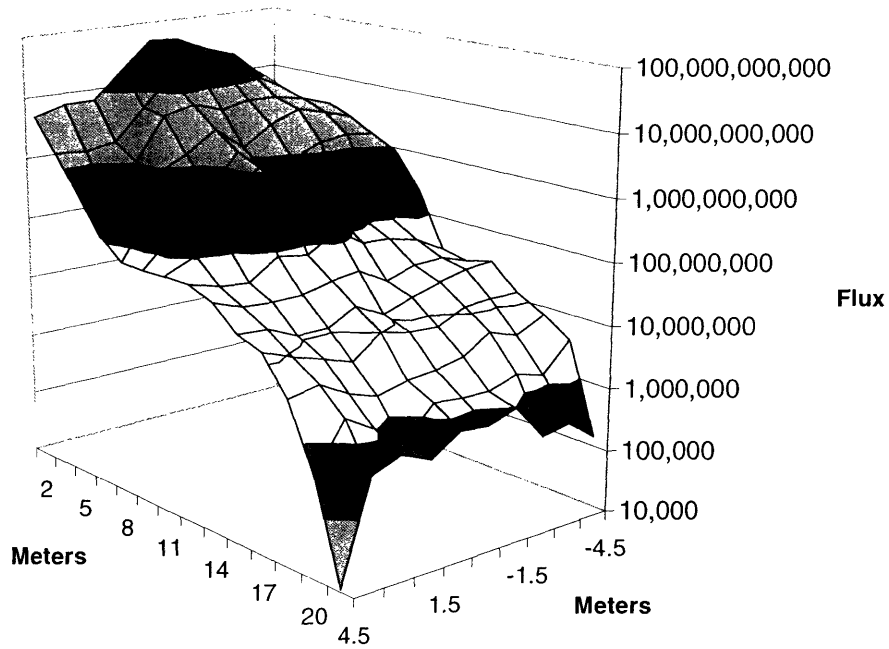


Figure 7-50: Neutron flux 12 kg Pu, shielded with 20 cm of polyethylene,
pixel array #2

Neutron Flux per m² for 2 Week voyage, 12 kg Pu,
Pixel Array #3, Shielded with 20 cm of Polyethylene

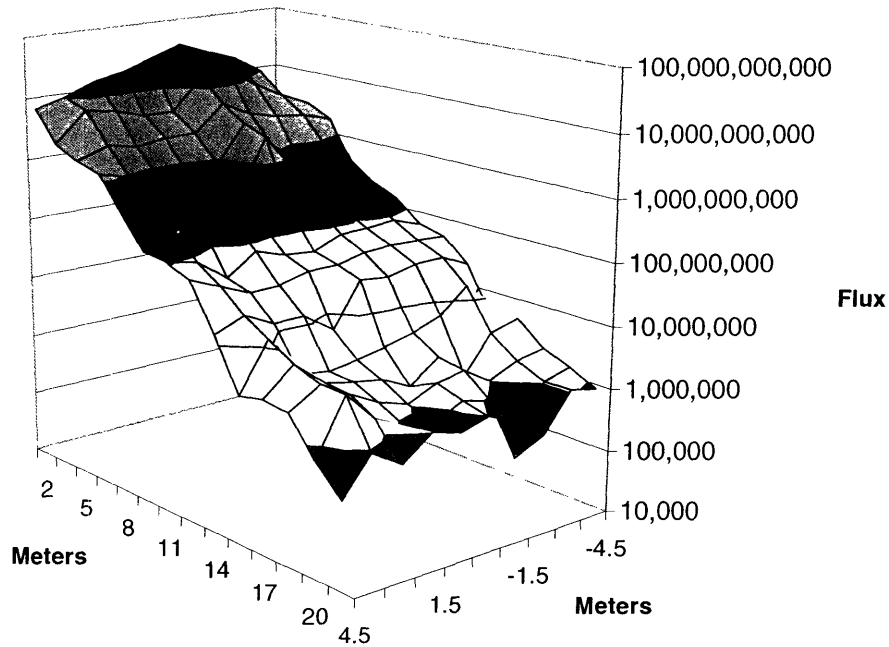


Figure 7-51: Neutron flux 12 kg Pu, shielded with 20 cm of polyethylene,
pixel array #3

Pixel array #3 is presented in Figure 7-51. Pixel array #3 resembles pixel array #2 in that the flux at greater than 21 meters consistently falls below one million particles per m². The same distance to threshold is found in this case and is taken as 23 meters.

7.7.4.5.3 Concrete Filled Container

In what was expected to be a worst-case shielding scenario, an attempt was made to completely remove neutrons from the system before they ever reached the pixel array. This was done by completely filling the space inside the container with Portland concrete of density 2.3 gm/cm³. The case is obviously impractical, but the results are interesting enough that they warrant some attention and actually produce an important conclusion.

Pixel array #2 was chosen with 4 kilograms of plutonium for this case and the results are shown in Figure 7-52.

The surprising results speak for themselves. Operating over a two-week period, the flux of neutrons actually making it out of a concrete-filled container is significant. Out to a distance of 10-11 meters, neutrons can be seen with a three-sigma confidence level. The conclusion is, of course, that a terrorist will not be able to completely shield a 4-kilogram plutonium-based weapon such that it cannot be seen through 10 meters of cargo. This is a very significant statement.

**Neutron Flux per m² for 2 Week voyage, 4 kg Pu,
Pixel Array #2, Container filled with Concrete**

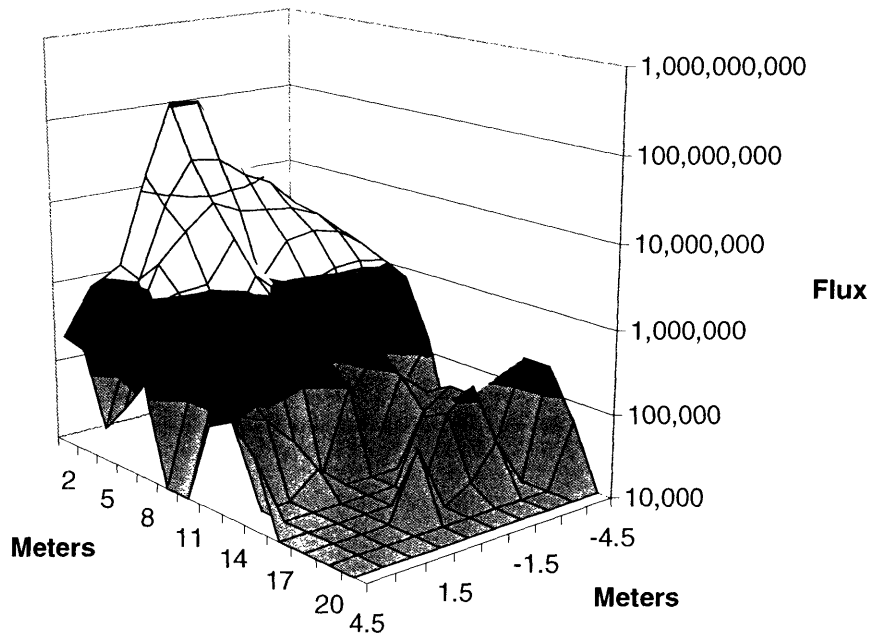


**Figure 7-52: Neutron flux 4 kg Pu, container backfilled with concrete,
pixel array #2**

7.8 Summary of Results

Clearly, the physics behind the ship-based approach is favorable; radiation signal attenuation is extremely high, often losing 10-12 orders of magnitude through 20 meters of cargo, but it is still significant enough to identify a weapon. Nature has created nuclear structure such that energetic gammas and neutrons from frequent nuclear decay provide a signature that can identify an arrangement of fissile material in such a manner that the threat can be mitigated. Simulations of shielded material measure a strong enough signal that significantly more shielding might have been assumed.

It has been firmly established that the potential for detection on a containership is attainable, but it remains to show that the ship-based approach is practical. From a

physics standpoint, the most important numbers reported above are the fluxes; but from a practical point of view, the most important results in the multitude of graphs and surface plots shown above are the average distance to threshold numbers. Recall that distance to threshold is the distance where the flux falls below the 3σ detectability limit. This distance can be translated directly into the number of containerized detectors needed to cover every container in each ship and then to cover all inbound containerships. To set the stage for the translation and to summarize this chapter, the average distances to threshold are organized in Table 7-1. The last column is a simple weighted average of the three pixel arrays. It is weighted for photons such that the worst-case pixel #3 carries a 10% contribution, which is clearly an overstatement given the extremely low probability (1 in 10,000) of such an occurrence.

Table 7-1: Average distance to threshold

Summary of Average Distance to Threshold					
Pixel Array	Fissile Mass (kg)	Energy (keV)	Shielding	Distance to Threshold (meters)	Case Average Distance to Threshold
#1	12	2615	Self	25.0	
#2	12	2615	Self	21.0	
#3	12	2615	Self	13.0	22.0
#1	50	2615	Self	20.5	
#2	50	2615	Self	19.0	
#3	50	2615	Self	12.0	19.0
#1	12	1001	Self	15.5	
#2	12	1001	Self	13.5	
#3	12	1001	Self	9.5	14.0
#1	12	2615	2 cm Lead	19.5	
#2	12	2615	2 cm Lead	19.0	
#3	12	2615	2 cm Lead	10.5	18.4
#1	50	2615	2 cm Lead	18.5	
#2	50	2615	2 cm Lead	17.5	
#3	50	2615	2 cm Lead	11.0	17.3
#1	4	Full Spectrum	Self	23.5	
#2	4	Full Spectrum	Self	23.5	
#3	4	Full Spectrum	Self	23.5	23.5
#1	12	Full Spectrum	Self	29.0	
#2	12	Full Spectrum	Self	26.0	
#3	12	Full Spectrum	Self	24.0	26.3
#1	4	Full Spectrum	5 cm Water	25.0	
#2	4	Full Spectrum	5 cm Water	25.0	
#3	4	Full Spectrum	5 cm Water	24.0	24.7
#1	12	Full Spectrum	20 cm Polyethylene	24.5	
#2	12	Full Spectrum	20 cm Polyethylene	23.5	
#3	12	Full Spectrum	20 cm Polyethylene	23.0	23.7
#2	12	Full Spectrum	Concrete	10.5	10.5

Chapter 8: Deployment of the Ship-Based Detector Network

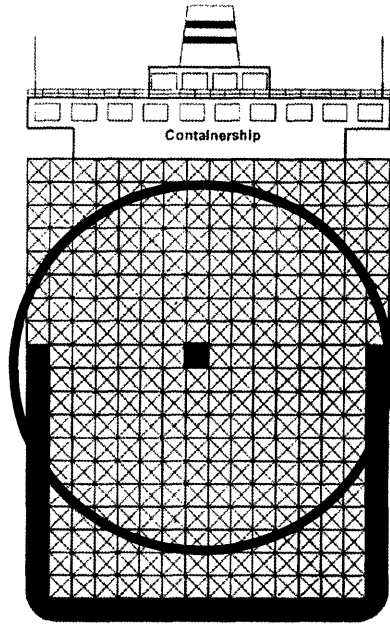
Given the results presented in Chapter 7, the next step is to quantify the number of containers needed on each ship with varying degrees of coverage. Due to previous thesis work by Broderick, this task is a straightforward cross-reference [Broderick, 2004]. One of the important outputs of Broderick's thesis was to set the framework for an easy translation of distance to threshold into number of containerized detectors needed on each ship. The details of his calculations and simulations are not summarized here, but are instead taken as completely relevant since they were created in anticipation of the numbers produced in this thesis.

Broderick's work delineates two fundamental types of container loading patterns. One "centerline" pattern is considered where each containerized detector is placed in the center of the ship for optimal coverage volume. The other is a random pattern where no control is assumed over the placement of the containerized detectors [Broderick, 2004].

Another major conclusion of Broderick's thesis is that achieving coverage volumes of 80-90 percent or more shows diminishing returns if done by adding additional containerized detectors [Broderick, 2004]. It is not cost effective to achieve 100% coverage of a fully loaded containership from a practical standpoint because the small benefit gained from adding extra detectors is not worth the additional resources. Some degree of coverage with respect to cost optimization is therefore necessary, but should be considered in context of the diminishing increases in deterrence gained by adding additional containers. It seems safe to assert that a terrorist is unlikely to adjust his level of deterrence if the system is increased from 75% coverage to 85% coverage; significant gains in deterrence by denial are likely achieved with much lower coverage percentages.

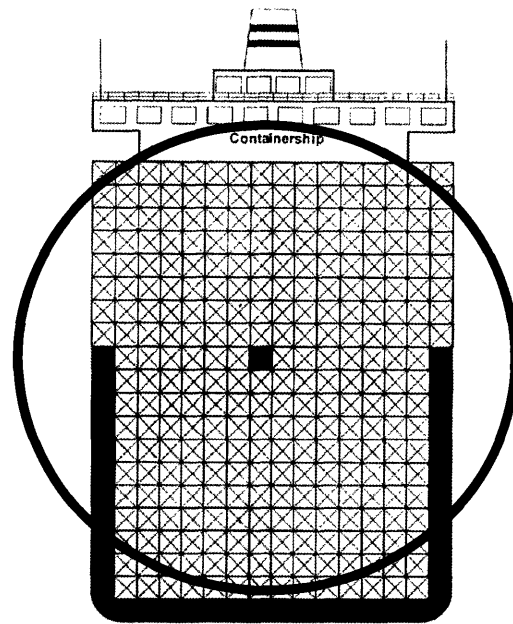
To help illustrate the concept of coverage volume, the following containership diagrams have been adapted to show how distance to threshold affects the number of containers covered [CPIP, 2003].

Shielded Uranium



R = 17.3 meters

Shielded Plutonium



R = 23.7 meters

Figure 8-1: Coverage volumes in two-dimensions

The schematic is meant for illustrative purposes and does not match the exact dimensions of a containership hull; however, it does represent precisely scaled dimensions of containers and distances to threshold. The shaded containers represent detector units and "R" defines the distance to threshold. A weapon within the sphere of containers delineated by R will be detected with a three-sigma confidence level.

The two cases shown above represent the lowest average distance to threshold numbers resulting from pixel arrays #1 and #2 (see Table 7-1). The left figure is a lead-shielded 50-kg uranium weapon and the right is a polyethylene-shielded 12-kg plutonium weapon. Much larger circles could be drawn for other cases. For instance, the 29-meter average distance to threshold for the bare 12-kg plutonium weapon would extend to easily encompass the entire diagram.

Of course, this diagram only shows two dimensions of the coverage volume and is potentially misleading. The total number of containers within the coverage volume cannot be calculated by cubing the number of containers along R. The container's 40-foot dimension (perpendicular to the diagram) must be taken into account. Calculations made by Broderick carefully include all dimensions of both the container and containership.

8.1 Detectors Needed on a Typical Containership

For deployment of the ship-based network of detectors, it is important to know how many containerized units are required on each ship to give varying degrees of coverage. There are over a thousand different containerships operating around the globe, but fortunately, most can be categorized by TEU capacity. Because many containerships are manufactured to the same specifications, they are easily categorized by capacity: 1440, 2496, 3600, 4800 and 6460 TEU. It is noteworthy that several large containerships with capacities over 7,000 TEU are currently in shipyards or on order so that a new category will have to be defined within the next decade [Sallas, 2002].

The number of containerized detectors needed to cover each type of containership is listed in Table 8-1 for each weapon and shielding case. The average distance to threshold numbers are taken from the last column in Table 7-1 and the remainder of the chart is cross-referenced with work from Broderick. Detector coverage volumes are reported as a percentage of the total volume of the ship. These percentages are, in essence, the amount of coverage achieved for a fully loaded containership. Under each ship capacity column, the "R" refers to a randomized placement of containerized detectors and the "C" refers to the centerline placement of detectors. Some centerline scenarios are blocked out because they are not physically possible. For instance, with a distance to threshold of only 14 meters, it is not geometrically possible to cover 95% of a 6460 TEU containership with a centerline deployment.

Table 8-1: Containerized detectors needed per containership

Containerized Detectors Needed per Containership													
Weapon Case	Distance to Threshold (meters)	Percent Covered	Ship Capacity (TEU)										
			1440		2496		3600		4800		6460		
			R	C	R	C	R	C	R	C	R	C	
2615 keV, 12 kg U	22.0	75	5	3	7	4	9	4	11	4	14	6	
		85	6	3	9	5	12	4	15	5	18	7	
		95	3	4	15	5	19	5	24	7	31	9	
2615 keV, 50 kg U	19.0	75	6	3	9	5	12	5	15	6	20	8	
		85	8	4	12	5	17	5	20	7	27	15	
		95	14	4	21	6	27	7	34	14	45		
4 kg Pu	23.5	75	4	2	6	3	8	4	9	4	12	5	
		85	6	3	8	4	10	4	13	5	17	6	
		95	9	3	14	5	17	5	21	7	29	8	
12 kg Pu	26.3	75	4	2	5	3	7	3	8	4	10	5	
		85	5	3	8	4	9	4	11	4	15	5	
		95	8	3	12	4	15	4	19	5	25	6	
2615 keV, 12 kg U, Lead Shielding	18.4	75	7	4	11	5	15	5	18	7	24	12	
		85	10	4	15	6	20	6	26	12	33		
		95	15	5	25	7	34	9	43		55		
2615 keV, 50 kg U, Lead Shielding	17.3	75	9	4	13	6	18	7	23	12	30		
		85	12	5	19	6	25	8	31		41		
		95	19	5	30	10	41		53		70		
4 kg Pu, Water Shielding	24.7	75	4	2	6	3	8	4	9	4	12	5	
		85	6	3	8	4	10	4	13	5	17	6	
		95	9	3	14	5	17	5	21	7	29	8	
12 kg Pu, Polyethylene Shielding	23.7	75	4	2	6	3	8	4	9	4	12	5	
		85	6	3	8	4	10	4	13	5	17	6	
		95	9	3	14	5	17	5	21	7	29	8	
1001 keV, 12 kg U	14.0	75	13	5	21	10	30		37		59		
		85	19	5	31		40		52		68		
		95	32	7	50		69		88		117		

Some significant conclusions can be drawn from the above table. Most importantly, the majority of ships can be covered enough to confidently find a weapon in almost any configuration. Restrictive scenarios do occur; for example, it is probably not practical to cover every 6460 TEU containership having a concealed virgin uranium weapon. Much more discussion will follow on deployment scenarios (see section 8.3), but in response to credible intelligence or substantiated threats, even 50-100 detectors is not out of the question. Conversely, it is highly practical to cover just about any other scenario on the above chart, many of which require less than 10 containerized units. Still, the above table is conservative in that it does not take into consideration practical shipping constraints such the inefficiencies of loading to full capacity.

8.2 Load Factor Adjustment

Table 8-1 is extremely useful as a guide to the number of containerized detectors needed to cover a filled containership, but is not entirely applicable to the real world. While fully loaded voyages do occur, the likelihood of filling a containership to capacity is very low. In fact, most containerships travel with a much lower capacity to both expedite commerce and optimize fuel efficiency. The shipping industry defines “load factor” as the volume of containers actually loaded divided by the volume at full capacity. Average load factors tend to be in the 65% range [PIERS, 2001; San, 2004]. This fact alone vastly improves the practical deployment of the ship-based system. It is also easy to see how the coverage volume diagrams of Figure 8-1 would easily encompass all the cargo once nearly a third of the containers are removed.

Depending on loading patterns, the 65% load factor is translatable into Table 8-1. A containership loaded to 65% capacity should be almost fully covered with the 75% numbers from Broderick. This increase of 10% is a conservative estimate, but is required because the possibility of uneven loading patterns, which would reduce the coverage volume of some containerized detectors, must be taken into account. For example, Coverage A in Figure 8-2 is not as great as coverage B so some extra percent above loading factor should be built in to the estimate.

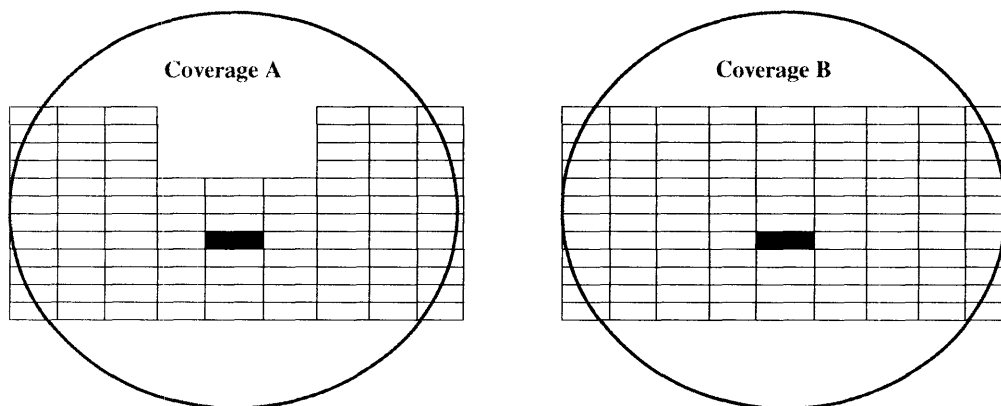


Figure 8-2: Coverage volume inefficiencies due to loading factor

Due to erratic container loading patterns, an estimate is made that 65% uneven loading requires 75% uniform coverage. This estimate is conservative in that irregular loading will only occur on top and containers throughout the rest of the vessel will be closely packed. Accounting for the 65% average load factor, the 75% coverage numbers given by Broderick translate into nearly 100% coverage of the ship. As such, Table 8-1 above can be reduced to include just the 75% coverage lines as other rows would be superfluous, corresponding to well over 100% coverage

Table 8-2: Containerized detectors needed per containership with 65% loading factor

Containerized Detectors Needed per Containership, 65% Loading Factor												
Weapon Case	Distance to Threshold (meters)	Percent Covered	Ship Capacity									
			1440		2496		3600		4800		6460	
			R	C	R	C	R	C	R	C	R	C
2615 keV, 12 kg U	22.0	~100	5	3	7	4	9	4	11	4	14	6
2615 keV, 50 kg U	19.0	~100	6	3	9	5	12	5	15	6	20	8
4 kg Pu	23.5	~100	4	2	6	3	8	4	9	4	12	5
12 kg Pu	26.3	~100	4	2	5	3	7	3	8	4	10	5
2615 keV, 12 kg U, Lead Shielding	18.4	~100	7	4	11	5	15	5	18	7	24	12
2615 keV, 50 kg U, Lead Shielding	17.3	~100	9	4	13	6	18	7	23	12	30	
4 kg Pu, Water Shielding	24.7	~100	4	2	6	3	8	4	9	4	12	5
12 kg Pu, Polyethylene Shielding	23.7	~100	4	2	6	3	8	4	9	4	12	5
1001 keV, 12 kg U	14.0	~100	13	5	21	10	30		37		59	

The results tabulated above directly quantify the capabilities of the ship-based approach in a practical, real-world environment. There are almost no impractical deployment scenarios in the above table, and most scenarios require a rather low number of containerized detectors. The deployment of a ship-based network of detectors is well within reason and is perhaps surprisingly practical.

8.3 Deployment Scenarios

While deployment of the ship-based detector network will ultimately fall under control of the government, it is useful to suggest some deployment scenarios on the conceptual level. A three-stage deployment will be outlined here with the realization that in practice a much more detailed analysis is required. It is also likely that the broad view given here (and to an extent, a detailed strategy) will not be static. Rather, the strategy will be dictated by the world landscape at the time of deployment.

8.3.1 Containerized Units Required for Complete Coverage

Before beginning a discussion of particular deployment scenarios, it remains to quantify the total number of containerized detector units that are required for complete coverage of all incoming containerships. Again, Broderick performed much of the work in anticipation of distance to threshold numbers from this thesis. It is a straightforward cross-referencing task to produce Table 8-3. Broderick uses detailed analysis to calculate the total number of detectors needed; for perspective, the number of TEU imported in 2002 was 12,916,00 with an average of 17 port calls per detector [Broderick, 2004].

Table 8-3: Containerized detectors needed for to cover all incoming containerships

Containerized Detectors Needed for Complete Coverage			
Weapon Case	Cargo Percent Covered	Random	Centerline
2615 keV, 12 kg U	~100	7,578	3,790
2615 keV, 50 kg U	~100	9,861	4,607
4 kg Pu	~100	6,406	3,106
12 kg Pu	~100	5,706	2,890
2615 keV, 12 kg U, Lead Shielding	~100	11,951	5,233
2615 keV, 50 kg U, Lead Shielding	~100	14,705	
4 kg Pu, Water Shielding	~100	6,406	3,106
12 kg Pu, Polyethylene Shielding	~100	6,406	3,106
1001 keV, 12 kg U	~100	23,798	

The ability to cover all inbound containerships is well within reason. Most random deployments can be covered by between 5,000 and 10,000 detectors with the lead shielded scenarios requiring more. A Defense Science Board Report to the Department of Defense provides a rough estimate of a suggested total deployment, defending against all modes of attack at between 100,000 and 400,000 detectors [DSBTF, 2004]. Even 15,000 detectors are not at all impractical for the containership mode, consuming only a small fraction of estimated needs. Thus, the results of the Table 8-3 are extremely encouraging.

Some optimization of random and centerline deployment is likely to occur. While it is well within reason to deploy even 15,000 detector units, it might be desirable to limit the number of random detectors and rely on centerline deployment for many scenarios. For example, if the government decides to allow the adversary to know that all containerships from the Middle East are covered, it might be reasonable to choose a large percentage of centerline deployed detectors and leave only a few random detectors to maintain the advantage of stealth. In other cases, it might be reasonable to deploy most of the detectors clandestinely. Table 8-3 serves to bracket the two extremes and the final deployment will require many checks and balances, necessitating much more detailed analysis.

8.3.2 Deployment Outline

A three-stage, tiered approach might offer the most practical and cost-effective deployment of the entire ship-based network. The deployment of a fleet of containerized detectors could begin on a small-scale with enough units located in “holding pens” throughout high-risk locations of the world to adequately respond to credible intelligence or substantiated threats. Containers would be simply shipped back and forth between the U.S. and their holding pens. Each holding pen could also perform any maintenance, calibration, or upgrades. A build-up of enough units to cover every inbound containership could then occur over the course of a few years, with the first detectors likely deployed to cover the Middle East, which accounts for only around a third of a percent of total imports (see Table 6-2). A secondary deployment might broaden the scope of covered inbound ships from ports in or around the Mediterranean and the Far East. Still more

holding pens could be added in a secondary deployment as a continuous ramp of ship coverage is initiated. In a final deployment, all incoming ships could be covered.

8.3.3 Initial Deployment

An initial deployment might consist of mostly containers in “holding pens”. Holding pens could initially house 10-20 detector units and could be established throughout the world with a concentration in suspect regions. Containerized units would then be ready to respond to emerging threats or be deployed to cover ships leaving ports of greatest concern. Holding pens would be a necessary component of the initial deployment because the units would need a point of origin, and upon return, a point of destination.

Once holding pens have been established, consistent routes could be defined such that detectors are always on board any ship originating from the most threatening ports. As part of the initial deployment, the entire Middle East could be covered with a minimal number of detectors. It turns out that only around a third of a percent of containerized cargo is imported from the Middle East (see Table 6-2); and given the low volume, containerships leaving the region are likely to be of lower capacity, requiring even fewer detectors. It would therefore be a minimal investment of resources to achieve complete coverage of this entire volatile region.

Assuming around 100 detectors for various holding pens throughout the world, and accounting for around 0.32% of the total detectors needed for the Middle East, Table 8-4 shows the number of units that would be required in the initial stage for each weapon case. Most of the initial deployment comes from the 100 units in holding pens. Only on the order of tens of containerized detectors are required to cover every port in the Middle East.

Table 8-4: Containerized detectors needed for an initial deployment

Containerized Detectors Needed for Initial Deployment (Middle East + 100 in Holding Pens)			
Weapon Case	Cargo Percent Covered	Random	Centerline
2615 keV, 12 kg U	~100	124	112
2615 keV, 50 kg U	~100	132	115
4 kg Pu	~100	120	110
12 kg Pu	~100	118	109
2615 keV, 12 kg U, Lead Shielding	~100	138	117
2615 keV, 50 kg U, Lead Shielding	~100	147	
4 kg Pu, Water Shielding	~100	120	110
12 kg Pu, Polyethylene Shielding	~100	120	110
1001 keV, 12 kg U	~100	176	

A rapid and noticeable initial deployment is necessary to achieve deterrence by denial, even if the entire layer of defense is not yet implemented. The deployment should occur as soon as possible after a reduction to practice and subsequent demonstration of capabilities. Such a step-deployment must be substantial enough so that it is noticeable to the adversary. Once the terrorist is aware that ships are being covered, he will likely not risk the loss of his weapon, even if the percentage of ships covered is low. This discussion also brings to light the advantage of operating covertly. While the terrorist knows that the containerized detectors are operating, he will not be aware of their exact location. It is this element of stealth that affords the system the ability to cover only a small percentage of ships in an initial deployment and still deter the enemy.

There are two deployment objectives that must be achieved so that a level of deterrence by denial can be attained. First, the enemy must be aware that containerized detectors exist and are operational; and second, the enemy must know that he cannot locate a significant percentage of the detectors. Knowing and believing that containerized detectors are operational achieves a level of deterrence by denial. An element of ambiguity is essential to any deployment such that the enemy does not know where the defenses lie [DSBTF, 2004]. Given the desirability of covert deployment and necessity of

visible deployment, some percentage of containerized detectors must operate covertly to ensure the element of fear and some percentage must be visible to ensure the credibility of the deterrent. Therefore, a combination of centerline and random deployments is recommended to achieve both objectives.

8.3.3 Extended Deployment

An extended deployment would not be as step-like as the initial deployment. It could consist of a slow ramp-up in coverage as budgetary freedom dictates. In the second stage, many more ports of origin would be targeted according to their level of concern. A list of sorts could be dynamically compiled, which would serve as a guideline for the ramp-up. To quantify the secondary deployment, some other regions of concern might be included. For this stage, coverage of the Middle East, Southeast Asia, the Mediterranean and all of Africa is attained with just under 22% of a full deployment. Simply multiplying through Table 8-3, the following estimate for a secondary deployment is shown in Table 8-5 for each weapon case.

Table 8-5: Containerized detectors needed for secondary deployment

Containerized Detectors Needed for Secondary Deployment (Middle East, Southeast Asia, Mediterranean and Africa)			
Weapon Case	Cargo Percent Covered	Random	Centerline
2615 keV, 12 kg U	~100	1,766	933
2615 keV, 50 kg U	~100	2,268	1,113
4 kg Pu	~100	1,509	783
12 kg Pu	~100	1,355	736
2615 keV, 12 kg U, Lead Shielding	~100	2,728	1,251
2615 keV, 50 kg U, Lead Shielding	~100	3,334	
4 kg Pu, Water Shielding	~100	1,509	783
12 kg Pu, Polyethylene Shielding	~100	1,509	783
1001 keV, 12 kg U	~100	5,333	

To cover a major portion of the world, only between 1,000 and 2,000 units are required for a completely random deployment. Less than 1,000 are needed for a most cases in a centerline deployment. Again, an optimization between the centerline and random deployment is necessary and the final number of units could fall anywhere between the extremes.

8.3.4 Final Deployment

A final deployment would constitute coverage of every inbound containership and would insert an extra layer of defense against containerized nuclear terror. It would entail nearly 100 percent coverage of all incoming containerized cargo at the three-sigma detection level. For number of detectors needed in a full deployment see Table 8-3 at the beginning of this chapter. While a full deployment would shield the United States from a containerized nuclear event, it could be argued that complete coverage is not necessary. For instance, it might be found too costly to cover all containerships from places such as Oceania or the Caribbean. Some trade offs could be made as parts of the world are deemed safe or of little threat. It is likely that these trade-offs would be dynamic, never exposing the same ports to a complete lapse in coverage.

8.4 Cost

The cost analysis of the ship-based network of detectors is outside the scope of this thesis because it will depend on many design trade-offs not yet analyzed. It is at least appropriate to state that the system is not cost-prohibitive, especially given the relatively low number of units required to ensure the national security of the United States should a terrorist or rogue group intend containerized nuclear attack. One way to gauge the relative value of the system to the government might be through analogy. The government requested just over 9 billion dollars in 2004 on a national missile defense (NMD) to shield the United States from nuclear missile attack [Isaacs, 2004]. Given the findings of the Defense Science Board Task Force report for the Department of Defense, which state that the threat of nuclear terrorism should be treated “as serious as that

devoted missile defense” [DSBTF, 2004], it seems only rational that at least a small fraction of the \$9 billion requested for NMD should be apportioned for nuclear terrorism defenses and at least a fraction of that spent on the system described in this thesis.

One other option might be to fund the system in part by charging a small “security fee” to the shipping company. Using the 12,916,000 TEU imported in 2002, a \$10 fee per TEU would generate over \$120 million per year for the ship-based system. A nuclear incident involving containerships would likely cripple the shipping industry for an extended period of time, thus providing motivation for shipping companies. Contrasted with the vested interest that the shipping companies have in minimizing the threat of nuclear terrorism, a small fee seems reasonable.

The instant that a terrorist places a functional nuclear weapon inside a container bound for the United States, a nuclear attack has been committed. The slow transit time of a containerized delivery as compared to a missile launch should not force a distinction between the two modes of attack: both threaten American soil with nuclear force. The question remains, by analogy, what would the United States be willing to pay to attach detectors to every foreign nuclear missile so that an interception can be made while still in transit? The ship-based network of detectors would not be so dissimilar for the containerized mode of attack. The fundamental property that the system increases nuclear deterrence and strengthens the U.S. nuclear defense posture for a relatively small cost all but ensures the eventual deployment of the ship-based network of detectors.

Chapter 9: Reassessment and Conclusion

9.1 Reassessment of Assumptions

The distance to threshold given by MCNP simulation and the number of containerized detectors required for a practical deployment are so encouraging that a reassessment of assumptions leading to these conclusions is necessary. It is useful to step back at this point and recount what assumptions have been made to reach the point at which Tables 7-1 and 8-2 can be stated with confidence. In this thesis, the following have been assumed, with corresponding justification immediately following:

Assumption: The threat of containerized nuclear terrorism is real.

Justification: The possibility that a terrorist has or at some point could have a functional nuclear weapon is inherently assumed as part of the problem and given the rhetoric and monetary investment of government officials, there appears to be at least some concern that the threat is real.

Assumption: A critical mass of weapons grade material is weaponized and concealed.

Justification: The critical mass used in simulations is given by Fetter and a functional device must be assumed (as opposed to unassembled fissile material) because there is no way of knowing, *a priori*, the adversary's capabilities. The system will also detect unassembled fissile material.

Assumption: There are at least 100 parts per trillion of ^{232}U in WgU.

Justification: 100 parts per trillion is on the lower end of Figure 4-4, representing U.S. Orallo. Measurements indicate that Russia also used reprocessed uranium. Virgin uranium can still be detected from ~15 meters.

Assumption: Weapons grade plutonium containing no more than 6% ^{240}Pu , which provides a large portion of the neutron signal.

Justification: Fetter provides this as a model for WgPu. Plutonium less than weapons grade will have a stronger neutron signal and will be easier to detect.

Assumption: A normal neutron background and practical gamma background is present, not 1,000 tons of Café Brown granite

Justification: There are virtually no neutron sources in cargo and the cosmic muon flux is known. The chances of large amounts of rare types of granite all located near the weapon are extremely low and shipping manifestos will indicate their presence.

Assumption: A non-restrictive and concealable amount of shielding is used.

Justification: For uranium, lead shielding could be thicker, but this might raise the suspicions of foreign customs officials. Thicker shielding of lead will still be detected, but with lower distance to threshold. Almost no amount of neutron shielding will conceal plutonium over a two week voyage.

Assumption: A lumped density cargo model with $\frac{3}{4}$ air by volume.

Justification: The pixel approach is not an assumption, but rather an improved model. The volume calculation is based only on *known* shipping data.

One major contention of this thesis is that above list of assumptions are reasonable and a more detailed attempt to justify them has been made in Chapters 1-8. Based on the accuracy of the assumptions, direct calculation and simulation has been performed which shows that the ship-based approach is both practical and necessary.

9.2 Conclusion

A new approach to the detection of concealed nuclear weapons and fissile material aboard cargo containerships has been detailed. The novel approach removes constraints of current port-based solutions by placing detectors outside the perimeter of a U.S. city. Current defenses exist within the city's perimeter such that a terrorist could remotely detonate the weapon while taxiing past urban areas, but the ship-based system does not allow a concealed nuclear weapon to ever approach the U.S. homeland.

Simply a detector in a box, the system is essentially only a rearrangement of commercially available technology, and will therefore require very little further research and development. Going forward, the next task is to build a prototype and demonstrate the accuracy of the results presented here. The intention of this thesis is both to provide a thorough description of the concept and to indicate expected capabilities with accurate simulation. The above analysis provides a framework by which the ship-based network of detectors can be developed and deployed.

Chapters 2-5 describe the ship-based system, outline the advantages of standoff, sensitivity and stealth over current technology, identify unique radiation signatures of fissile material and characterize potential radiation background. Chapter 6 describes a new, more accurate model of cargo—based only on known shipping data—that includes random pathways of air allowing for improved radiation transport. The results of MCNP simulations are presented in Chapter 7 with the intent of quantifying a distance to threshold, which is found to be quite far. Simulations suggest that due to long count times during a typical two week voyage, radiation transport is significant enough such that containerized units will detect weapons grade uranium and plutonium with three-sigma confidence from distances averaging greater than 22 meters. Given the distance to threshold, the capabilities of the system are quantified in Chapter 8. The vast majority of containerships require between 3 and 15 units deployed on each ship depending on its capacity and degree of control over container placement. Given the low number of units needed for each ship, deployment of a containerized detector network is practical. Even

an initial limited deployment, not yet covering all inbound ships, at least increases the level of deterrence by denial against containerized nuclear terror.

The ship-based system has been described in detail throughout this thesis. The new approach accomplishes all of the objectives of port-based systems such as detection of unassembled fissile material and dirty bombs, but it most importantly offers the ability to detect an assembled nuclear device before the perimeter of a U.S. city is breached. Its attributes and advantages over existing technology are clear, but the most important characteristic of the system is its ability to achieve deterrence by denial. Current solutions offer little deterrence because the rational terrorist will likely detonate the weapon before it ever reaches port-based detectors. With the ship-based system aboard containerships, the nuclear terrorist will not risk his one-time shot where he has a high likelihood of failure. If in fact containerized nuclear terrorism looms on the horizon, the ship-based system will most likely achieve its goal not by detection, but by deterrence.

As one final thought, consider that an irrational terrorist has concealed a shielded, 12-kilogram, plutonium-based nuclear weapon onto a large 6460 TEU containership bound for New York with the intent of detonation as the ship passes near Lower Manhattan. Only 5 containerized detectors would be necessary to cover almost 100% of the ship with a three-sigma confidence level and send an alarm condition so that the weapon never approaches the U.S. homeland. *There is no understating the importance of having detectors aboard that ship.*

Appendix A: 2615 keV Gamma Origin Determination Procedure

In rare instances where imaging is not enough to resolve false alarms, such as granite slabs in the very far field, it may be necessary to distinguish between gammas from the granite and gammas from the weapon. If the intensity factor (see Table 5-6) is substantially lowered due to large differences in granite and weapon locations, the following procedure can be employed to distinguish benign cargo and fissile material. The procedure takes advantage of the fact that actinium gamma lines will be present in the spectrum of natural thorium but not in the spectrum of the weapon.

Referring to Table 5-1, the fact that there will be no actinium lines in the weapon can be used to distinguish the thorium's 2615 keV contribution to the measurement from weapon's contribution. Armed with knowledge of the nearly exact relative decay intensities of ^{228}Ac and ^{236}Pu and ^{232}U daughter lines, the contribution of daughter isotopes such as ^{208}Tl from the natural background can be essentially subtracted from the total measurement. Once the background has been removed, a more accurate representation of the weapon can be made and potential false alarms can be minimized. Since the half lives of all daughters below ^{228}Th in both decay chains are short relative to the parent nuclides, secular equilibrium can be assumed to excellent approximation. Secular equilibrium allows the formulation of nearly exact ratios of gamma intensities between different daughters. For example, one of the most useful ratios is that of the 911 keV ^{228}Ac gamma intensity to the 2615 keV ^{208}Tl gamma intensity. Defining η as the ratio between the two energy line intensities, I_{wpn} for photons of weapon origin and I_{bgd} for photons of background origin, the simple ratio can be constructed as

$$\eta = \frac{I_{wpn}}{I_{bgd}} \quad (\text{A-1})$$

Letting I_{wpm} be the ^{208}Tl 2615 keV relative intensity of 0.1405 and I_{bgd} be the ^{228}Ac 911 keV intensity of 0.1050, then η takes a value of 1.3383.⁶ There will be 1.3383 counts at 2615 keV for every count at 911 keV. For convenience, the notation $\eta = \langle \text{energy of weapon gamma, energy of background gamma} \rangle$ will be used with energies in keV. The above example would then be $\langle 2615, 911 \rangle = 1.3383$. Some important values of η are shown in Table A-1.

Table A-1: Important values of η , the weapon to background intensity ratio

Nuclide		Ac-228						
	Energy (keV)	911.204	968.971	964.766	463.000	794.947	1630.627	1459.138
Pb-212	238.362	1.6391	2.6914	8.5490	9.9091	10.1395	27.2500	54.5000
Bi-212	727.330	0.2519	0.4136	1.3137	1.5227	1.5581	4.1875	8.3750
	1621.500	0.0564	0.0926	0.2941	0.3409	0.3488	0.9375	1.8750
	785.370	0.0414	0.0679	0.2157	0.2500	0.2558	0.6875	1.3750
	1078.620	0.0203	0.0333	0.1059	0.1227	0.1256	0.3375	0.6750
Tl-208	2614.533	1.3383	2.1975	6.9804	8.0909	8.2791	22.2500	44.5000
	583.191	1.1429	1.8765	5.9608	6.9091	7.0698	19.0000	38.0000
	861.564	0.1692	0.2778	0.8824	1.0227	1.0465	2.8125	5.6250

^{208}Tl intensities have been adjusted for their 35.04% branching ratio for ^{212}Po from ^{212}Bi . Values of η as close to 1 as possible are statistically desirable. Resolution issues will likely keep the detector from distinguishing the ^{228}Ac 965 and 969 keV lines, so their intensities will need to be combined and some statistical accuracy sacrificed. Not considering intensity for the moment, the most probable candidates are $\langle 727, 795 \rangle$ and $\langle 862, 795 \rangle$ because of their nearly 1 to 1 ratio and their proximity in energy, which minimizes attenuation differences and energy variations in the detector. The most intense

⁶ See Appendix C for tabulated thorium series relative intensities and Appendix D for ^{232}U series relative intensities.

gammas from thallium and actinium, <2615,911>, are extremely useful even though their energies differ by 1704 keV. Also of interest may be <862,463> and <583,911> for close proximity scenarios. <1620,1630> could have been of great importance considering the proximity in energy and η of 0.9375, but the 1630 keV line from actinium will not resolve itself from the 1638 keV ^{234m}Pa line of the ambient ^{238}U decay chain. Similarly, the relatively intense 1245 keV line from actinium may not be of use because of a 1238 keV gamma from ^{214}Bi of the ^{238}U chain. The 1588 keV line from actinium will likely prove to be useless because the interference of the double escape peak at 1592 keV from the 2615 keV ^{208}Tl gamma. The relatively intense 511 keV ^{208}Tl gamma is of little use since it coincides with the line from positron annihilation. The ^{212}Pb , 239 keV peak may be useful only because of its high relative intensity, but self-shielding severely attenuates these gammas. The combination <2615,911> will have the most utility, but there are a few others with some limited value.

Shielding Effects

For high energy and short distances, equation A-1 is a good approximation; however, looking for lower energy gammas passing through dense material, the approximation fails. Materials such as tungsten or natural uranium tampers and lead shielding surrounding the fissile material will greatly attenuate the low energy gammas (see the spectrum in Figure 7-4). For η to remain accurate, this attenuation must be taken into account. Complex and unknown weapon geometries and shielding configurations may cause the results to become unreliable. However, if geometric approximations can be made and weapon-self shielding scenarios assumed within a reasonable degree of error, a valid η can still be calculated. To account for attenuation, η is modified from (A-1) to

$$\eta_a = \frac{\sum_i^m I_{wpm} e^{-\mu_i x_i}}{\sum_j^n I_{bgd} e^{-\mu_j x_j}} \quad (\text{A-2})$$

for m materials between the weapon and detector and n materials between the background and detector. x_i is the i^{th} material thickness traversed by photons from the weapon and x_j is the j^{th} material thickness traversed by natural background photons, usually air; and

$$\mu = \left\{ \tau \left(1 - \frac{\delta}{h\nu} \right) + \sigma \left(\frac{T_{avg}}{h\nu} \right) + \kappa \left(1 - \frac{2mc^2}{h\nu} \right) \right\} (1 - g) \quad (\text{A-3})$$

where τ , σ and κ are the linear attenuation coefficients for the photoelectric effect, Compton effect and pair production, respectively; $T_{avg}/h\nu$ is the average fraction of the incident gamma energy converted into initial kinetic energy of Compton electrons and g is the average fraction of initial kinetic energy lost to electrons emitted as bremsstrahlung [Turner, 1995]. Background contributions can be simply subtracted from the total count if detector efficiencies are not taken into account.

Detector Efficiency

In all crystal detectors, there is a reduction in counts due to intrinsic efficiency associated with the scintillation material, photo-multiplier tube and electronic pulse discrimination. This efficiency is dependant on the energy of the incident photon. Because of the energy dependence, a further modification of η_a is needed. Adjusting (A-3) to account for the scintillation material's absorption efficiency, η_a is now redefined as

$$\eta_{a,e} = \frac{\mathcal{E}(E_{wpn}) \sum_i^m I_{wpn} e^{\mu_i x_i}}{\mathcal{E}(E_{bgd}) \sum_j^n I_{bgd} e^{\mu_j x_j}} \quad (\text{A-4})$$

where $\varepsilon(E)$ is the efficiency of the given type of detector crystal and photon energy E . For the commonly used sodium iodide (NaI) detectors, the dependence of efficiency on energy is shown in Figure A-1 to provide a general trend [Knoll(1), 2000].

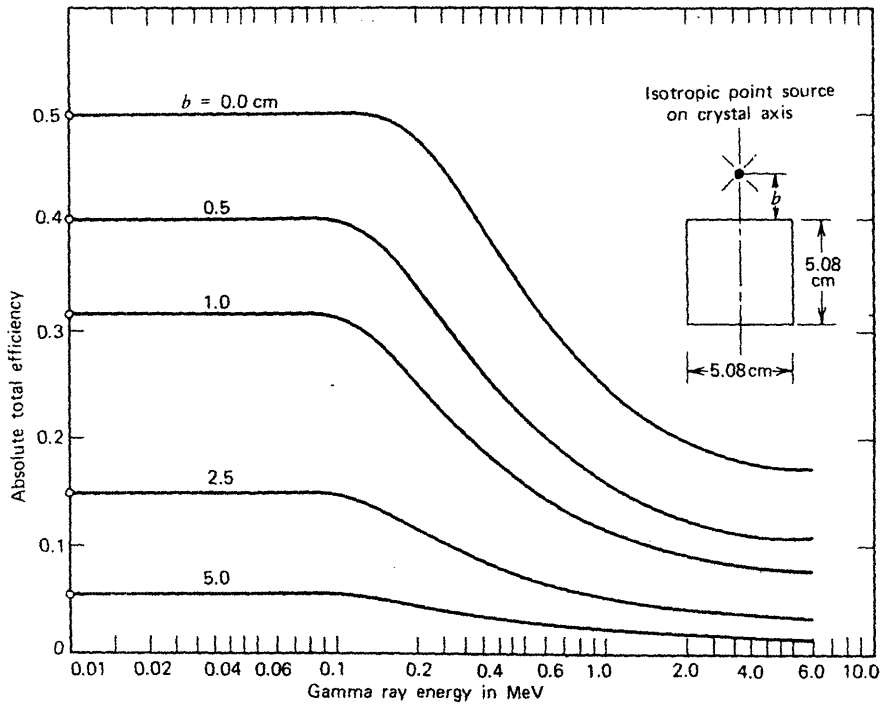


Figure A-1: NaI Scintillator efficiency

Detector efficiencies with each CsI crystal should be thoroughly measured for energies between 0 and 3 MeV before deployment for optimal results.

Total Counts from the Weapon

Without knowledge of background, the total contribution of counts from a weapon at a specific energy can now be calculated. N is defined as the total number of counts at a specific energy, Γ_{wpn} as the number of counts from the weapon and Γ_{bgd} as the number of counts from the background, so that

$$\mathbf{N} = \Gamma_{wpn} + \Gamma_{bgd} \quad (\text{A-5})$$

substituting (A-4) since $\Gamma \propto \mathbf{I}$,

$$\mathbf{N} = \Gamma_{wpn} + \frac{\Gamma_{wpn}}{\eta_{a,e}} \quad (\text{A-6})$$

and rearranging,

$$\Gamma_{wpn} = \frac{\mathbf{N}}{\left(1 + \frac{1}{\eta_{a,e}}\right)} \quad (\text{A-7})$$

This expression gives the total counts from the weapon for different $\eta_{a,e}$ and \mathbf{N} .

Appendix B: Radioactive Cargo

Table B-1 is a list of potential radioactive materials in cargo. The list was compiled by a joint IAEA/Interpol/Europol/WSC project to familiarize guards at border crossings about the types of materials they might encounter [IAEA, 2002]. The most intense gamma energies as well as spontaneous fission rates are included from other sources [Parrington, 1996].

Table B-1: Gamma energies from common background isotopes

Radiation from Common Medical and Industrial Radionuclides	
Isotope	Gamma Energy (keV) (Neutron yield per gm per sec)
Sodium-22	1274
Phosphorus-32	n/a
Calcium-47	1297
Cobalt-58	810
Cobalt-60	1332; 1173
Gallium-67	93; 300
Selenium-75	264; 136
Krypton-81m	276
Yttrium-88	1836; 898
Strontium-89	909
Strontium-90	n/a
Yttrium-90	2186; 2319
Technetium-99	89
Technetium-99m	140
Ruthenium-106	n/a
Palladium-103	39; 357
Indium-111	245; 141
Iodine-123	159
Iodine-125	35
Iodine-129	39
Iodine-131	364
Xenon-133	80
Barium-133	356; 81

Cesium-137	662
Promethium-147	121
Iridium-192	316; 468
Mercury-197	134
Thallium-201	167; 135
Radon-222	510
Radium-226	186
Plutonium-238	43 (1,800)
Californium-252	43 (2,430)

Appendix C: Thorium Series Relative Gamma Intensities

Table C-1: Thorium Series Relative Gamma Intensities [ENSDF, 2003]

Nuclide	Energy (keV)	Relative Intensity	Nuclide	Energy (keV)	Relative Intensity
Th-232	126	0.000170	Th-228	84.4	0.005133
	59	0.000750		216	0.001027
				132	0.000553
Ra-228	30.6	0.000032		166	0.000434
	26.4	0.000006		206	0.000079
	19.4	0.000055		74.4	0.000002
	18.8	0.000829			
	16.2	0.002843	Ra-224	422	0.000011
	15.5	0.000632		404	0.000008
	13.5	0.006318		645	0.000021
	12.8	0.001185		293	0.000024
	6.7	0.000000		241	0.015795
	6.3	0.000000			
			Rn-220	550	0.000434
Ac-228	1631	0.006318			
	1502	0.001856	Po-216	805	0.000008
	814	0.000028			
	672	0.000011	Pb-212	177	0.000201
	42.5	0.000037		300	0.013031
	1588	0.013031		415	0.000111
	1459	0.003159		239	0.172164
	1250	0.000253		115	0.002330
	677	0.000253			
	666	0.000253	Bi-212	1079	0.002132
	629	0.000182		1806	0.000434
	623	0.000043		1074	0.000063
	555	0.000186		1801	0.000000
	523	0.000434		952	0.000711
	492	0.000095		1679	0.000269
	419	0.000083		893	0.001461
	115	0.000039		1621	0.005923
	1345	0.000367		785	0.004344
	1135	0.000039		1513	0.001224

Nuclide	Energy (keV)	Relative Intensity	Nuclide	Energy (keV)	Relative Intensity
	562	0.003435		727	0.026456
	509	0.001856		576	0.000003
	440	0.000513		620	0.000014
	378	0.000099		453	0.001422
Ac-228	99.5	0.005133	Bi-212	493	0.000024
	1374	0.000055		434	0.000055
	1245	0.000387		288	0.001343
	1103	0.000059		474	0.000197
	463	0.017374		328	0.000553
	452	0.000063			
	409	0.007503	Po-212	0	0.000000
	341	0.001501			
	264	0.000162	Tl-208	1283	0.000075
	1111	0.001224		1185	0.000024
	840	0.003712		883	0.000043
	772	0.005923		1161	0.000016
	649	0.000162		1744	0.000003
	199	0.001303		588	0.000055
	146	0.000632		821	0.000055
	77.3	0.000103		705	0.000031
	1154	0.000553		983	0.000288
	1096	0.000513		650	0.000051
	322	0.000908		928	0.000186
	279	0.000790		1381	0.000010
	185	0.000284		253	0.000987
	174	0.000142		486	0.000071
	1065	0.000553		763	0.002567
	795	0.016979		749	0.000059
	727	0.002527		211	0.000253
	154	0.002922		722	0.000284
	100	0.000379		233	0.000434
	965	0.020138		511	0.031985
	836	0.006713		1094	0.000553
	969	0.063969		277	0.009082
	911	0.105036		861	0.017769
	782	0.001974		583	0.120041
	338	0.044620		2615	0.140574

Nuclide	Energy (keV)	Relative Intensity	Nuclide	Energy (keV)	Relative Intensity
	209	0.015400			
	328	0.011846			
	270	0.013426			
	129	0.009872			
	57.8	0.001935			

Appendix D: $^{236}\text{Pu}/^{232}\text{U}$ Relative Gamma Intensities

Table D-1: ^{236}Pu and ^{232}U Relative Gamma Intensities [ENSDF, 2003]

Nuclide	Energy (keV)	Relative Intensity	Nuclide	Energy (keV)	Relative Intensity
Pu-236	48	0.833649	Th-228	206	0.010926
	109	0.151573		74.4	0.000229
	165	0.008336		166	0.060095
	515	0.002147		216	0.142044
	563	0.001263		132	0.076485
	645	0.003031		84.4	0.710220
U-232	58	0.750261	Ra-224	241	0.995966
	129	0.226730		293	0.001494
	270	0.011856		645	0.001295
	327	0.010622		422	0.000722
	191	0.000117		404	0.000523
	332	0.000185			
	338	0.000139	Rn-220	550	1.000000
	209	0.000040			
	773	0.000017	Po-216	805	1.000000
	141	0.000012			
	478	0.000005	Pb-212	239	0.916563
	503	0.000005		300	0.069373
	547	0.000004		115	0.012403
	817	0.000003		177	0.001072
	831	0.000003		415	0.000589
Th-232	59	0.815451	Bi-212	727	0.519038
	126	0.184549		1621	0.116203
				785	0.085215
Ra-228	13	0.530938		39.9	0.085215
	16	0.238922		1079	0.041833
	12	0.099551		893	0.028663
	18	0.069686		453	0.027889
	15	0.053094		288	0.026339
	19	0.004646		1513	0.024015
	30	0.002655		952	0.013944

Nuclide	Energy (keV)	Relative Intensity	Nuclide	Energy (keV)	Relative Intensity
Ra-228	26	0.000498	Bi-212	328	0.010846
	6	0.000010		1806	0.008522
	6	0.000000		1679	0.005268
				474	0.003873
Ac-228	911	0.263019		1074	0.001239
	969	0.160185		434	0.001085
	338	0.111734		620	0.000279
	965	0.050429		493	0.000473
	463	0.043507		576	0.000061
	795	0.042518			
	209	0.038563	Po-212	0	0.000000
	270	0.033619			
	1588	0.032630	Tl-208	2614	0.431875
	328	0.029664		583	0.368792
	129	0.024720		511	0.098264
	409	0.018787		861	0.054591
	836	0.016810		277	0.027902
	1631	0.015821		763	0.007885
	772	0.014832		253	0.003033
	99.5	0.012854		1094	0.001698
	840	0.009295		233	0.001334
	562	0.008603		983	0.000886
	1459	0.007910		722	0.000873
	154	0.007317		211	0.000776
	727	0.006328		928	0.000570
	782	0.004944		486	0.000218
	57.8	0.004845		749	0.000182
	1502	0.004647		821	0.000170
	509	0.004647		588	0.000170
	341	0.003757		650	0.000158
	199	0.003263		883	0.000133
	1111	0.003065		705	0.000096
	322	0.002274		1185	0.000074
	279	0.001978		1161	0.000049
	146	0.001582		1381	0.000030
	1154	0.001384		1744	0.000009
	1065	0.001384			
	1096	0.001285			

Nuclide	Energy (keV)	Relative Intensity	Nuclide	Energy (keV)	Relative Intensity
Ac-228	440	0.001285			
	523	0.001088			
	1245	0.000969			
	100	0.000949			
	1345	0.000920			
	185	0.000712			
	1250	0.000633			
	677	0.000633			
	666	0.000633			
	555	0.000465			
	629	0.000455			
	649	0.000405			
	264	0.000405			
	174	0.000356			
	77	0.000257			
	378	0.000247			
	492	0.000237			
	419	0.000208			
	452	0.000158			
	1103	0.000148			
	1374	0.000138			
	623	0.000109			
	1135	0.000099			
	115	0.000099			
	42.5	0.000092			
	814	0.000071			
	672	0.000027			

Appendix E: Self-Shielding Effect in 50 Kilograms of Uranium

A rough estimate of the expected signal attenuation shows that 50 kilograms of uranium is actually less detectable than 12 kg. In the MCNP model, the distribution of source particles follows the r^2 power law in both the 12 kg and 50 kg case so that particles are evenly distributed along a radial line. A good approximation of the origin for an average gamma decay is therefore the average radius of the uranium shell. For the 12 kg case, the average is $\frac{7cm - 5.75cm}{2} = 6.373cm$ and for the 50 kg case, $\frac{9.34cm - 5.75cm}{2} = 7.545cm$.

Taking the difference of these numbers to quantify the average amount of extra material the gammas will have to travel through

$$\Delta r = 1.17 \tag{E-1}$$

For signal intensity, I , the exponential signal attenuation due to the extra material is then

$$\frac{I}{I_0} = e^{-\mu\rho\Delta r} \tag{E-2}$$

Taking $\mu = 4.878 \times 10^{-2} cm^2 / gm$ from the NIST online reference for uranium [NIST, 2005] and the input density of uranium at $\rho = 19.05 gm / cm^3$, a signal reduction of 0.337 is seen, which accounts almost exactly for the lower fluxes in Figure 7-21.

Appendix F: Randomized Pixel Arrays of Materials

Table F-1: Pixel Array Arrangement

Pixel Array #1, Row 1									
Air	Air	Air	Air	Air	Air	Air	Air	Air	Vehicles
Air	Air	Miscellaneous	Air	Air	Beverages	Air	Air	Air	Air
Air	Air	Air	Air	Air	Air	Coffee	Miscellaneous	Air	Edible Preparations
Miscellaneous	Air	Air	Air	Miscellaneous	Fertilizers	Inorganic Chemicals	Cereals (rice)	Air	Air
Miscellaneous	Air	Air	Air	Air	Air	Air	Air	Air	Cereals (wheat)
Pixel Array #1, Row 2									
Air	Miscellaneous	Air	Air	Air	Fertilizers	Air	Miscellaneous	Air	Air
Air	Air	Air	Air	Furniture	Air	Air	Air	Air	Air
Miscellaneous	Air	Paper & Books	Air	Air	Air	Air	Air	Fertilizers	Air
Air	Fruits	Miscellaneous	Air	Air	Air	Air	Miscellaneous	Air	Air
Air	Coffee	Air	Organic Chemicals	Air	Air	Fertilizers	Air	Air	Machinery
Pixel Array #1, Row 3									
Rubber	Air	Air	Air	Air	Air	Fruits	Air	Air	Air
Air	Ceramic	Air	Air	Air	Air	Air	Organic Chemicals	Air	Air
Air	Air	Wood	Air	Air	Miscellaneous	Air	Air	Air	Beverages
Miscellaneous	Air	Air	Air	Organic Chemicals	Air	Air	Miscellaneous	Apparel	Miscellaneous
Air	Paper & Books	Air	Miscellaneous	Air	Air	Vegetable	Air	Air	Fertilizers
Pixel Array #1, Row 4									
Air	Air	Fertilizers	Air	Air	Wood	Fertilizers	Air	Air	Fertilizers
Air	Air	Miscellaneous	Air	Air	Air	Air	Air	Air	Air
Air	Air	Air	Air	Air	Organic Chemicals	Fertilizers	Air	Miscellaneous	Air
Air	Air	Air	Fertilizers	Air	Air	Air	Plastics	Organic Chemicals	Air
Air	Beverages	Air	Air	Vegetable	Fruits	Air	Air	Vegetable	Paper & Books
Pixel Array #1, Row 5									
Fertilizers	Organic Chemicals	Air	Fertilizers	Air	Air	Air	Plastics	Miscellaneous	Air
Air	Air	Air	Air	Inorganic Chemicals	Air	Air	Air	Air	Miscellaneous
Air	Air	Beverages	Fertilizers	Air	Miscellaneous	Miscellaneous	Miscellaneous	Air	Air
Air	Air	Air	Miscellaneous	Air	Fish	Miscellaneous	Air	Beverages	Air
Paper & Books	Air	Air	Air	Air	Fertilizers	Air	Air	Air	Air

Pixel Array #1, Row 6									
Organic Chemicals	Air	Air	Stone	Air	Air	Air	Air	Air	Air
Miscellaneous	Air	Air	Organic Chemicals	Vegetable	Fruits	Air	Air	Air	Air
Air	Air	Air	Vegetable	Air	Air	Air	Air	Air	Air
Miscellaneous	Air	Dairy	Air	Fertilizers	Air	Air	Beverages	Air	Air
Air	Paper & Books	Air	Fertilizers	Edible Preparations	Air	Air	Air	Air	Air
Pixel Array #1, Row 7									
Air	Air	Air	Air	Air	Miscellaneous	Furniture	Air	Fertilizers	Air
Miscellaneous	Air	Air	Air	Air	Fertilizers	Air	Air	Air	Air
Air	Miscellaneous	Air	Air	Air	Air	Air	Miscellaneous	Air	Air
Air	Miscellaneous	Sugars	Air	Air	Fruits	Air	Air	Air	Air
Air	Air	Air	Miscellaneous	Air	Fertilizers	Fertilizers	Air	Air	Miscellaneous
Pixel Array #1, Row 8									
Air	Air	Miscellaneous	Cocoa	Organic Chemicals	Air	Air	Miscellaneous	Air	Air
Air	Air	Coffee	Vegetable Fats/Oils	Air	Air	Air	Air	Miscellaneous	Apparel
Miscellaneous	Air	Air	Plastics	Air	Air	Air	Air	Air	Air
Air	Iron/Steel Bulk	Air	Air	Air	Air	Air	Air	Fish	Air
Air	Fertilizers	Organic Chemicals	Air	Glass	Air	Air	Air	Plastics	Vegetable
Pixel Array #1, Row 9									
Air	Air	Air	Air	Miscellaneous	Air	Air	Air	Air	Air
Wood	Air	Air	Air	Air	Air	Air	Fertilizers	Air	Miscellaneous
Air	Air	Air	Miscellaneous	Air	Air	Air	Fertilizers	Air	Air
Organic Chemicals	Air	Air	Miscellaneous	Vegetable	Air	Miscellaneous	Air	Air	Air
Fertilizers	Air	Air	Air	Air	Miscellaneous	Air	Air	Air	Air
Pixel Array #1, Row 10									
Furniture	Air	Air	Air	Air	Air	Air	Air	Miscellaneous	Air
Air	Air	Air	Air	Miscellaneous	Inorganic Chemicals	Edible Preparations	Air	Air	Miscellaneous
Miscellaneous	Fruits	Air	Toys	Air	Air	Air	Air	Air	Sugars
Fertilizers	Air	Miscellaneous	Miscellaneous	Air	Air	Air	Air	Dairy	Air
Miscellaneous	Air	Air	Miscellaneous	Air	Air	Air	Air	Air	Apparel

Pixel Array #1, Row 11									
Fertilizers	Machinery	Air	Air	Air	Air	Miscellaneous	Fertilizers	Air	Air
Air	Air	Air	Air	Air	Miscellaneous	Air	Air	Air	Air
Air	Air	Air	Air	Air	Air	Air	Air	Fertilizers	Air
Plastics	Air	Air	Air	Air	Air	Air	Fertilizers	Air	Vehicles
Air	Fertilizers	Air	Air	Air	Air	Plastics	Air	Air	Air
Pixel Array #1, Row 12									
Sugars	Air	Air	Air	Air	Air	Air	Air	Air	Air
Air	Organic Chemicals	Air	Air	Air	Air	Air	Air	Beverages	Air
Air	Fertilizers	Air	Air	Miscellaneous	Air	Air	Air	Vegetable	Air
Air	Air	Air	Air	Air	Air	Air	Air	Air	Air
Air	Air	Air	Organic Chemicals	Air	Air	Air	Air	Air	Air
Pixel Array #1, Row 13									
Air	Air	Coffee	Paper & Books	Air	Beverages	Miscellaneous	Wood	Air	Air
Vegetable	Air	Air	Air	Air	Air	Air	Air	Air	Air
Furniture	Inorganic Chemicals	Fish	Air	Air	Air	Air	Air	Fish	Air
Air	Air	Air	Air	Air	Miscellaneous	Air	Air	Air	Air
Air	Air	Air	Air	Air	Toys	Fertilizers	Air	Air	Air
Pixel Array #1, Row 14									
Air	Air	Air	Air	Air	Air	Organic Chemicals	Air	Air	Air
Air	Cereals (wheat)	Air	Air	Air	Air	Air	Cocoa	Air	Air
Miscellaneous	Vehicles	Air	Air	Fertilizers	Organic Chemicals	Air	Air	Air	Air
Air	Air	Air	Miscellaneous	Air	Miscellaneous	Air	Air	Air	Air
Air	Air	Air	Air	Air	Air	Air	Air	Fertilizers	Miscellaneous

Pixel Array #2, Row 1									
Air	Air	Glass	Air	Miscellaneous	Air	Air	Air	Air	Air
Air	Air	Air	Air	Air	Air	Air	Air	Air	Air
Air	Fruits	Air	Air	Air	Air	Paper & Books	Air	Air	Air
Air	Air	Air	Air	Beverages	Beverages	Miscellaneous	Air	Air	Air
Air	Miscellaneous	Fruits	Air	Cocoa	Air	Air	Air	Miscellaneous	Air
Pixel Array #2, Row 2									
Air	Air	Air	Air	Air	Air	Vegetable Fats/Oils	Air	Air	Air
Organic Chemicals	Air	Air	Air	Air	Air	Plastics	Air	Organic Chemicals	Air
Air	Air	Air	Air	Air	Air	Air	Beverages	Air	Air
Air	Air	Miscellaneous	Air	Air	Air	Air	Miscellaneous	Air	Air
Miscellaneous	Air	Air	Air	Air	Beverages	Air	Air	Air	Air
Pixel Array #2, Row 3									
Air	Paper & Books	Miscellaneous	Air	Vegetable	Air	Air	Air	Miscellaneous	Stone
Air	Air	Air	Air	Air	Organic Chemicals	Cereals (rice)	Air	Air	Miscellaneous
Air	Air	Air	Air	Vegetable	Air	Air	Air	Organic Chemicals	Air
Air	Air	Air	Air	Air	Air	Air	Air	Air	Beverages
Air	Wood	Air	Air	Air	Air	Air	Air	Air	Air
Pixel Array #2, Row 4									
Air	Beverages	Air	Air	Air	Air	Air	Air	Air	Air
Air	Air	Air	Air	Air	Miscellaneous	Air	Air	Air	Air
Air	Air	Air	Air	Air	Air	Vegetable Fats/Oils	Air	Air	Cocoa
Air	Air	Miscellaneous	Air	Fertilizers	Air	Air	Air	Furniture	Air
Miscellaneous	Air	Air	Air	Air	Air	Air	Air	Air	Fertilizers
Pixel Array #2, Row 5									
Air	Air	Fertilizers	Air	Miscellaneous	Air	Air	Air	Beverages	Vegetable
Air	Beverages	Apparel	Air	Fertilizers	Air	Fruits	Air	Air	Glass
Air	Air	Fruits	Miscellaneous	Air	Air	Air	Air	Miscellaneous	Fish
Air	Miscellaneous	Air	Air	Air	Air	Air	Air	Vegetable	Air
Air	Air	Air	Air	Air	Air	Miscellaneous	Air	Air	Air

Pixel Array #2, Row 6									
Cocoa	Air	Air	Air	Air	Air	Air	Air	Vegetable	Fertilizers
Air	Miscellaneous	Air	Miscellaneous	Air	Air	Air	Air	Air	Vegetable Fats/Oils
Air	Air	Air	Air	Air	Air	Air	Air	Air	Air
Air	Air	Air	Air	Air	Air	Air	Air	Air	Miscellaneous
Air	Air	Miscellaneous	Air	Air	Air	Air	Iron/Steel Bulk	Air	Air
Pixel Array #2, Row 7									
Air	Vegetable	Air	Air	Air	Air	Air	Air	Miscellaneous	Air
Air	Air	Organic Chemicals	Miscellaneous	Air	Vegetable	Organic Chemicals	Air	Air	Air
Miscellaneous	Air	Air	Air	Air	Miscellaneous	Miscellaneous	Furniture	Air	Air
Air	Air	Air	Air	Air	Cereals (wheat)	Air	Air	Air	Air
Air	Air	Air	Miscellaneous	Air	Air	Air	Miscellaneous	Air	Air
Pixel Array #2, Row 8									
Fruits	Air	Vegetable	Coffee	Air	Air	Miscellaneous	Air	Air	Air
Rubber	Air	Fertilizers	Air	Wood	Air	Air	Air	Air	Air
Air	Air	Air	Miscellaneous	Air	Air	Iron/Steel Bulk	Air	Air	Air
Air	Air	Air	Air	Air	Toys	Air	Ceramic	Air	Stone
Air	Air	Air	Furniture	Air	Miscellaneous	Miscellaneous	Air	Air	Air
Pixel Array #2, Row 9									
Air	Air	Air	Air	Air	Air	Air	Air	Air	Air
Air	Air	Air	Air	Air	Air	Air	Miscellaneous	Air	Plastics
Air	Air	Air	Air	Furniture	Air	Air	Air	Air	Air
Air	Air	Vegetable	Air	Air	Air	Edible Preparations	Air	Air	Air
Miscellaneous	Air	Fertilizers	Air	Air	Air	Wood	Plastics	Air	Air
Pixel Array #2, Row 10									
Air	Miscellaneous	Miscellaneous	Air	Air	Air	Air	Air	Air	Cocoa
Paper & Books	Air	Air	Fertilizers	Air	Air	Air	Air	Air	Air
Air	Air	Air	Air	Air	Air	Air	Air	Air	Air
Air	Air	Plastics	Air	Air	Beverages	Air	Air	Air	Coffee
Fruits	Air	Air	Air	Stone	Miscellaneous	Air	Air	Cocoa	Fertilizers

Pixel Array #2, Row 11									
Air	Air	Air	Air	Air	Air	Air	Miscellaneous	Air	Miscellaneous
Air	Air	Plastics	Air	Air	Miscellaneous	Air	Air	Air	Beverages
Air	Air	Air	Vegetable	Air	Miscellaneous	Vegetable	Air	Air	Air
Air	Sugars	Rubber	Air	Air	Fertilizers	Air	Furniture	Air	Air
Miscellaneous	Vegetable Fats/Oils	Air	Air	Air	Air	Air	Air	Air	Air
Pixel Array #2, Row 12									
Air	Air	Air	Air	Air	Beverages	Air	Air	Air	Air
Toys	Air	Air	Air	Air	Air	Air	Air	Air	Air
Air	Miscellaneous	Air	Air	Beverages	Air	Miscellaneous	Air	Air	Beverages
Air	Air	Furniture	Miscellaneous	Air	Air	Air	Air	Air	Miscellaneous
Air	Miscellaneous	Air	Toys	Air	Air	Air	Air	Fruits	Air
Pixel Array #2, Row 13									
Vegetable	Air	Air	Air	Air	Air	Air	Air	Air	Miscellaneous
Air	Air	Air	Air	Air	Air	Air	Air	Air	Air
Vegetable	Air	Miscellaneous	Air	Air	Air	Air	Air	Miscellaneous	Air
Air	Air	Air	Air	Air	Fruits	Air	Air	Air	Air
Miscellaneous	Air	Air	Air	Air	Air	Air	Air	Air	Air
Pixel Array #2, Row 14									
Air	Air	Air	Air	Air	Miscellaneous	Air	Air	Air	Air
Air	Air	Air	Miscellaneous	Air	Air	Air	Air	Air	Miscellaneous
Miscellaneous	Organic Chemicals	Miscellaneous	Air	Air	Air	Air	Air	Air	Air
Air	Air	Air	Air	Air	Air	Air	Air	Air	Air
Air	Miscellaneous	Air	Air	Air	Air	Air	Air	Air	Air

Pixel Array #3, Row 1									
Air	Air	Air	Air	Air	Air	Beverages	Air	Air	Air
Air	Air	Air	Air	Air	Air	Air	Air	Air	Miscellaneous
Furniture	Miscellaneous	Air	Air	Air	Ceramic	Air	Air	Air	Air
Air	Beverages	Air	Air	Air	Miscellaneous	Air	Air	Air	Air
Organic Chemicals	Air	Air	Air	Air	Air	Air	Air	Air	Glass
Pixel Array #3, Row 2									
Plastics	Organic Chemicals	Air	Air	Air	Beverages	Air	Fertilizers	Air	Fertilizers
Air	Air	Air	Air	Air	Air	Air	Air	Air	Miscellaneous
Air	Air	Miscellaneous	Air	Air	Miscellaneous	Air	Air	Air	Organic Chemicals
Air	Air	Air	Air	Furniture	Air	Air	Air	Air	Air
Vegetable	Air	Coffee	Air	Air	Cereals	Air	Air	Air	Air
Pixel Array #3, Row 3									
Air	Miscellaneous	Air	Air	Air	Air	Air	Air	Air	Air
Miscellaneous	Air	Air	Vegetable	Air	Air	Miscellaneous	Air	Air	Air
Miscellaneous	Air	Air	Fertilizers	Air	Air	Air	Air	Air	Air
Furniture	Air	Air	Air	Air	Fertilizers	Vegetable	Air	Air	Air
Air	Vegetable	Air	Air	Air	Air	Air	Air	Air	Air
Pixel Array #3, Row 4									
Air	Air	Air	Air	Paper & Books	Air	Air	Air	Air	Air
Miscellaneous	Air	Air	Air	Air	Air	Air	Air	Air	Air
Fertilizers	Miscellaneous	Fertilizers	Air	Air	Wood	Air	Air	Air	Air
Air	Air	Air	Air	Vegetable	Air	Air	Air	Air	Air
Air	Air	Air	Miscellaneous	Air	Air	Air	Air	Air	Air
Pixel Array #3, Row 5									
Air	Air	Air	Air	Air	Miscellaneous	Air	Organic Chemicals	Air	Air
Air	Air	Air	Air	Miscellaneous	Air	Air	Air	Air	Coffee
Vegetable Fats/Oils	Miscellaneous	Cocoa	Toys	Air	Fertilizers	Miscellaneous	Air	Air	Furniture
Fertilizers	Air	Air	Air	Paper & Books	Air	Air	Beverages	Air	Air
Iron/Steel	Air	Air	Air	Fruits & Vegetables	Fertilizers	Air	Fertilizers	Plastics	Miscellaneous

Pixel Array #3, Row 6									
Miscellaneous	Air	Organic Chemicals	Air	Miscellaneous	Miscellaneous	Miscellaneous	Air	Air	Beverages
Vegetable	Air	Air	Vegetable	Air	Miscellaneous	Air	Vehicles	Paper & Books	Air
Air	Air	Miscellaneous	Air	Machinery	Air	Air	Cocoa	Air	Air
Miscellaneous	Air	Air	Air	Air	Air	Air	Fruits & Vegetables	Air	Air
Air	Air	Air	Air	Air	Air	Air	Air	Miscellaneous	Air
Pixel Array #3, Row 7									
Miscellaneous	Air	Air	Air	Beverages	Air	Air	Air	Air	Dairy
Air	Air	Air	Air	Fruits & Vegetables	Air	Vegetable	Air	Air	Air
Air	Air	Air	Air	Air	Air	Air	Air	Air	Air
Vegetable Fats/Oils	Fertilizers	Air	Air	Air	Air	Miscellaneous	Air	Air	Air
Air	Air	Miscellaneous	Air	Air	Air	Air	Air	Stone	Air
Pixel Array #3, Row 8									
Air	Air	Air	Air	Air	Air	Air	Miscellaneous	Miscellaneous	Air
Air	Cocoa	Air	Air	Air	Air	Air	Air	Miscellaneous	Air
Air	Air	Air	Air	Air	Air	Air	Air	Air	Air
Beverages	Air	Miscellaneous	Miscellaneous	Air	Air	Air	Air	Air	Vegetable
Air	Air	Air	Air	Coffee	Fertilizers	Air	Air	Air	Miscellaneous
Pixel Array #3, Row 9									
Plastics	Air	Air	Miscellaneous	Beverages	Iron/Steel Bulk	Miscellaneous	Beverages	Air	Air
Coffee	Air	Air	Air	Edible Preparations	Air	Fertilizers	Air	Air	Air
Plastics	Air	Air	Vegetable	Air	Iron/Steel	Vegetable	Coffee	Air	Furniture
Air	Vegetable	Air	Furniture	Fruits & Vegetables	Air	Air	Vehicles	Air	Air
Vegetable Fats/Oils	Vegetable Fats/Oils	Air	Miscellaneous	Vegetable Fats/Oils	Plastics	Air	Air	Air	Air
Pixel Array #3, Row 10									
Air	Miscellaneous	Furniture	Miscellaneous	Air	Air	Air	Air	Air	Air
Air	Miscellaneous	Fruits & Vegetables	Air	Air	Air	Air	Furniture	Miscellaneous	Air
Air	Air	Fertilizers	Air	Fertilizers	Air	Air	Air	Air	Air
Air	Miscellaneous	Air	Air	Air	Air	Air	Miscellaneous	Air	Air
Wood	Coffee	Air	Air	Air	Air	Air	Air	Air	Air

Pixel Array #3, Row 11									
Air	Air	Air	Air	Air	Air	Miscellaneous	Vegetable Fats/Oils	Air	Air
Air	Air	Air	Air	Air	Air	Air	Miscellaneous	Air	Air
Air	Air	Air	Air	Air	Air	Air	Air	Air	Air
Air	Air	Ceramic	Air	Air	Air	Coffee	Miscellaneous	Air	Air
Air	Fertilizers	Organic Chemicals	Air	Air	Air	Air	Miscellaneous	Organic Chemicals	Air
Pixel Array #3, Row 12									
Furniture	Beverages	Air	Air	Air	Fruits	Air	Miscellaneous	Air	Air
Air	Air	Air	Furniture	Air	Air	Air	Air	Air	Air
Air	Air	Cocoa	Air	Air	Miscellaneous	Air	Air	Air	Air
Beverages	Air	Air	Vegetable	Furniture	Air	Air	Fruits	Vehicles	Air
Air	Miscellaneous	Miscellaneous	Air	Air	Air	Air	Air	Wood	Air
Pixel Array #3, Row 13									
Air	Air	Air	Air	Vegetable	Air	Miscellaneous	Miscellaneous	Air	Air
Air	Air	Air	Air	Air	Air	Air	Air	Air	Air
Air	Air	Air	Air	Air	Air	Air	Air	Air	Iron/Steel
Air	Coffee	Air	Air	Air	Air	Air	Air	Air	Air
Air	Miscellaneous	Air	Coffee	Air	Plastics	Air	Fertilizers	Air	Air
Pixel Array #3, Row 14									
Air	Air	Air	Air	Fruits	Air	Miscellaneous	Air	Air	Air
Air	Air	Air	Air	Air	Coffee	Air	Air	Air	Miscellaneous
Paper & Books	Air	Air	Air	Air	Air	Fertilizers	Fruits	Organic Chemicals	Air
Air	Organic Chemicals	Air	Coffee	Air	Coffee	Air	Air	Fertilizers	Air
Air	Beverages	Air	Air	Vegetable Fats/Oils	Air	Air	Air	Air	Coffee

Appendix G: Cargo Imported to the Port of New York/New Jersey

Table G-1: Port of NY/NJ Import Material Tonnages [Harlingen, 2002]

Import Data for Port of NY/NJ		
Code	Cargo	Metric Tons
25	Crude Fertilizers & Minerals	7,441,496
29	Organic Chemicals	2,957,632
22	Beverages	2,721,911
87	Vehicles, /Except Railway	2,139,004
84	Machinery	1,377,754
20	Prep. Vegetables	1,358,524
39	Plastics	1,350,073
94	Furniture	1,236,492
48	Paper	1,226,841
73	Iron & Steel Articles	1,196,708
68	Art of Stone	1,024,583
72	Iron & Steel Bulk	898,939
8	Fruits	895,484
69	Ceramic Products	875,203
15	Animal or Vegetable Fats	867,002
18	Cocoa	723,678
44	Wood	720,008
9	Coffee	681,737
85	Electric Machinery	585,960
28	Inorganic Chemicals	569,990
17	Sugars	498,905
95	Toys	476,707
70	Glass	457,304
19	Prep. Cereals	451,862
40	Rubber	444,504
62	Apparel Articles not Knit	442,346
3	Fish	366,262
4	Dairy Products	348,738
61	Apparel Articles Knit	330,586
74	Copper	309,682
21	Misc. Edible Preparations	300,337
38	Misc. Chemical	273,783
64	Footwear	234,454
16	Edible Preparations	229,564
76	Aluminum	199,502
12	Oil Seeds	195,294
63	Textile Art	188,221
10	Cereals and Cereal Products	167,071

7	Vegetables	165,614
32	Tanning Dye	161,795
34	Soap	157,479
98	Special Class	148,342
49	Books	146,563
42	Leather	130,267
83	Misc. Base Metal	121,694
33	Essential Oils	115,397
26	Ores	107,534
35	Albuminoidal Subst.	93,406
11	Milling Products	90,998
90	Optic	76,371
55	Manmade Staple Fibers	76,281
52	Cotton	75,156
82	Tool, Cutlery	72,859
56	Wadding	70,041
54	Manmade Filaments	69,307
57	Carpets	69,114
96	Misc. Articles	68,229
6	Trees	66,767
13	Gum	65,259
5	Animal Origin	64,635
23	Food Residues	64,119
37	Photographic Goods	57,191
81	Base Metals	53,553
53	Veg. Text. Fib.	42,744
2	Meats	40,787
47	Pulp and Waste Paper	39,366
30	Pharmaceutical Products	32,897
46	Straw	25,293
86	Railway	24,359
75	Nickel	23,141
93	Arms	22,727
67	Prep Feathers	22,314
24	Tobacco	22,136
66	Umbrellas	21,550
97	Works of Art	21,318
41	Hides	18,056
80	Tin	16,390
92	Musical Instruments	15,738
59	Text Fabrics	14,842
31	Fertilizers	11,208
60	Knitted Fabrics	11,191
65	Headgear	10,764
51	Wool	9,374
71	Pearls	8,508
89	Ships	8,243

91	Clocks	8,032
14	Vegetable Plaiting	7,492
79	Zinc	7,434
58	Woven Fabrics	6,118
78	Lead	4,565
36	Explosives	3,434
45	Corks	3,405
88	Aircraft	2,660
43	Fur skins	1,930
50	Silk	260
1	Live Animals	20
	Total	39,660,408

References

Accorsi, R. et al., "A Coded Aperture for High-Resolution Nuclear Medicine Planar Imaging with a Conventional Anger Camera: Experimental Results," *IEEE Transactions on Nuclear Science*, **48**, No. 6, December 2001, p. 2412 (2001).

Allison, G., et al., "Avoiding Nuclear Anarchy: Containing the Threat of Loose Russian Nuclear Weapons and Fissile Material," The MIT Press, Cambridge, Massachusetts (1996).

Argonne National Laboratory, "Tiny Device Can Detect Hidden Nuclear Weapons, Materials," available on the Internet at:
<<http://www.anl.gov/OPA/news02/news020621.htm>> (accessed June, 2003).

Associated Press, "N.J. Seaport Gets Radiation Detectors," available on the Internet at:
<http://cbsnewyork.com/topstories/wcbsky_story_082141925.html> (accessed January, 2005).

Belyaev, S.T., et al., "The Use of Helicopter-Borne Neutron Detectors to Detect Nuclear Warheads in the USSR-US Black Sea Experiment," available on the Internet at:
<http://www.princeton.edu/~globsec/publications/pdf/1_3-4Belyaev.pdf> (accessed March 2004)

Bertozi, W., "Material Identification and Object Imaging using Nuclear Resonance Fluorescence," MIT Bates Linear Accelerator Center, Poster (2003).

Bicron Corporation, "Handling and Care of Crystal Scintillation Detectors," Product Specification Sheet and Unpacking Instructions (1992).

Bowen, W.Q., "Deterring Mass-Casualty Terrorism," *Joint Force Quarterly*, Summer (2002).

Broderick, B. P., "Systems-Based Analysis of a Ship Borne Approach for the Detection of Fissile Material Concealed in Cargo Containers," MS Thesis Massachusetts Institute of Technology, Department of Nuclear Engineering, (2004)

Bunn, M., "Proliferation Resistance (and Terror Resistance) of Nuclear Energy Systems," unpublished lecture series, Managing the Atom Project, Harvard University, available in the Internet at: <<http://www.ksg.harvard.edu/bcsia/atom>> (accessed November 2004).

Bush, G.W., "Weekly Compilation of Presidential Documents," President's Weekly Radio Address, February 14, 2004, text available on the Internet at:
<www.gpoaccess.gov/wcomp> (Accessed February, 2005).

CBS/AP, “Madrid Massacre Leader Named,” CBS News, available on the Internet at: <<http://www.cbsnews.com/stories/2004/03/11/world/main605222.shtml>> (accessed February 2005).

Chen, Y.W., et al., “Three-Dimensional Reconstruction of Laser Irradiated targets using URA Coded Aperture Cameras,” *Opt. Commun.*, **71**, p. 249-255 (1989).

Cheney, R. B., “The Cheney-Edwards Vice-Presidential Debate,” Commission on Presidential Debates, October 5, 2004, available on the Internet at: <<http://www.debates.org/pages/trans2004b.html>> (accessed January, 2005).

CNN, “Ashcroft: Nuclear Terror Greatest Threat,” January 28, 2005, available on the Internet at: <<http://www.cnn.com/2005/ALLPOLITICS/01/28/ashcroft.interview.ap/index.html>> (accessed January, 2005).

Comprehensive Port Improvement Plan Staff, “NY & NJ Comprehensive Port Improvement Plan,” presented July 10, 2003, DMMIWG Meeting for Market Demand and Port Capacity (2003).

Crane, T. W. and Parker, M. B., “Neutron Detectors,” available online at: <<http://astrophysics.fic.uni.lodz.pl/lectures/neut-det.pdf>> (accessed January, 2005).

Defense Science Board Task Force (DSBTF), “Preventing and Defending Against Clandestine Nuclear Attack,” report for the Undersecretary of Defense for Acquisition, Technology and Logistics.

Department of Energy, “Restricted Data Declassification Decisions 1946 to Present,” RDD-7 (2001).

Driscoll, M., MIT, personal correspondence (2005).

ENSDF, “Evaluated Nuclear Structure Data File,” Brookhaven National Laboratory, available on the Internet at: <<http://www.nndc.bnl.gov/ensdf/index.jsp>> (accessed June, 2003).

Fetter, S., et al., “Detecting Nuclear Warheads,” *Science and Global Security*, **1**, p. 226 (1992).

Fetter, S. et al., “Gamma-Ray Measurements of a Soviet Cruise-Missile Warhead,” *Science*, New Series, **248**, Issue 4957, May 18, 1990 p. 828-34 (1990).

Frank, M.I. et al, “A Monte Carlo Model of Sea-Level Neutron Background: Directionality, Spectra and Intensity,” *Journal of Radioanalytical and Nuclear Chemistry*, **249**, No. 1, p.148 (2001).

Garamone, J., “Wolfowitz Says Dirty Bomb Plot Highlights WMD Dangers,” American Forces Press Service, June 11 2002.

Gedcke, D.A., “How Counting Statistics Controls Detection Limits and Peak Precision,” ORTEC application note AN59, available on the Internet at: <www.ortec-online.com/application-notes/an59.pdf> (accessed February 2005).

Gosnell (1), T. B., “Detecting Fissile Material: Limitations of Current Technology,” presented March 29, 2000, Alternative Signatures for Detecting Fissile Materials Workshop, Livermore, CA (2000).

Gosnell (2), T. B., “Uranium Measurements and Attributes (preprint),” UCRL-JC-139450, submitted to 41st Annual Meeting of the Institute of Nuclear Materials Management, July 15-20, New Orleans, LA (2000).

Hammel, E. F., “Plutonium Metallurgy at Los Alamos, 1943-1945,” Library of Congress Catalog-in-Publication data, ISBN 0-9412342-20-4 (1998).

Harlingen Intelmart, “U.S. Port Vessel Movement and Foreign Trade Database,” available on the Internet at: <http://harlingen.intelemart.com/vessel_movements/portqueryform.cfm> (accessed February 2005).

Hasson, J., “Customs on the Lookout,” available on the Internet at: <<http://www.fcw.com/fcw/articles/2002/0715/web-extra-07-15-02.asp>> (accessed February 2005).

IAEA, “Detection of Radioactive Materials at Borders,” IAEA-TECDOC 1312 (2002).

Isaacs, J., “Current Status of Missile Defense Program, May 2004,” Center for Arms Control and Non-Proliferation, available on the Internet at: <http://64.177.207.201/pages/16_571.html> (accessed April, 2005).

Ivanovich, M. and Harmon, R. S., *Uranium Series Disequilibrium: Applications to Environmental Problems*, Clarendon Press, Oxford, p.399 (1982).

Kernan, W. J. et al. “Ship Effect Measurements Aboard the USNS Regulus,” Bechtel-Nevada Remote Sensing Laboratory, (2003).

Knoll(1), G. F., *Radiation Detection and Measurement*, Third Edition, John Wiley & Sons (2000).

Knoll(2), G. F., “Radiation Detection,” in *Arms Control and Nonproliferation Technologies*, Department of Energy, DOE/NN/ACNT-97 (1997).

Koch, C., “The State of Maritime Security”, testimony of March 24, 2004 before the Senate Committee on Commerce, Science and Transportation (2004).

Kok, J., “Smart and Secure Trade Lanes,” presented November 5, 2004, HPH Corporation, Shanghai, China, (2004).

Kudryavtsev, V. A., “Measurement of the Neutron Flux Produced by Cosmic-Ray Muons with LVD at Gran Sasso”, 26th International Cosmic Ray Conference, Salt Lake City, UT, USA, 17-25 Aug 1999, pp.e-proc, 2.HE.3.1.15 (1999).

Lamarsh, J. R., *Introduction to Nuclear Reactor Theory*, Addison-Wesley Publishing Company, Reading Massachusetts (1966).

Lanza, R., Massachusetts Institute of Technology, Personal Communication (2005).

Lasche, G. P., et al., “Limits of Detection for Special Nuclear Materials with an Advanced High-Pressure Xenon Detector and Robust Fitting Analysis,” IAEA-CN-86-68P.

Lawrence Berkeley Laboratory, “Radioactivity in the Natural Environment,” available on the Internet at: <<http://www.lbl.gov/abc/wallchart/chapters/15/3.html>> (accessed February 2005).

Lugar, R., *Foreword* in Ellis, J., “Defense by Other Means,” Praeger, London (2001).

Luke, S. J. et al., “Neutron Symmetry and Gamma Ray Measurements for the Fissile Material Transparency Technology Demonstration,” Lawrence Livermore National Laboratory, unpublished report.

Mearsheimer, J. J., “Conventional Deterrence,” Cornell University Press, p. 14 (1983).

Morgado, R. E. and Bounds, J. A., “High-Energy Gammas from Fissile Material,” unpublished report, Advanced Nuclear Technology (N-2), Los Alamos National Laboratory (2003).

National Institute of Standards and Technology, “Tables of X-ray Mass Attenuation Coefficients and Mass Energy-Absorption Coefficients,” available on the Internet at: <<http://physics.nist.gov/PhysRefData/Xray/MassCoef/ElemTab/z92.html>> (accessed January 2005).

National Weather Service, “Comparative Climactic Data Publication,” National Oceanic and Atmospheric Administration, available on the Internet at: <<http://ols.nndc.noaa.gov/plolstore/plsql/olstore.prodspecific?prodnum=C00095-PUB-A0001#TABLES>> (accessed June, 2003).

Nuclear Threat Initiative (NTI), “The Nunn-Lugar Cooperative Threat Reduction (CTR) Program,” available on the Internet at: <http://www.nti.org/db/nisprofs/Russia/forasst/nunn_lug/overview.htm> (accessed February, 2005).

O’Brien, K., et al., “Cosmic Ray Induced Neutron Background Sources and Fluxes for Geometries of Air over Water, Ground, Iron, Aluminum,” *Journal of Geophysical Research*, **83**, No. A1, (1978).

Palmer, D., “NY & NJ Port Improvement Plan”, presented at the CPIP Stakeholder Committee Market Forecasting Meeting” April 15, 2003, available on the Internet at: <http://www.cpiponline.org/plan/events/4_14_2003/PortCapacityPres.pdf> (accessed February 2005).

Parrington, J. R., et al., *Nuclides and Isotopes*, Distributed by General Electric company and Lockheed Martin (1996).

Powers, M. J., “Deterring Terrorism with CBRN Weapons: Developing a Conceptual Framework”, CBACI/Sandia National Laboratory, available on the Internet at: <> (accessed February, 2005).

Perrung, A. J., “Predicting ²³²U Content in Uranium,” Pacific Northwest National Laboratory, Richland, WA, PNNL-12075 (1998).

PIERS, “A Capacity Utilization Analysis of the U.S. Container Trade,” *Journal of Commerce*, On Board Review, Summer 2001, Volume VI, Number II. (2001).

Rhodes, R., *The Making of the Atomic Bomb*, Simon & Schuster, New York, (1986).

Sachs, J., “Formation of the Solar System and Structure of the Earth,” MIT Open Courseware, available on the Internet at: <<http://ocw.mit.edu/NR/rdonlyres/Earth--Atmospheric--and-Planetary-Sciences/12-007Spring2003/08C63216-0C54-41FA-9109-3E8912E1D7E0/0/Lec02.pdf>> (accessed January, 2005).

Sallas, B.R., “The Containership Market in 2002,” infoMare, available on the Internet at: <<http://www.infomare.it/news/forum/2003/brs/container-auk.asp>> (accessed May 2004).

San, W.J. “Poon Slams Shipping Industry for Failure to Meet Demands of Modern Global Economy,” available on the Internet at: <http://www.tdctrade.com/shippers/vol24_4_seafr02.htm> (accessed January, 2005).

Schumer, C.A., “Senate Passes Schumer Effort to Provide \$150 Million to Strengthen Port Security, Stop Nuclear Bombs from being Smuggled into U.S.,” United States Senate Internet Press Room, Charles A. Schumer, January 17, 2003, available on the Internet at: <http://schumer.senate.gov/SchumerWebsite/pressroom/press_releases/PR01410.html>

(accessed February, 2005).

Sheu, R.J., et al., “A Study of the Cosmic-Ray Neutron Field near Interfaces,” *Nuclear Instruments and Methods in Physics Research*, Section A 476, p. 74-9 (2002).

Slaughter, D., et al., “Detection of Special Nuclear Material in Cargo Containers using Neutron Interrogation,” UCRL-ID-155315, (2003).

Slevin, P. and Lancaster, J. “At Least 7 Nations Tied to Pakistani Nuclear Ring,” *Washington Post*, February 8, 2004, available on the Internet at: <<http://www.washingtonpost.com/ac2/wp-dyn/A22508224Feb7>> (accessed February, 2004)

Smith, D. E., “Technical Testing of Portable Isotope Identification Instruments,” US Customs Service, IAEA-CN-86-70P, p. 177.

Stern, J., “The Ultimate Terrorists,” Harvard University Press, p 11-17 (1999).

Transport Information Services, “Notes on Stowage and Securing of Various Goods,” German Insurance Association (GDV), available on the Internet at: <http://www.tis-gdv/tis_e/inhalt.html> (accessed February 2005).

Turner, J. E., *Atoms, Radiation and Radiation Protection, Second Edition*, John Wiley and Sons, (1995).

Tzortzis, M. and Tsertos, H., “Gamma Radiation measurements and dose rates in commercially-used natural tilling rocks (granites),” UCY-PHY-02/03 (physics/0212104) *Radiation Measurements*, p. 17-9 (2003).

Uphoff, K. “Osama bin Laden’s Mandate for Nuclear Terror,” The Jewish Institute for National Security Affairs, December 10, 2004, available on the Internet at: <<http://www.jinsa.org/articles/articles.html/function/view/catagoryid/1701/documentid/2762/history/3,2360,655,1701,2762>> (accessed January, 2005).

Wagner, R., Los Alamos National Laboratory, Personal Communication (2004).

Wampler, S., “Cell Phone Doubles as Radiation Detector,” Lawrence Livermore National Laboratory, available on the Internet: <http://www.llnl.gov/pao/news/news_releases/2003/nr-03-04-06.html> (accessed February 2005).

Ziock, K. P., et al., “Large Area Imaging Detector for Long-Range Passive Detection of Fissile Material,” *IEEE Trans. Nucl. Sci.*, **51**, no. 5 p. 2238-2244, (2004).